

(NASA-CR-179287) OPTICAL PROPERTIES OF
SOUTHERN HEMISPHERE AEROSOLS: REPORT OF THE
JOINT CSIRO/NASA STUDY Final Report (NASA)
156 p CSCL 04A

N88-21605

Unclas
0137322

G3/46

COHERENT



TECHNOLOGIES, INC.

P.O. Box 7488 Boulder, Colorado 80306-0403

TECHNICAL REPORT CTI-TR-8801

REPORT OF THE JOINT CSIRO/NASA STUDY

OPTICAL PROPERTIES OF
SOUTHERN HEMISPHERE AEROSOLS

FINAL REPORT
FEBRUARY 1988

CONTRACT NO. NAS8-36722

Prepared for

George C. Marshall Space Flight Center
National Aeronautics and Space Administration
Marshall Space Flight Center, AL 35812

Prepared by

John L. Gras¹
C. Martin Platt¹
R. Milton Huffaker²
William D. Jones³
Michael J. Kavaya²

1. CSIRO Division of Atmospheric Research, Aspendale, Victoria, Australia
2. Coherent Technologies, Inc., Boulder, Colorado
3. NASA-Marshall Space Flight Center, Huntsville, Alabama

Coherent Technologies, Inc.
P.O. Box 7488
Boulder, CO 80306 USA

ACKNOWLEDGEMENT

The Coherent Technologies, Inc. analysis effort was sponsored by the NASA-Marshall Space Flight Center (MSFC) on Contract NAS8-36722. The technical monitors of this contract were Daniel E. Fitzjarrald and James W. Bilbro of NASA-MSFC. Their assistance and support during the study are appreciated. The Commonwealth Scientific and Industrial Research Organization (CSIRO) of Australia contributed significantly to the total program effort in providing the F-27 aircraft, flight costs, and personnel to analyze a large part of the data. The cooperation of Dr. Merv Lynch of Curtin University, Perth, Australia in providing the 0.532 μm lidar data, and the cooperation of Dr. Dean Cutten of the Department of Defense in Adelaide, Australia in the 0.532 lidar data analysis is appreciated.

REPORT OF THE JOINT CSIRO/NASA STUDY
OPTICAL PROPERTIES ON SOUTHERN HEMISPHERE AEROSOLS

TABLE OF CONTENTS

	<u>Page</u>
1. Background	1
2. Summary	2
3. Joint CSIRO/NASA Program	3
4. The Experiment	7
5. Data Analysis - Summary	11
6. Comparison of Measured and Calibrated Backscatter Coefficients .	17
7. Recommendations	19
8. Appendix A - Aerosol Measurements, Eastern Australia and Papua New Guinea. May 25 - June 11, 1986	A1
9. Appendix B - Australian Aerosol Backscatter at 10.6 Microns Using an Airborne CW CO ₂ Coherent Lidar	B1
10. Appendix C - The Joint CSIRO/NASA WINDSAT Experiment: Atmospheric Backscatter Measurements at 0.694 Microns	C1
11. Appendix D - Lidar Observations of Tropospheric Aerosols at Cowley Beach, North Queensland: May-June, 1986	D1

REPORT OF THE JOINT CSIRO/NASA STUDY

OPTICAL PROPERTIES ON SOUTHERN HEMISPHERE AEROSOLS

1. BACKGROUND

The global measurement of wind is an important aim for meteorologists, particularly for numerical weather prediction. Although global winds derived from pressure observations using the geostrophic relationship have been popular up until the present, it has recently become increasingly clear that direct wind data are also extremely effective for use in numerical weather prediction. This is particularly true of tropical and southern hemisphere regions where there is a paucity of conventional wind and pressure data.

The realization of global wind measurements from satellites has become feasible recently with technological research and development in the field of coherent Doppler lidar. Coherent lidar, using visible or infrared wavelengths, can provide winds along a cloudless line of sight by measuring the frequency change of the laser radiation when backscattered from aerosol particles moving with the wind flow.

The design of a suitable lidar, and even the choice of a suitable wavelength, depends on a number of factors such as power and weight requirements and eye safety. The design also depends on a knowledge of the abundance of aerosol particles in the atmosphere and their geographical variation throughout the troposphere. A global Doppler wind lidar system would obviously be of most use in those remote regions of the globe which are poorly served by conventional observations. Many of these remote regions are, by definition, far from centers of population and therefore have a relatively low level of atmospheric aerosol pollution. It is thus imperative for design considerations to know the abundance of aerosols, as well as their physical and chemical properties, in remote regions of the globe.

Recently, international programs such as the Global Backscatter Experiment (GLOBE) (sponsored by NASA) and the Laser Atmospheric Wind Sounder (LAWS) project (also sponsored by NASA) have been set up both to measure the global aerosol backscatter and to design a suitable satellite instrument. The

GLOBE program will operate in the 1988/89 timeframe.

A preliminary conceptual design for a space-based Doppler lidar was undertaken by R. M. Huffaker et al, NOAA TM ERL WPL-37 (1978) and NOAA TM ERL WPL-63 (1980). The system was named WINDSAT. The apparent feasibility of measuring winds from space, based on this study, together with the necessity of obtaining aerosol data in "clean" areas of the global atmosphere, led to the initiation of collaboration in 1984 between CSIRO Division of Atmospheric Research, NASA, and Coherent Technologies, Inc., a company situated in Boulder, Colorado.

2. SUMMARY

This study was made in support of the LAWS and GLOBE programs, which aim to design a suitable Doppler lidar system for measuring global winds from a satellite. Observations were taken from 5°S to 45°S along and off the E and SE Australian coast, thus obtaining representative samples over a large latitude range. Observations were made, between 0 and 6 km altitude, of aerosol physical and chemical properties in situ from the CSIRO F-27 aircraft; of lidar backscatter coefficients at 10.6 μm wavelength from the F-27 aircraft; of lidar backscatter profiles at 0.694 μm at Sale, SE Australia; and of lidar backscatter profiles at 0.532 μm at Cowley Beach, NE Australia.

Both calculations and observations in the free troposphere gave a backscatter coefficient of $1-2 \times 10^{-11} \text{ m}^{-1} \text{ sr}^{-1}$ at 10.6 μm , although the accuracies of the instruments were marginal at this level. Equivalent figures were $2-8 \times 10^{-9} \text{ m}^{-1} \text{ sr}^{-1}$ (aerosol) and 9×10^{-9} to $2 \times 10^{-8} \text{ m}^{-1} \text{ sr}^{-1}$ (lidar) at 0.694 μm wavelength at Sale; and $3-7 \times 10^{-9} \text{ m}^{-1} \text{ sr}^{-1}$ (aerosol) and $10^{-8}-10^{-7} \text{ m}^{-1} \text{ sr}^{-1}$ (lidar) at 0.532 μm wavelength at Cowley Beach. The measured backscatter coefficients at 0.694 μm and 0.532 μm were consistently higher than the values calculated from aerosol size distributions by factors of typically 2 to 10.

It is recommended that much more experimental data be taken and that all instrumentation be upgraded, at least to some extent, before further measurements are made, in order to infer the levels of backscatter in the free troposphere with sufficient accuracy and sensitivity.

3. JOINT CSIRO/NASA PROGRAM

The desirability for the development of a viable space program in Australia has been recognized recently. In 1984 CSIRO identified participation in the development of the Australian space industry as an important strategic goal for the Organization, and formed the CSIRO Office for Space Science Applications, or COSSA. COSSA has progressed from that beginning to an active agency, promoting space research and development between Industry, Government Research Laboratories, and Universities. This GLOBE/LAWS experiment was sponsored by COSSA and supported by CSIRO, Division of Atmospheric Research.

The joint field program had four principal aims:

- (i) to make direct measurements of 10.6 μm backscatter in the southern hemisphere over a wide enough latitude range to be representative and during conditions as close as possible to "background". Specifically, this meant avoiding periods when dust transport, cloud, or other short period enhancements would be likely.
- (ii) to attempt to identify the aerosol component responsible for 10.6 μm backscatter. This was seen as a two part process:
 - (a) by determining the aerosol size distribution and using Mie theory to calculate backscatter as a function of particle size thereby identifying the "active" size range;
 - (b) obtain (qualitative) composition data by morphological identification of individual particles in the "active" size range.
- (iii) to directly measure the ratio of backscatter at 10.6 μm and 0.693 μm and also the ratio of backscatter at 10.6 μm and 0.53 μm to derive empirical conversion factors for backscatter at these wavelengths. Also, to investigate the aerosol size distribution over the size range responsible for this scattering and whether such a conversion procedure is in fact valid.
- (iv) to obtain size distribution and species data to add to the very limited data set on southern hemisphere free troposphere aerosol.

The selected area of operation, near 150°E and ranging in latitude from 4°S to 42°S was chosen to include conditions ranging from tropical to the Southern Ocean.

The program was planned as a cooperative venture bringing together five organizations in two countries. Participants in the field program were:

- CSIRO Division of Atmospheric Research - airborne microphysics/ground-based ruby lidar

- NASA Marshall Space Flight Center - airborne 10.6 μm CW lidar

- Curtin University (formerly WAIT) and DSIR - ground-based doubled YAG lidar

Analyses were performed by the individual investigators, with overall collation of the data analyses and the analysis of the NASA CW lidar data the responsibility of Coherent Technologies, Inc., Boulder, Colorado, who also coordinated the experiment.

CSIRO, DAR conducted two main experiments. The first involved obtaining vertical profiles of aerosol backscatter from the ground and at a visible wavelength of 0.694 μm using the CSIRO lidar, and at a site near the south-eastern coast of Australia. The second involved flying instruments in the CSIRO F-27 aircraft to measure aerosol sizes, numbers and chemical properties, at different altitudes. The aircraft could obtain data from selected altitudes from the ground up to a maximum of about 6 km.

NASA participation took the form of a coherent continuous-wave CO₂ lidar, developed at Marshall Space Flight Center, Huntsville, Alabama. The lidar was mounted in the F-27 and looked out sideways. It was able to measure the aerosol backscatter coefficient directly at a wavelength of 10.6 μm and at a nominal distance from the aircraft of 10 m. The lidar measured the aerosol backscatter coefficient continuously during aircraft experiments.

The West Australian Institute of Technology, (WAIT), now Curtin University), Department of Applied Physics, also collaborated substantially in the experiment. Their participation was part of a program studying lidar

backscatter for the Department of Defense, Electronics Research Laboratory. They measured backscatter profiles at 0.532 μm at a tropical location in Northern Queensland simultaneously with the present experiment.

The Department of Defense, Electronics Research Laboratory also contributed financial support to CSIRO, DAR for the aircraft operations around Cairns.

Coherent Technologies, Inc., Boulder, Colorado coordinated the experiment and also the data analysis. They undertook analysis of the NASA CO₂ lidar data and also provided facilities for CSIRO to analyze much of the aerosol data, and supported one CSIRO scientist for a period during the analysis phase.

A formal agreement based on the proposal was set up between CSIRO, COSSA, and the NASA Office of International Affairs, Washington, DC. The formal lines of communication and responsibilities of the participating agencies are shown schematically in Figure 1.

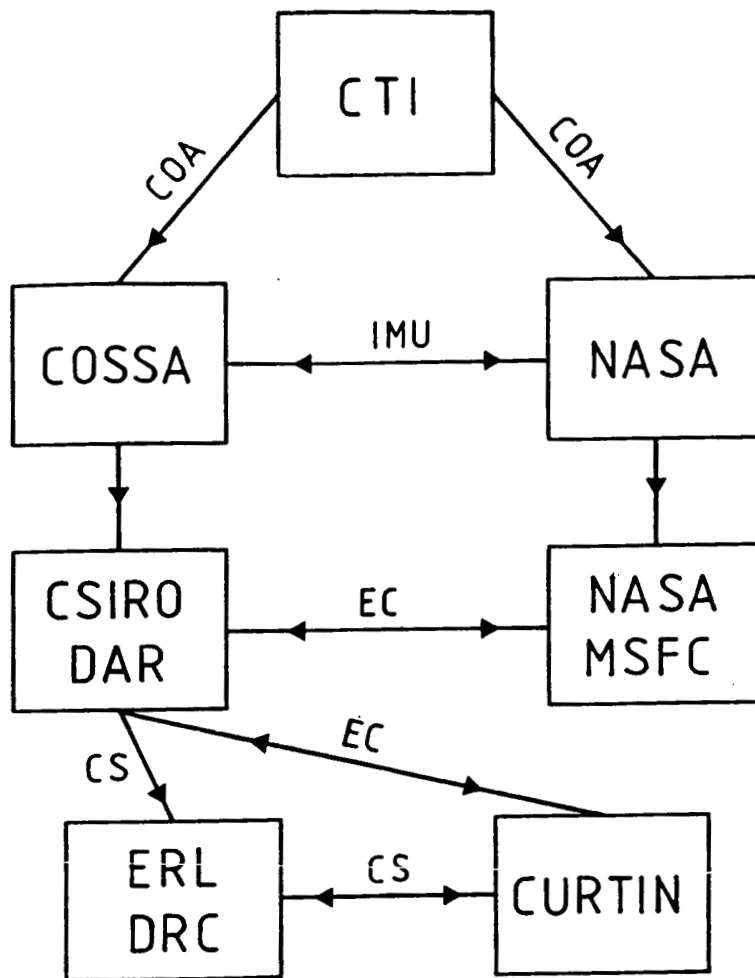


Figure 1. Formal Structure of the Study.

Agencies

NASA National Aeronautics and Space Administration
MSFC Marshall Space Flight Center
COSSA CSIRO Office of Space Science Applications
CSIRO Commonwealth Scientific and Industrial Research
Organization
DAR Division of Atmospheric Research
ERL, DRC Electronics Research Lab, Defense Research Centre, Dept. of
Defense, S. Australia
CURTIN Curtin University
CTI Coherent Technologies, Inc.

Abbreviations

COA Coordination and Analysis
IMU International Memorandum of Understanding
EC Experimental Collaboration
CS Collaboration and Support

4. THE EXPERIMENT

4.1 INSTRUMENTATION OUTLINE

4.1.1 AIRBORNE

Airborne instrumentation was carried in the CSIRO Space Science and Applications Branch (COSSA) Fokker F-27 aircraft. This is a twin turbo-prop with a typical cruise speed of 180 knots and ceiling altitude of 6.5 km. Support instrumentation included doppler radar and INS for determination of wind and location, pitot-static for true air speed and altitude, reverse flow temperature sensor, and dew-point hygrometer.

The main experiment included the NASA-Marshall Space Flight Center's 10.6 μm CW lidar system operating through an 18-cm diameter germanium window. To conform to the aircraft operational requirements, the lidar orientation was perpendicular to its usual disposition requiring some modification to the final optics train.

Aerosol microphysics instrumentation included some real-time devices and some particle collectors. A modified GE condensation nucleus counter was used for total particle concentrations and in conjunction with a diffusion

battery to give size data for radii less than 0.1 μm . Concentrations of particles with radii from 0.05 to 1.5 μm were determined with a PMS ASASP-X particle spectrometer. Both the GE and ASASP were internally mounted and fed from the aircraft isokinetic sampling line. A modified CLIMET 208 size spectrometer was externally pod-mounted. The normal radius sensing range is 0.18 to 10 μm , however an engineering problem arose in the operation of this instrument and data from it has not been included in size distribution determinations at this point. Particles were collected for later analysis using two impaction systems, an external 7-mm wide, free-stream impactor that allows up to 5 samples per flight and a 1-mm jet sampler with morphological identification where possible. Because of the problems with the CLIMET 208 spectrometer, large particle concentrations were determined on representative impaction samples despite the intensive manual effort this involves.

4.1.2 SURFACE

The CSIRO ruby lidar was an incoherent lidar transmitting at a wavelength of 0.694 μm , with a pulse energy of typically 500 mJ, pulse length of 60 ns, and maximum pulse repetition frequency of 1 Hz. The receiving mirror was Cassegrain, 30 cm in diameter and aperture of from 1 to 10 milliradians. The detector was an RCA photomultiplier.

The new CSIRO tunable incoherent CO_2 infrared lidar was also operated, but due to several engineering problems its range was considered too limited to be of any use.

The Curtin University Nd:YAG incoherent lidar operated at a frequency-doubled wavelength of 0.532 μm , pulse energy of 0.2 mJ, pulse length of 5 ns, and pulse repetition frequency of 1 Hz. The receiver was of Newtonian design and 25.4 cm aperture.

4.2 WEATHER CONDITIONS

During the experiment period, weather conditions were typical for late autumn-early winter. In southern Australia there was a slow progression of anti-cyclonic systems followed by a rapid progression of a series of cold fronts across Victoria, after which deep south or southwesterly streams penetrate into continental southeastern Australia. Measurements at the Cape Grim baseline station in northwest Tasmania show that these deep southwest streams usually produce clean or "baseline" conditions for both gases and

condensation nuclei. The frequency of baseline conditions varies from year to year, but is typically 30 to 40% (depending on definitions). Weather conditions for the northern section of the experiment were also quite typical for the season with low level southeasterly trades giving way to the upper level westerly zonal flow above the inversion.

4.3 LOCATIONS AND FLIGHT PLANS

This study was planned around two principal sites, each with a ground-based lidar and a series of "excursion" and "transit" flights. The two fixed sites were at Sale ($38^{\circ}06'S$, $147^{\circ}04'E$) in eastern Victoria where the CSIRO ruby lidar was located, and Cowley Beach ($17^{\circ}41'S$, $146^{\circ}07'E$) in northern Queensland where the Curtin University doubled YAG lidar was sited for the experiment. In both of these locations, aircraft flights were planned as a series of straight and level legs, each of approximately 20 to 30 minutes duration centered on the lidar site. Altitudes were stepped between the boundary layer and the aircraft ceiling (usually between four and six levels). Flights normally finished with a spiral descent sounding. Excursion flights south from Sale to the Cape Grim ($40^{\circ}41'S$, $144^{\circ},41'E$) area, and north from Cairns to Rabaul ($4^{\circ}12'S$, $152^{\circ}12'E$) in New Guinea were included to extend the geographic range of measurements. Both the excursion flights and transit flights used stepped levels in the free troposphere to obtain representative samples (see Figure 2).

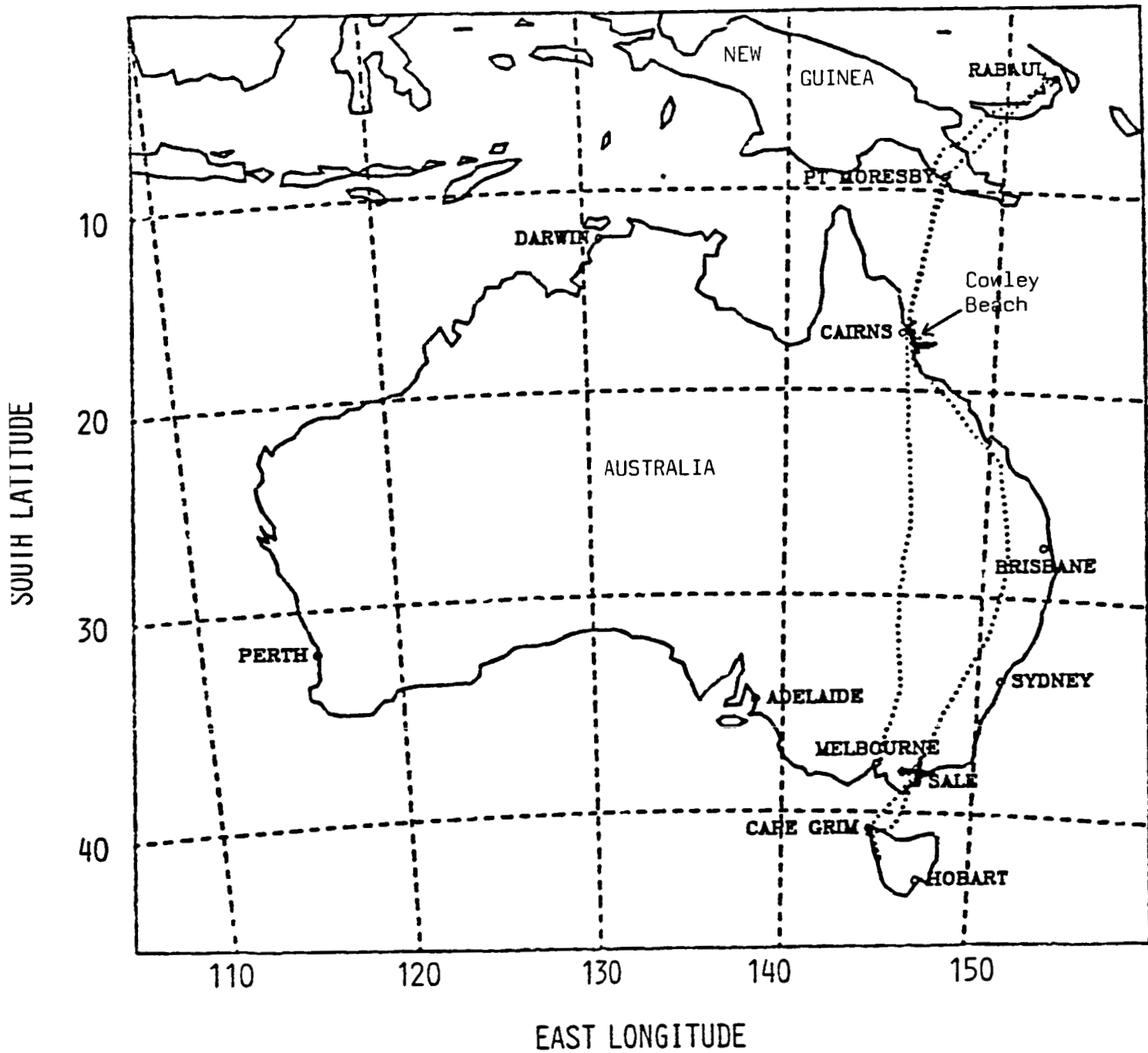


Figure 2. Flight track of CSIRO F-27 Aircraft.

5. DATA ANALYSIS - SUMMARY OF MEASURED DATA

Details of the data analyses are given in the various appendices. Only the final analyzed data are presented here.

5.1 AEROSOL

Details of the data analysis and the results are given in Appendix A. This section summarizes the most significant results. Profiles of concentration for particles with radii larger than selected values plotted as a function of altitude showed several important features. Concentrations of optically important particles were relatively uniform or declined slowly with increasing altitude in the boundary layer, but above the inversion, decreased steadily to an altitude of about 2.5 or 3 km above which concentrations were relatively constant. The larger the particle size the more rapidly concentrations fell off with altitude above the mixed layer. In Sale, the lower inversion meant that free troposphere conditions were approached at a lower altitude than at Cairns and also the concentration of large particles, for example, those with radii larger than 0.2 μm , was somewhat lower there also. Total particle concentrations indeed confirmed a very clean air mass during the period at Sale when large particle concentrations were low, and more typical conditions during the observations near Cairns.

Particle size distributions were obtained as means over selected altitude bands and geographic regions. The measured distributions followed the well known multi-modal form but typically only exhibited two main modes. In the lower layers (below 2.3 km) the individual morphology of the large particles ($r > \text{approx. } 1 \mu\text{m}$) was predominantly a sea-salt type; however, the recrystallization did not produce as regular cubes as is usual. Approximately 12% of particles for these altitudes were irregularly shaped and could not be classed in this way. Low level winds were either maritime or continentally modified maritime during the experiment.

Most free troposphere particles from both main sites, when examined by electron microscopy, had a morphology typical of sulfuric acid or lightly ammoniated sulfate. Only 24% of the free-troposphere particles examined didn't have this morphology.

Day to day variations in particle concentration are an important and regular feature of the atmospheric aerosol. During this flight series, the

most obvious variations in the free troposphere occurred at Sale in a post-frontal, deep southwesterly flow where the concentrations of large particles were about one-tenth of the average (for the whole period). This was followed by an increase of about two orders of magnitude (at some altitudes) with the reversion to a continental airstream.

5.2 MIE ANALYSIS

Full details of calculation and analysis are given in Appendix A. Computation of backscatter coefficients from the aerosol size distribution data serves two purposes. First, by calculating and plotting differential backscatter distributions, e.g. as $\log (d \log b / d \log r)$ as a function of $\log r$ the 'active' aerosol, that is the fraction contributing significantly to the backscatter at a given wavelength is readily identified. Second, the calculated value of backscatter over the whole distribution gives a means for comparing experimentally determined backscatter coefficient values and experimentally determined aerosol concentration values.

Backscatter values were calculated for a series of specific bimodal size distribution models corresponding with the chosen altitude bands, and at wavelengths of 0.53 μm , 0.693 μm and 10.6 μm . Refractive indices were selected to encompass a likely range of compositions. The first assumption is that the aerosol mode centered at 0.06 μm radius (the ubiquitous 'accumulation' mode) is sulfate, however the degree of neutralization is unknown and a wide range of cation composition and hydration combinations is possible. As a simplification this was assumed to be ammonium bi-sulfate. More evidence is available on the composition of the large mode particles. In the boundary layer and just above the inversion ($z = 2.3$ km) impaction samples indicated a high proportion of sea-salt particles. In contrast, the upper troposphere samples showed predominately sulfate and only partially ammoniated. For the lower levels two model compositions were used for the large mode component; 'maritime' or water. Since the refractive index of sea-salt is quite strongly dependent on the actual relative humidity, particularly for $\text{RH} > 60\%$, this approach should span the likely range of refractive indices.

Separation of the two aerosol modes for the calculations demonstrated clearly that at 10.6 μm the backscatter was dominated by large mode particles for all altitude bands and regardless of the refractive index model used. In the free troposphere the contribution fell to 10% at radii of 0.3 μm and 2 μm ,

peaking at around 0.8 μm radius. In contrast, at shorter wavelengths, particles in the smaller 'sulfate' or 'accumulation' mode made an equivalent or dominant contribution to the backscatter compared with the large mode. It follows that backscatter at these widely different wavelengths may be dominated by particles with different sources, sinks and histories. In the boundary layer at all the wavelengths considered, backscatter was dominated by the large particle mode with radii from around 0.5 μm and up to 10 or 20 μm being important in the integrated value.

5.3 AIRBORNE CW CO₂ LIDAR

Full details of the analysis and results of the CO₂ lidar aerosol backscatter measurements in Australia are given in Appendix B. Plots of measured aerosol backscatter with altitude are presented for: 0 to 6.5 km altitude, 5° S to 42° S latitude, and 145° to 153° E longitude. Measurements with the NASA-MSEFC CW CO₂ lidar in the free troposphere gave aerosol backscatter coefficient values of 1-2 x 10⁻¹¹ m⁻¹sr⁻¹ at 10.6 μm . The aerosol backscatter in the free troposphere at 10.6 μm did not change significantly from 5° S (Rabaul) to 42° S (Tasmania). The accuracy of the lidar was marginal at this level. The minimum sensitivity of the lidar was found to be approximately 2 x 10⁻¹¹ m⁻¹sr⁻¹. The lidar data was taken in two modes of operation; a volume scattering mode and a single particle counting mode. Only the volume scattering mode data was analyzed. For the CW CO₂ coherent lidar at 10.6 μm , particles around 1 μm were the most important due to the rapid falloff in number density above 1 μm .

It is recommended that more experimental data be taken in Australia to measure the data base in this very "clean" southern hemisphere environment. The CW CO₂ lidar needs to have increased sensitivity to levels of 5 x 10⁻¹² m⁻¹sr⁻¹. An increase in laser power seems the most effective way to increase the CW lidar aerosol backscatter sensitivity.

5.4 SURFACE LIDAR

5.4.1 CSIRO/DAR RUBY LIDAR AT SALE

Full details of the analysis and results are given in Appendix C. The final data are presented as height profiles of aerosol backscatter coefficient representing different time and height averages. The main features in the backscatter were the generally high, but variable values below the mixed

layer inversion, followed by the rapid decrease by several orders of magnitude to a minimum value which lay at altitudes between 1.2 km and about 4 km. On one day when the air above the inversion was essentially of continental origin, a very sharp minimum at 1.2 km was followed by a recovery in aerosol backscatter which then remained fairly constant with altitude.

The backscatter coefficient in the mixed boundary layer varied by more than an order of magnitude from day to day, with high values immediately following an incursion of moist southwesterly air, and lower values in air which had a more continental origin.

5.4.2 CURTIN UNIVERSITY Nd:YAG LIDAR AT COWLEY BEACH

Full details of the analysis and results are given in Appendix D. Lidar data are presented as height profiles of aerosol volume backscatter function (at 532 nm) for the 9th and 10th of June 1986, the two days on which useful comparisons could be made between the ground-based lidar and the airborne particle samplers. Both profiles were averages of 50 lidar firings and showed enhanced aerosol scattering in the mixing layer, with maximum values of $5 \times 10^{-7} \text{ m}^{-1} \text{ sr}^{-1}$ to $2 \times 10^{-6} \text{ m}^{-1} \text{ sr}^{-1}$. Above the temperature inversion, aerosol backscattering, as measured by the lidar, decreased steadily with height to values of $10^{-8} \text{ m}^{-1} \text{ sr}^{-1}$ or less. Aerosol profiles were normalized to molecular scattering values at around 4.5 km altitude, so that any significant aerosol scattering at these levels meant that the lidar data underestimated the aerosol scattering at all other levels. Because aerosol scattering was weak around these levels, any underestimate is expected to be minimal.

As explained in Appendix D, a single measured value of the aerosol backscatter-to-extinction ratio was used in the calculation of the transmittance correction during data analysis. If this value was not constant with height or differs from the value used, the profiles of backscatter would have to be scaled accordingly.

5.5 UNCERTAINTIES, DATA RELIABILITY

5.5.1 AEROSOL

From the outset it should be appreciated that sampling large aerosol particles from aircraft is difficult. Concentrations may be very low, dictating large flow rates and/or long sample times to obtain good estimates of concentration. Furthermore, there are potential losses or gains in

concentration in sampling non-isokinetically and due to the effects of flow compression and expansion around the aircraft as well as screening off certain areas to particle flow. Plumbing particles along sampling lines with decelerator stages, bends, stepped sizes, or joins may involve particle losses through turbulence or impaction. These effects will vary with particle size, altitude and aircraft speed. In general, quantifying the magnitude of such losses if possible, is exceedingly difficult.

Light-scattering, particle-size spectrometers are subject to uncertainties in size determination relating to the accuracy of the calibration relation, unknown refractive index of sample particles, conversion from calibration particle refractive index to assumed refractive index of sample particles, dependence of response on particle shape, and finite response width of the counter (particularly where the distribution slope is very steep). Small errors in size can appear as large concentration errors. A reasonable estimate of the sizing error if the composition is known is around 5 to 10%, but this could be much larger with unknown composition (and if no conversion from a PSL calibration size is used). Other techniques such as impaction require a model to convert the impacted, desiccated electronmicrographed image back to an equivalent ambient particle size. If the impactor operates in a region where the collection efficiency is less than unity, the uncertainty in the collection efficiency, which is usually determined empirically, must also be included. All possible efforts were taken to reduce the potential for errors in sizing and counting, as an overall estimate sizing error should lie in the range of around $\pm 5\%$ for particles with radii around $0.1 \mu\text{m}$ to about $\pm 20\%$ for radii greater than about one micrometer.

5.5.2 AIRBORNE CW CO₂ LIDAR

Techniques were developed during this study effort, and described in Appendix B for determining the minimum sensitivity of the CW CO₂ lidar by analyzing the noise records of the lidar data. There has been considerable effort at NASA-MSC to develop the CW CO₂ lidar and to develop proper calibration techniques. The volume scattering mode is more understood than the single-particle counting mode and was used in the data analysis. However, the minimum sensitivity of the CW CO₂ lidar was found to be approximately the same value as the measured data in the free troposphere. The CW CO₂ lidar needs additional laser power to increase the lidar sensitivity to $5 \times 10^{-12} \text{ m}^{-1}\text{sr}^{-1}$, as well as special care in calibration. The single-particle mode needs to be

better understood and calibrated for future testing. Improvements can also be made in using calibration targets when in flight and by verifying that the processing bandpass filter is correctly matched to the true airspeed of the aircraft. The Dicke switching technique is subject to true airspeed errors, pointing angle errors, and filter tuning errors. Techniques should be developed to confirm that the processing bandpass filter setting is correct. Quick-look analysis procedures should also be developed to obtain a near real-time assessment of the data quality. The data gathered in Australia indicated that the 10.6 μm aerosol backscatter in the free troposphere is of the same level as the noise of the lidar. It is recommended that similar flight experiments be again conducted in Australia, but with increased CW CO_2 lidar sensitivity, improved system calibration, and an on-board quick-look analysis procedure.

5.5.3 SURFACE LIDAR

The measurement of aerosol backscatter coefficient in the visible spectrum and in the free troposphere is difficult in several respects. First, in the clean maritime atmosphere of the Southern Hemisphere, the aerosol backscatter coefficient in the free troposphere is found to be typically one to two orders of magnitude less than the molecular backscatter, particularly at the shorter wavelengths. Thus, errors involved in extracting a (usually) slowly varying aerosol signal from the molecular signal, and the associated normalization problem, are considerable. Second, the $(\text{range})^2$ decrease in lidar signal implies that signal-to-noise ratios required to extract the aerosol signal from the molecular signal are marginal, at best, in the upper free troposphere, unless many hundreds of profiles are averaged. Third, offset errors due to background radiances (a daytime problem) and due to amplifiers in the signal line can cause appreciable, consistent departures from reality in the aerosol signal.

In many respects, the accurate measurements of the free tropospheric aerosol backscatter coefficient in clean atmospheres requires techniques similar to those used for many years in the stratosphere. In particular, photon counting methods would appear to have some advantages over analog amplification techniques.

6. COMPARISON OF MEASURED AND CALCULATED BACKSCATTER COEFFICIENTS

Backscatter coefficients were calculated as a function of altitude for the three wavelengths used in the field experiment from the mean aerosol concentration profiles measured with the ASASP and measured (altitude dependent model) aerosol particle size distributions. Backscatter coefficients calculated for the model size distributions were scaled for different altitudes using the ratio of the number of particles larger than a specified radius (0.06 μm or 0.25 μm) in the mean concentration profiles and the corresponding concentration in the mean distribution. This gives continuous profiles of calculated backscatter with altitude but with breaks at the altitude boundaries where the size distribution model changes. The profiles for 10.6 μm , 0.694 μm , and 0.532 μm backscatter calculated in this way are given in Figures 3 to 5, respectively, with experimentally observed profiles of backscatter.

The comparison for 10.6 μm backscatter shown in Figure 3 differs from the shorter wavelength comparisons with respect to the data sets actually compared. For 10.6 μm both aerosol and backscatter data apply to the whole experimental period, although the calculated profiles were derived from aerosol averages (and selected size distributions) in the three different geographic regions. For the shorter wavelength profiles, a mean experimental profile is plotted for 0.694 μm which comprises data from four of the seven days that are included in the aerosol data, and for 0.532 μm only two profiles (two days) from the seven days with aerosol data in the Cairns region are included (at this time). This complicates the comparisons to some degree, however there are a number of conclusions that can be drawn.

Considering first the 10.6 μm data, it is clear from the distribution of data points and their associated errors bars in Figure 3 that the 10.6 μm CW lidar was operating just on or in its noise threshold in the free troposphere for most of the conditions sampled. With the reduced complement of particle measuring equipment, the same can be said for the 10.6 μm backscatter. Despite this the agreement between the observed and calculated backscatter at 10.6 μm is surprisingly good. The backscatter profile was calculated (as above) from the concentration (profile) of particles with radii greater than 0.25 μm and also assumed a free troposphere composition of ammonium sulfate and boundary layer composition of ammonium sulfate in the accumulation mode and water in the large particle mode. In the transition between boundary layer and free troposphere, a maritime refractive index was used for the large particle mode.

The more rapid fall off in observed backscatter contribution is strongest at 10.6 μm for particles with radii around 1 μm . Above about 1 km, the concentration of these particles falls off with increasing altitude significantly faster than the 0.25 μm particles on which the profile was based. The peak in backscatter at about 4.5 km in both the observed and calculated profiles is an artifact due to the presence of widespread altostratus cloud north of New Guinea.

Perhaps the greatest difficulty with analysis of data from both of the shorter wavelength lidars, which were operating in daylight conditions, has been establishing the absolute calibration. In both cases the aerosol backscatter in the free troposphere was only a small fraction of the molecular backscatter. Because of this and also because of the (range)² effect on gain, the signal due to aerosol backscatter could not be resolved in the random noise at the upper levels. For comparisons at both wavelengths, two calculated backscatter profiles are given in Figures 3 and 4 for each location. Backscatter coefficients were again determined from the ratio of the mean concentration of particles with $r > 0.06 \mu\text{m}$ (continuous line) and $r > 0.25 \mu\text{m}$ (dashed line) determined with the ASASP and the corresponding concentration in the model size distribution used for that altitude with the backscatter coefficient calculated for the mean size distribution. Calculations of the contribution to backscatter as a function of particle size in Appendix A, indicated that for both of these wavelengths the major contribution to backscatter in the free troposphere and about 25% in the boundary layer was due to particles in the accumulation mode. On this basis, the concentration profile for particles with radii greater than 0.06 μm should give a better representation than the 0.25 μm profile. In comparing the observed and calculated 0.694 μm backscatter profiles for Sale, Figure 4, backscatter calculated using the larger than 0.06 μm radius particle profile agrees more closely with the observed profile between about one and five kilometers altitude, but both give considerably smaller backscatter coefficients than was observed directly at around 1 km altitude. However, the direct observation of backscatter coefficient at 1 km was nearly an order of magnitude greater than on any other days. Above about 4 km there is an increasing divergence between the observed and calculated backscatter coefficients. This could arise either from background and range corrections in the lidar or could represent an increasing loss of some particle fraction with increasing altitude; however, for this short wave scatter the principal contributing size fraction is not the

most difficult to measure. To some extent here also, the lidar data was biased upwards by two profiles on May 25 where the backscatter was consistently higher in the free troposphere than on the other days.

Comparison of the observed and calculated variation of $0.532 \mu\text{m}$ backscatter coefficient with altitude shows an evidently even greater discrepancy than was observed at $0.694 \mu\text{m}$, although as explained above, only two observed profiles have been included at this time. As well, the calculated profiles include a number of days where the concentrations were relatively low compared with the days of the directly measured profiles. Despite this, there appears to be a systematic difference in the shape of the observed and calculated mean profiles above the inversion with the aerosol data indicating a rapid drop in backscatter coefficient above the inversion and a much more gradual drop in the lidar profiles. The rapid drop in the lidar profiles at about 4 km indicates a close proximity to the height of normalization to the molecular profile.

In conclusion, it was found that measured visible wavelength backscatter coefficients were consistently greater than values calculated from aerosol size and concentration measurements but that agreement between observation and calculation was better than $10.6 \mu\text{m}$. Thus, assuming that the shorter wavelength lidars are correctly normalized (and therefore calibrated correctly), they are either "seeing" particles which the aerosol instrumentation doesn't detect or there may be a consistent undersizing of particles.

7. RECOMMENDATIONS

The performances of all three lidars are marginal for measurements of the free troposphere Southern Hemisphere aerosol. It is thus recommended that effort is put into improvement of these instruments before further observations are made. Specifically:

LIDAR INSTRUMENTATION

7.1 For the CW $10.6 \mu\text{m}$ lidar, a greater sensitivity, that is, a better signal-to-noise ratio for a given aerosol backscatter coefficient is required. The calibration of the instrument should include a measure of the real zero.

7.2. Lidar experiments in the visible region should be done at night. Many profiles integrated over an extended time are required. Photon counting methods of signal recovery would be preferable. Some form of independent calibration is required.

7.3 There is some difficulty in tying up the relationship in reconciling measured and calculated values of backscatter coefficients, particularly in the visible region. Support instrumentation to measure extinction coefficients, such as nephelometers, would be desirable.

AEROSOL INSTRUMENTATION

7.4 As wide a range of instrumentation as possible is desirable, particularly instruments that can be mounted externally and have a minimum disturbance on airflow. For calculating 10.6 μm backscatter, particular emphasis should be placed on particles in the size range 0.5 μm to 50 μm . Further, the composition of the particles for this size range should also be determined.

7.5 Measured aerosol concentrations in the Southern Hemisphere appear to cover a wide range of magnitudes, both spatially and temporally. Many more measurements are needed before a reasonably accurate assessment of aerosol backscatter probability distribution can be made.

NASA CW CO₂ LIDAR MEASURED BACKSCATTER

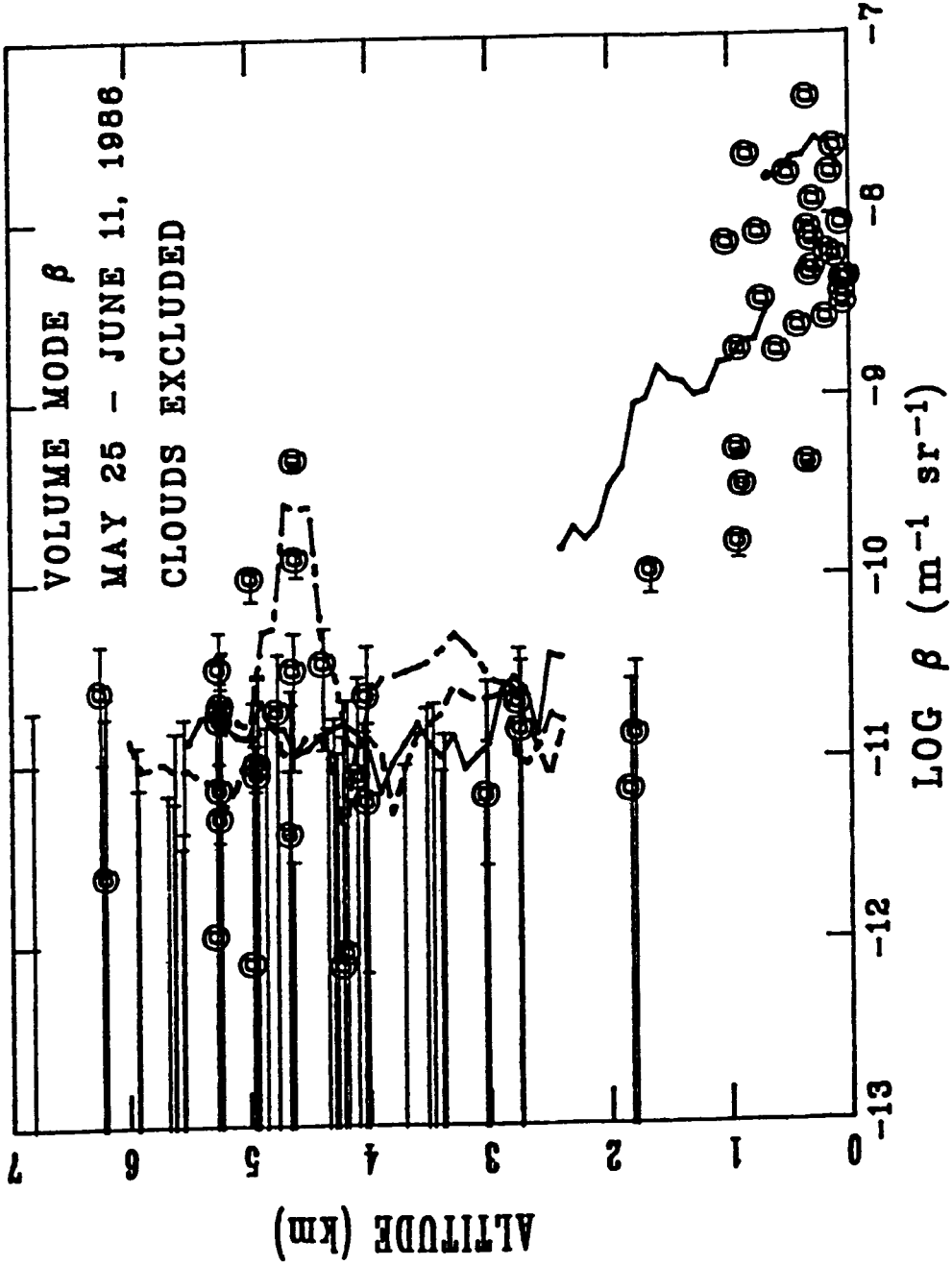


Figure 3. Measured 10.6µm backscatter coefficients from the NASA CW lidar for the whole experiment, cloud-free conditions (points with error bars). Calculated values based on number of particles with $r > 0.25\mu\text{m}$ are for Sale (dash line), Cairns (solid line) and New Guinea (dot-dash line).

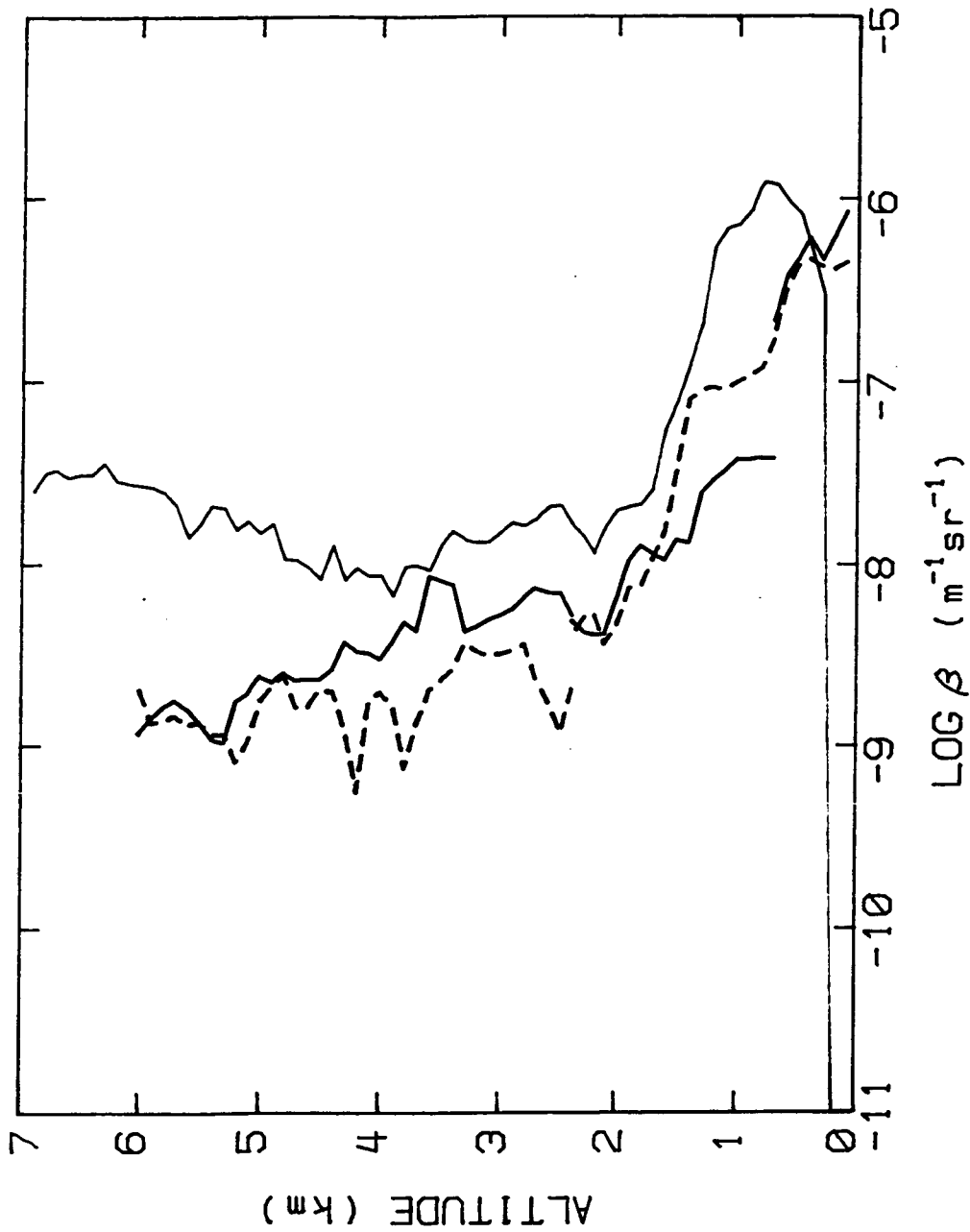


Figure 4. Mean profile of measured 0.694 μm backscatter coefficient from Sale (light continuous line) and two calculated profiles derived using averaged size distributions normalized by the concentration of particles with $r > 0.06 \mu m$ (continuous heavy line) and $r > 0.25 \mu m$ (dashed line), from the mean of all ASASP data for Sale.

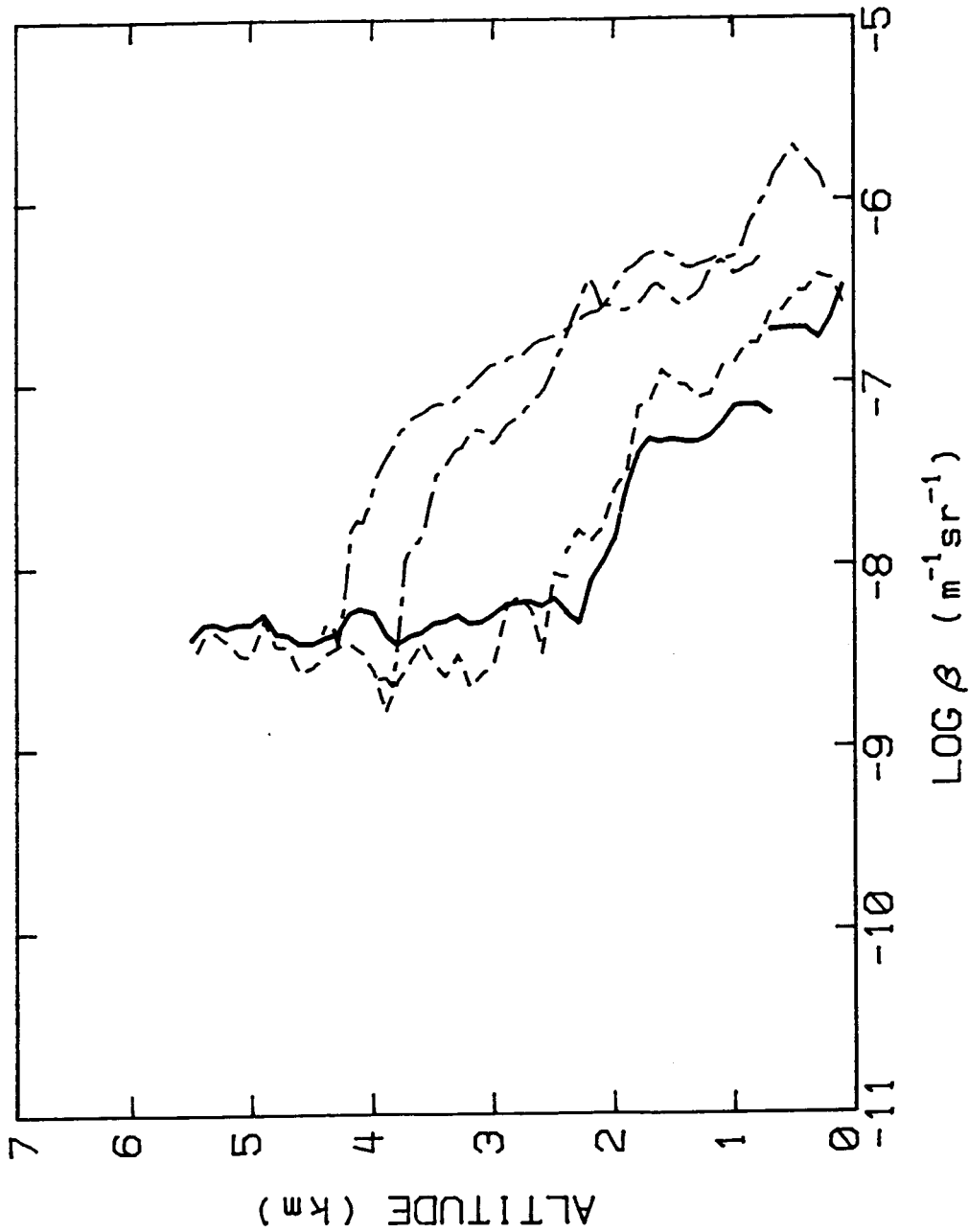


Figure 5. Two observed 0.532 μm backscatter coefficient profiles from Cairns (dot-dash line) and two calculated profiles using averaged size distributions normalized by the concentration of particles with $r > 0.06\mu\text{m}$ (continuous heavy line) and $r > 0.25\mu\text{m}$ (dashed line), from the mean of all Cairns area ASASP data.

APPENDIX A

Aerosol measurements, Eastern Australia and Papua New Guinea

May 25 - June 11 1986

John L. Gras

CSIRO Division of Atmospheric Research

Aspendale, Australia

December 1987

INTRODUCTION

This report describes results obtained from a series of airborne aerosol-particle-microphysics measurements made during a joint CSIRO-NASA field experiment in the eastern Australia-Papua New Guinea region, between May 25 and June 11 1986. These aerosol measurements were made concurrently with (and from the same aircraft as) 10.6 μ m backscatter determinations by W.Jones of NASA MSF. During the same period backscatter was also measured at two shorter wavelengths, 0.693 μ m and 0.532 μ m, using ground-based lidars sited at Sale in south-eastern Victoria and Cowley Beach in north Queensland respectively. Descriptions of the lidar systems, their methods of operation and results are described elsewhere. The altitude range covered during the airborne measurements was surface to approximately 6km.

EXPERIMENT DETAILS

Instrumentation

All of the airborne instrumentation was carried in the CSIRO Fokker F27 research aircraft. This is a high-wing twin turbo-prop. aircraft with a nominal ceiling of 6.5km. Environmental data recorded during the flights using the microphysics instrumentation were drybulb temperature, using a reverse flow thermometer, dew-point temperature using a Bendix cooled mirror hygrometer and pitot and static pressures, for air-speed and altitude. Position information and wind speeds were derived from INS and doppler radar systems operated by the aircraft facility.

Aerosol microphysics instrumentation

Summary

1. Modified GE condensation nucleus (CN) counter with six stage screen type screen diffusion battery. Radius range approximately 0.002 μ m to 0.1 μ m.
2. PMS ASASP-X active cavity laser single particle size spectrometer, fed from aircraft isokinetic sampling line. Radius range nominally 0.05 μ m to 1.5 μ m.
3. Climet 208 white light single particle size spectrometer, modified and mounted in external pod. Two selectable inlet nozzles, one isokinetic the

other sub-kinetic. Two radius ranges $0.2\mu\text{m}$ to $1\mu\text{m}$ and $0.5\mu\text{m}$ to $10\mu\text{m}$.

4. External, free-stream impactor. A pneumatically operated five slide impactor used for collecting particles with $r > \text{apx. } 2\mu\text{m}$ on 7mm by 25mm , silicone grease coated slides (mounted on 7 mm diameter support rods).

5. A 1mm diameter round jet, single stage inertial impactor used for collecting particles with $r > 0.3\mu\text{m}$ (apx.) at a nominal flow rate of 4 l min^{-1} . Particles were collected on standard, nitro-cellulose coated, 3mm diameter electron microscope grids further strengthened with a thin film of carbon.

Operation of aerosol sizing instrumentation

Aerosol particle concentrations were determined in-situ as a function of particle size using a PMS ASASP-X size spectrometer fed from the aircraft isokinetic sampling line. This spectrometer covers a nominal radius range of $0.05\mu\text{m}$ to $1.5\mu\text{m}$ in four overlapping groups of fifteen size channels, however the sampling rate is quite low, typically $1.5\text{ cm}^3\text{s}^{-1}$. It is usually necessary to integrate for considerable periods to obtain meaningful concentrations for particles with radii greater than a few tenth micrometre. Normally, level flight legs were about thirty minutes duration giving around 2.7 litre samples with the ASASP per altitude section per flight. Calibrations with PSL particles were carried out before, during and after the flight series and corrections made for expected refractive index based on the work of Garvey and Pinnick¹. Throughout the flight series the ASASP performed well. One problem that appears to be common to this family of instruments is a tendency to count excess particles in the most sensitive channel when operating at altitudes above about 5km and using the recommended ratio of sample to purge air. This happened occasionally in the early flights but in general was avoided by operating at a flow ratio of around 1 to 15 compared with the recommended 1 to 20. There are some indications of a possible inertial loss problem somewhere in the sampling-counting process. As it will be shown later concentrations of particles measured with the ASASP for radii greater than around $1\mu\text{m}$ appear to fall too rapidly (with increasing radius). This effect is only evident in the boundary layer where the concentration of particles with $r > 1\mu\text{m}$ is large enough to measure (with the ASASP) and there is another measurement of concentration independent of the isokinetic sampling line.

For this flight series the main instrument for sizing and counting particles with radii greater than about $0.2\mu\text{m}$ was to have been a (modified) Climet 208 externally (pod) mounted and using either an isokinetic or subkinetic (concentrating) inlet nozzle. This instrument operates at a nominal flow rate of 7 l m^{-1} and can be used to greater than $10\mu\text{m}$ radius. Examination of the PHA subsequent to the flight series however revealed an incorrect internal setting that rendered data for radii larger than about $1\mu\text{m}$ totally irretrievable and greater than about $0.5\mu\text{m}$ likely to be low in concentration. Consequently data from the Climet has been excluded entirely from size distribution determinations although it is used to show comparative altitude variation and day to day changes in concentrations.

For smaller particles (typically $r < 0.1\mu\text{m}$) penetrations through a screen diffusion battery² were determined with a modified GE type condensation nucleus counter³. These penetrations were inverted using Twomey's non-linear iterative scheme⁴ to derive size distributions in the radius range $0.002\mu\text{m}$ to $0.1\mu\text{m}$. These diffusion battery determinations were initiated manually during the flight at fairly regular intervals and for the remaining time the condensation nucleus counter was used to monitor the CN concentration.

Larger particles were collected with a free-stream (externally mounted) remotely operated impaction system on 7mm-wide silicone grease coated slides (principally in the boundary layer) and on 3mm diameter electron microscope grids using a 1mm diameter jet impactor fed from the aircraft isokinetic sampling line at a flow rate of $4\text{ to }5\text{ l min}^{-1}$. These collection systems were included principally to obtain compositional data but were used for size information also because of the failure of the Climet spectrometer PHA. Collected particles were sized by first photographing slide cross-sections (or grids) in either secondary emission or transmission scanning electron microscopy, measuring the particle images and converting the dry impacted volume to an equivalent preimpaction spherical size. Where appropriate, further correction was made to account for ambient humidity using the relations given by Hanel⁵. For sizing sulfate particles in the free troposphere the model of Gras and Ayers⁶ was used. Salt particles were modelled as "blocks"; for samples

measured using transmission microscopy the height was determined by measuring the length of individual particle shadows obtained from a non-reactive coating evaporated at a known angle onto the sample before microscopy. The mean ratio of height to width obtained in this way was also used for samples measured using secondary emission microscopy. Particles that could not be identified morphologically were treated as spheres with a diameter equal to the mean of the measured dimensions. Collection efficiency for the jet impactor has previously been determined experimentally⁷ and for the slide impactor an empirical determination by Wong et al.⁸ was used. In both cases only particles for which the collection efficiency was greater than 50% were included in the analyses (after correcting the concentration for collection efficiency).

Locations and flight plans

This study was planned around two main sites, each with a ground based lidar system and included a series of supporting "excursion" and "transit" flights. The two sites were Sale (38°06'S, 147°04'E) in eastern Victoria where the CSIRO ruby lidar was located, and Cowley Beach (17°41'S, 146°07'E) in north Queensland where the Curtin University doubled YAG lidar was located, both lidars being temporarily sited for the experiment. In both of these locations aircraft flights were planned as a series of straight and level legs, each of approximately thirty minutes duration centred on the lidar site. Locations of the main sites, local, transit and excursion flights are all given in Fig.1. Altitudes were stepped between the boundary layer and the aircraft ceiling (usually between four and six levels). Flights normally included a spiral descent sounding. Excursion flights south from Sale to the Cape Grim area (40° 41' S, 144° 41'E) and north from Cairns to Rabaul (4°12'S, 152°12'E) in New Guinea were included to extend the geographic range of the study. Excursion flights and transit flights were made at a series of altitudes in the free troposphere to obtain a range of representative data.

Weather conditions

During the experiment period weather conditions were fairly typical for late autumn early winter. In south-eastern Australia the dominant feature was the slow progression of an anti-cyclonic system and rapid progression

of a series of cold fronts across Victoria. Deep south-westerly streams associated with these fronts usually produce clean or "baseline" conditions for both gases and condensation nuclei. The frequency of the "baseline" conditions varies from year to year but at Cape Grim in north-western Tasmania (see Fig. 1) is typically 30 to 40% (depending on definition). Weather conditions for the northern section were also typical for the season with low level south easterly trades giving way to the upper level westerly zonal flow above the inversion.

OBSERVATIONS

Because aerosol particle concentration (and composition) is a function of size, altitude, location and time there is no one simple method to fully depict the state of the aerosol. The two procedures followed here will be to give representative profiles of the number concentration of particles larger than a given size, as a function of altitude for particular locations and times and to give averaged size distributions covering certain times, geographic locations and altitude ranges.

Concentration profiles were usually determined during a spiral descent but also occasionally during a normal ascent. Figures 2 to 5 show a series of representative profiles combining output from the GE CN counter and cumulative concentrations from the ASASP and Climet size spectrometers. Only two lower radius bounds from the ASASP (channels 2+ and 21+ giving the concentration of particles with radii greater than apx. 0.06 μm and 0.13 μm) and two from the Climet (channels 2+ and 6+ giving the concentration of particles with radii greater than apx. 0.2 μm and 0.5 μm) were used. In the configuration used the GE counter gives the concentration of particles with radii greater than about 0.002 μm .

The first of these profiles, Fig.2, a descent into Sale on May 29 1986 illustrates an important feature observed during the period in Sale. Following the passage of a cold front a deep south-westerly air stream bringing air from over the southern ocean crossed Victoria, see Fig.6. Particle concentrations in this airstream were exceedingly low. In Fig.2 two altitude regions, 0.7km-1.7km and about 3km-5km show total particle concentrations below 100 cm^{-3} and large particle concentrations are also severely reduced in the upper altitude band. With the normal descent rate of 300 m min^{-1} several of the ASASP records (one minute sample rate)

contain no counts for radii greater than $.13\mu\text{m}$, the Climet also shows marked depression of concentrations of particles with radii greater than $0.2\mu\text{m}$. Below the inversion (at 1.8 km) large particle concentrations are relatively constant with altitude but there is a strong decrease above the inversion. Cloud was thin strato-cumulus (apx. 300m thick) with tops to around 1.7km. The following day the eastwards progression of the anticyclonic system centred in the Great Australian Bight brought upper level air that had passed over central Australia to south-eastern Victoria and northern Tasmania, see Fig.7. Particle profiles illustrated in Fig.3 a descent off Cape Grim on May 30 show that there is still extensive scavenging of small particles evident below the inversion with total particle concentrations approaching a few per cubic centimetre and essentially no particles with radii less than $0.06\mu\text{m}$ but above the inversion there is now a marked increase in the concentration of large particles with the concentration of particles with $r > 0.13\mu\text{m}$ at 3.5km greater than observed anywhere else in the study except one descent in New Guinea. Comparison of Figures 3 and 2 shows in fact that in the region 3.5km-4km there is a change in concentration of approximately two orders of magnitude in the number of particles with radii greater than $0.2\mu\text{m}$ (and greater than $0.13\mu\text{m}$) over the period of one day in the same geographic region.

Profiles for the descent into Rabaul on May 4 are shown in Fig.4. Although there was considerable cloud in the area (cumulus with tops $> 6\text{km}$ and altostratus at 4.5km) the major part of the descent was cloud-free with one cloud layer at 3.3km and some rain at about 1km. As this descent was early afternoon, mixing was reasonably well developed. By comparison a subsequent morning ascent (see Fig.12) showed concentrations at 2km about two orders of magnitude lower than during this descent. The CN profile for this descent is interestingly flat with altitude outside the immediate boundary layer where there was a considerable amount of local smoke.

June 10 was selected to represent soundings taken at Cowley Beach in north Queensland and indeed is quite representative of the whole period. The 500 hPa stream analysis given in Fig. 8 shows that the immediate origin for air arriving at Cowley Beach on June 10 was over central Australia. Following the air stream back several days shows the origin to be to the north west of Australia. Large particles show a levelling out of concentration above about 2.3km the altitude of the inversion. During the

northern New Guinea show up as a large particle enhancement at about 4.5 km altitude in the New Guinea profiles.

Particle composition

Particles collected by impaction were individually sized and (where possible) morphologically identified. For the marine boundary layer samples the majority of particles examined could be clearly identified as having a marine (sea-salt) origin although occasional acidic particles and carbon clusters were observed. Fig. 20 shows a typical field of particles collected near Cowley Beach at about 1.7km and photographed using transmission electron-microscopy. The prevalence of cubic salt particles with their characteristic annular ring is clear. Another transmission photograph from the Cowley Beach area showing a rarer carbon cluster particle collected at about 900m in a maritime air stream is shown in Fig.21. Approximately 12% of particles in the (marine) boundary layer were irregular and could not be identified morphologically. Free-troposphere particles exhibited a completely different character as shown in Fig.22. The majority (76%) had the typical sulfuric acid or partially ammoniated sulfate morphology of a central cap-shaped particle or sulfate bar surrounded by rings of droplets. Again a fraction of the particles, but in this case 24%, could not be identified in this way. For the purposes of calibration of the ASASP all particles in the free-troposphere were assumed to be ammonium bi-sulfate and for the boundary layer, particles with radii less than $0.3\mu\text{m}$ were assumed to be ammonium bi-sulfate and larger particles hydrated sea-salt.

Particle size distributions

Because of the failure of the Climet PHA fewer size distributions than originally planned could actually be determined. Large particle concentrations were derived by manual sizing of impaction samples which is a tedious process and which to a large degree was limited by the available resources that could be applied to the analysis. Consequently not all of the collected samples have been analysed (sized). It is fairly clear from the observations however that particularly in the free troposphere the majority of variations in the aerosol involve changes in the overall concentration (as shown earlier, up to two orders of magnitude at least) with relatively minor changes in the relative concentrations of different

size particles, that is in the size distribution. The approach followed here has been to derive a number of "model" size distributions by combining data obtained in broad latitude ranges and a few fairly wide altitude ranges. The basic regions selected were 4°S-15°S, 15°S-25°S and 35°S-45°S and the altitude ranges 0-.76km, .76km-2.3km and 3.5km-6.7km. These altitude ranges principally separate free-troposphere and boundary layer particles with one transition range. For 2.3km-3.5km the 3.5km-6.7km model has been used. Some further rationalisation has been made by combining all the impaction data into sets (the majority obtained in the Cowley Beach area) differentiated only with respect to altitude and using the simultaneously observed concentrations of particles with radii greater than 0.2µm on the ASASP to merge this data with the other size data. This form of merging was required because the diffusion battery and impaction samples were not always concurrent whereas ASASP concentrations were obtained simultaneously with all other determinations.

The averaged data used to derive the Cairns region free-troposphere size model are shown in Fig. 23 identified for their method of measurement. Similar averaged data for the 0.76km-2.3km altitude range and the 0-.76km range are given in Figs. 24 and 25. Particles with radii less than 0.005µm were deleted from the set for fitting an analytic distribution function. Distribution functions comprising two log-normals were fitted to the data, expressed as $\log(dV/d\log R)$ by (non-linear) least squares methods. For the Cairns data the free troposphere and boundary layer distribution large particle mode radii were constrained to 0.3µm in order to obtain distributions that were reasonably physically realistic. This wasn't necessary for the 0.76-2.3km distribution. The separate and combined distribution functions are indicated with the measured data in Figs. 23 to 25. For the 0-0.76km data an alternate size distribution function for particles with radii larger than 0.22µm was derived by combining two power law segments fitted between the radii of 0.22µm to 0.5µm and 0.5µm-20µm using least squares methods. For the power law distributions shown, the data from the ASASP for radii greater than 1µm was excluded because of the possibility of an inertial loss mechanism that the rapid roll-off of this data suggests. In fact the removal of this data has very little effect on the fitted power law distribution. Model distribution parameters are summarised in Table 1.

Mean distributions for Sale for 0.76km-2.3km and 3.5km-6.7km obtained in the same manner as the Cairns data and similarly fitted size distributions

are given in Figs. 26 and 27. In both cases the large particle mode radius was constrained to $0.3\mu\text{m}$.

Uncertainty in aerosol size distributions

Aerosol particle size distributions measured from an aircraft platform are potentially susceptible to a large number of possible error sources. Some of these may be systematic, such as error in sizing particles in a light scattering spectrometer because of unknown refractive index or uncertainty in the calibration relation, or loss of particles in a sampling duct.

There is the statistical problem of collecting or counting enough particles to reduce the variability to an acceptable level, a typical problem at large radii, and the related problem of how representative are area, altitude or time averages used to bring up the number of particles which are present only in very small quantities. If an analytic function is fitted to the data there is the question of how well this function represents the data. Clearly the relative contributions of these various error sources can vary from instrument to instrument and even as a function of size for any one instrument.

Every effort has been taken to minimise the potential for errors in this work. Size spectrometers were calibrated with known size particles before, during and after the flights and the best known calibration factors have been used to convert to ambient particle sizes. As an estimate, particle sizes should be accurate to about 5%. Because the ASASP was sampling from an aircraft "isokinetic" line there should not be any systematic inertial sampling losses however there does appear to be an apparent significant loss of particles with $r > 1\mu\text{m}$ in the boundary layer with this instrument. Inertial losses certainly should not be a problem for particles with radii less than about $0.5\mu\text{m}$. An alternative explanation (for the apparent rapid roll-off in concentration for $r > 1\mu\text{m}$) may lie in the calibration relation for this instrument particularly at these large sizes where the theoretical and experimental agreement is not as good as at smaller sizes. For particles with radii less than about $0.5\mu\text{m}$ count statistics are not a limitation in the mean distributions although there may be some questions regarding the use of altitude averages, particularly at altitudes near the inversion where size distributions do in fact change quite rapidly. Flow rate was measured using a mass flow sensor and should have less than 5% uncertainty.

Estimation of the accuracy of distributions obtained from inverted diffusion battery penetrations where there is real noise present is a particularly difficult problem. The GE counter was calibrated against a "standard" Pollak counter and concentrations obtained with it should be accurate to about 10%. Previous simulations of inversions with typical noise⁹ showed that uncertainty in locating the distribution peak was about 5%-10% and in determining the magnitude of the peak about 20% in individual size distributions. Averaging many distributions as has been done here will reduce the statistical uncertainty but since not all distributions represent the same air parcel there is still a question of what the mean distribution actually represents.

Calculating size distributions from impaction samples is particularly troublesome with respect to uncertainty. It is very difficult to accurately gauge the accuracy of any particular model used for converting dry particle sizes to ambient humid pre-impaction conditions in an arbitrary situation. The model used for sulfate particles has been tested previously in the stratosphere¹⁰ and is believed to be better than to within 20%, possibly 10% for determination of pre-impaction radius. The model used for converting salt particles likewise is probably accurate to around 10 or 20% in deriving pre-impaction radius. Jet impaction samples were taken from the aircraft isokinetic line so there is some potential there for added inertial losses. In the free troposphere a major limitation is the small number of particles with radii larger than about 0.5 μ m, for the impaction sample means there were no particles larger than 1 μ m radius, statistical uncertainty is small for most of the impactor concentrations, shown for example in Fig 23, but increases fairly rapidly for the largest particle sizes. The third largest size has a standard deviation of 11% in concentration, the second largest 15% and the largest point at apx. 0.8 μ m radius 33%.

The overall good agreement between the concentrations obtained using quite different sizing methods as shown for example in Figs. 23 and 24 gives some confidence to the accuracy of the procedures and calibrations used. It is clear that for this type of work a diversity of measuring methods and instruments is almost mandatory.

Backscatter calculations

Computation of backscatter from particle size distributions serves two main purposes. First by determining the differential backscatter as a function of particle radius the "active scattering" size range of the particle population for the wavelength of interest is readily determined. Second, the calculated backscatter integrated over all particle sizes provides a means of comparing experimentally determined aerosol concentration values and experimentally determined backscatter values. Backscatter was determined from the aerosol particle model size distributions using a Mie solution program written by S. Banks and which utilises algorithms given by Wiscombe¹¹. For particles in the large particle mode refractive indices used were based on the morphologically identified major component. For the accumulation mode a composition of ammonium bi-sulfate was assumed in all cases. Three wavelengths have been considered, 0.532 μm , .693 μm and 10.6 μm . No values for the refractive index of ammonium bi-sulfate could be located for a wavelength of 10.6 μm and so a value of 1.98-0.06i, a value reported for ammonium sulfate¹² has been used.

Backscatter distributions for the Cairns free troposphere distribution (Fig. 23) are given in Fig. 28 for the wavelengths of 0.532 μm , 0.693 μm and 10.6 μm for a composition of ammonium bi-sulfate. (Particle morphology indicated only partially neutralised sulfate as the dominant large particle type). Backscatter at 10.6 μm is clearly dominated by particles in the 0.5 μm to 2 μm radius range whereas for the shorter wavelengths a little over 60% of the calculated backscatter is due to the accumulation mode particles (with radii less than about 0.15 μm). The remaining fraction is due to particles with radii up to about 1 μm .

The situation is somewhat different in the boundary layer (see Fig. 29) where at both short (0.532 μm) and long (10.6 μm) wavelengths the backscatter is controlled principally by particles in the 0.5 μm to about 3 μm radius range, although at 0.532 μm there is still about a 25% contribution from accumulation mode particles. For the boundary layer calculations a refractive index for water was used for the large particles, a reasonable approximation in line with the observed dry composition of sea-salt and the high humidities (>85% RH) which were observed during the measurements.

Mean profiles of calculated backscatter coefficient as a function of altitude are given in Fig. 30 and Fig. 31. These were derived by scaling the concentration of particles with radius greater than $0.25\mu\text{m}$ (ASASP channel 35+) from the mean concentration profiles (Figs. 17-19) with the backscatter per particle calculated from the model aerosol size distributions. In both cases the free troposphere size distribution model was used down to 2.3km. For the mean profiles of $10.6\mu\text{m}$ backscatter coefficient, Fig. 30 only the Cairns region profile below 2.3km is given but the effect of using two different refractive indices is shown. Profile (a) was derived with a refractive index for water $m=1.18-0.67i$ in the large particle mode and profile (b) for a "maritime" aerosol using $m=1.38-0.057i$ ¹³. The enhanced scattering coefficient at about 4.5km in the New Guinea profile results from the enhanced particle concentration due to widespread cloud that was discussed earlier. Backscatter profiles calculated for $0.532\mu\text{m}$ at Cairns and $0.693\mu\text{m}$ at Sale are given in Fig.31. For these shorter wavelengths the amount of scatter per particle larger than $0.25\mu\text{m}$ radius was nearly independent of altitude (for the three model altitude ranges) so discontinuities at the boundaries of the altitude regions are small. For the 0-0.76km altitude range at Sale ($0.693\mu\text{m}$) the scatter per particle determined for Cairns (at $0.693\mu\text{m}$) was used with the power law distribution and a refractive index for water. A similar model was used for the $0.532\mu\text{m}$ backscatter at Cairns in that altitude range but a profile segment for backscatter calculated using the log-normal distribution, again with water is also given. Calculated mean values of backscatter coefficient for the different wavelengths and locations determined from the aerosol distribution models are summarised in Table 2.

Conclusions

Model size distributions were derived from free-tropospheric particle measurements in the radius range $0.005\mu\text{m}$ and $1\mu\text{m}$, and for marine boundary layer from particles in the radius range $0.005\mu\text{m}$ to apx. $20\mu\text{m}$. In the free troposphere the majority of particles were found to have sulfate morphology typical of sulfuric acid or lightly ammoniated sulfate. Most of the marine boundary layer large particles were found to have sea-salt morphology. The concentration of large particles (radii greater than about $0.2\mu\text{m}$) was found to decrease to about the height of the inversion and thereafter to the maximum altitude studied remain relatively constant.

In the more southern latitudes (around 38°S) particle concentrations were exceedingly low (about one tenth of the average) in the deep south-westerly air stream from over the Southern Ocean following the passage of a cold front. Concentrations in this region also demonstrated a very large range in concentrations, around two orders of magnitude. Variability at about 17°S was considerably less and was typically within a factor of ten. Large variability principally between one morning sounding and several daytime soundings was also seen near the equator below 3km altitude. Calculations of backscatter using Mie theory have shown that 10.6µm backscatter in the free-troposphere for the regions studied is controlled mainly by particles in 0.5µm to 2µm radius range. At shorter wavelengths (0.532µm and 0.693µm) particles in the main accumulation mode with radii less than about 0.15µm produced most of the backscatter with a minor contribution up to about 1µm radius. Mean values of 10.6µm backscatter calculated for the free troposphere from the aerosol size distributions were $1 \times 10^{-11} \text{ m}^{-1} \text{ sr}^{-1}$ for the Sale area, $1.5 \times 10^{-11} \text{ m}^{-1} \text{ sr}^{-1}$ for the Cairns area and $1.7 \times 10^{-11} \text{ m}^{-1} \text{ sr}^{-1}$ for New Guinea.

References

1. D.M.Garvey and R.G.Pinnick *Aerosol Sci. and Technol.*, 2,477 (1983).
2. D.Sinclair and G.S.Hoopes, *Am.Ind.Hyg.Assoc.J.*, 36,39 (1975).
3. C.G.Michael, *J.Atmos. and Ocean Tech.*, 3,230 (1986).
4. S.Twomey, *J.Comp.Phys.*, 18,188 (1975).
5. G.Hanel, *Adv. in Geophys.*, 19,73 (1976).
6. J.L.Gras and G.P.Ayers, *J. Appl. Meteor.*, 18,64 (1979).
7. J.L.Gras and J.E.Laby, *J. Geophys. Res.*, 86,9767 (1981).
8. J.B.Wong, W.E.Ranz and H.F.Johnstone, *J. Appl. Phys.*, 26,244 (1955).
9. J.L.Gras, *Atmos. Environ.*, 17,883 (1983).
10. J.L.Gras and C.G.Michael, *J.Appl. Meteor.*, 18,855 (1979).
11. W.J.Wiscombe, *Appl. Opt.*, 19,1505 (1980)
12. O.B.Toone, J.B.Pollak, and B.N.Khare, *J.Geophys. Res.*, 33,5733 (1976).
13. J.A.Selby, E.P.Shettle and R.A.McClatchy, "Atmospheric Transmittance from 0.25 to 28.5µm: Supplement LOWTRAN 3B", AFGRL-TR-79-0214, Environmental Research Papers, 587 (1976).

Table 1a. Summary of fitted distribution parameters for bimodal log-normal distributions consisting of the sum of two equations of the form:

$$dN/d\ln r = A ((2\pi)^{1/2} \ln \sigma)^{-1} \exp\{ - [\ln(r/r_m)]^2 / [2 (\ln\sigma)^2] \}$$

Distribution	A ₁	r _{m1}	σ ₁	A ₂	r _{m2}	σ ₂
Cairns:						
3.5-6 km	122.6	.025	1.84	.040	.3	1.49
.76-2.3 km	653.7	.043	1.61	.649	.38	1.71
0-.76 km	375.3	.056	1.51	1.37	.3	2.40
Sale:						
3.5-6 km	92.1	.027	1.76	.038	.3	1.46
.76-2.3 km	104.0	.054	1.54	.083	.3	1.92

Table 1b. Power law segments for 0-.76km Cairns distribution, r>0.22μm. The equations have the form :

$$dN/d\log_{10}r = 10^{[A \log_{10}(r) - B]}$$

radius	A	B
0.22μm-0.55μm	.8281	.8619
0.55μm-20μm	-2.439	-.1129

Table 2. Backscatter coefficient values calculated from aerosol particle size distributions. New Guinea backscatter determined with Cairns size distribution.

Location	wave-length	aerosol type	mode	$\beta_{\pi} \text{ m}^{-1} \text{ sr}^{-1}$
Cairns 3.5-6km	0.532 μm	(NH ₄)HSO ₄	small	2.90*10 ⁻⁹
		"	large	1.75*10 ⁻⁹
	10.6 μm	(NH ₄) ₂ SO ₄	total	1.51*10 ⁻¹¹
Cairns .76-2.3km	0.532 μm	(NH ₄)HSO ₄	small	4.73*10 ⁻⁸
		maritime	large	3.86*10 ⁻⁸
	10.6 μm	(NH ₄) ₂ SO ₄	small	7.11*10 ⁻¹²
		maritime	large	7.86*10 ⁻¹⁰
		water	large	2.32*10 ⁻⁹
Cairns 0-.76km	0.532 μm	(NH ₄)HSO ₄	small	4.95*10 ⁻⁸
		water	large	1.66*10 ⁻⁷
		water	p.law	2.56*10 ⁻⁷
	10.6 μm	(NH ₄) ₂ SO ₄	small	6.92*10 ⁻¹²
		water	large	1.55*10 ⁻⁸
Sale 3.5-6km	0.693 μm	(NH ₄)HSO ₄	total	2.27*10 ⁻⁹
	10.6 μm	(NH ₄) ₂ SO ₄	total	1.04*10 ⁻¹¹
Sale .76-2.3km	0.693 μm	(NH ₄)HSO ₄	small	9.43*10 ⁻⁹
		maritime	large	3.50*10 ⁻⁹
		water	large	2.38*10 ⁻⁹
PNG 3.5-6km	10.6 μm	(NH ₄) ₂ SO ₄	total	1.71*10 ⁻¹¹

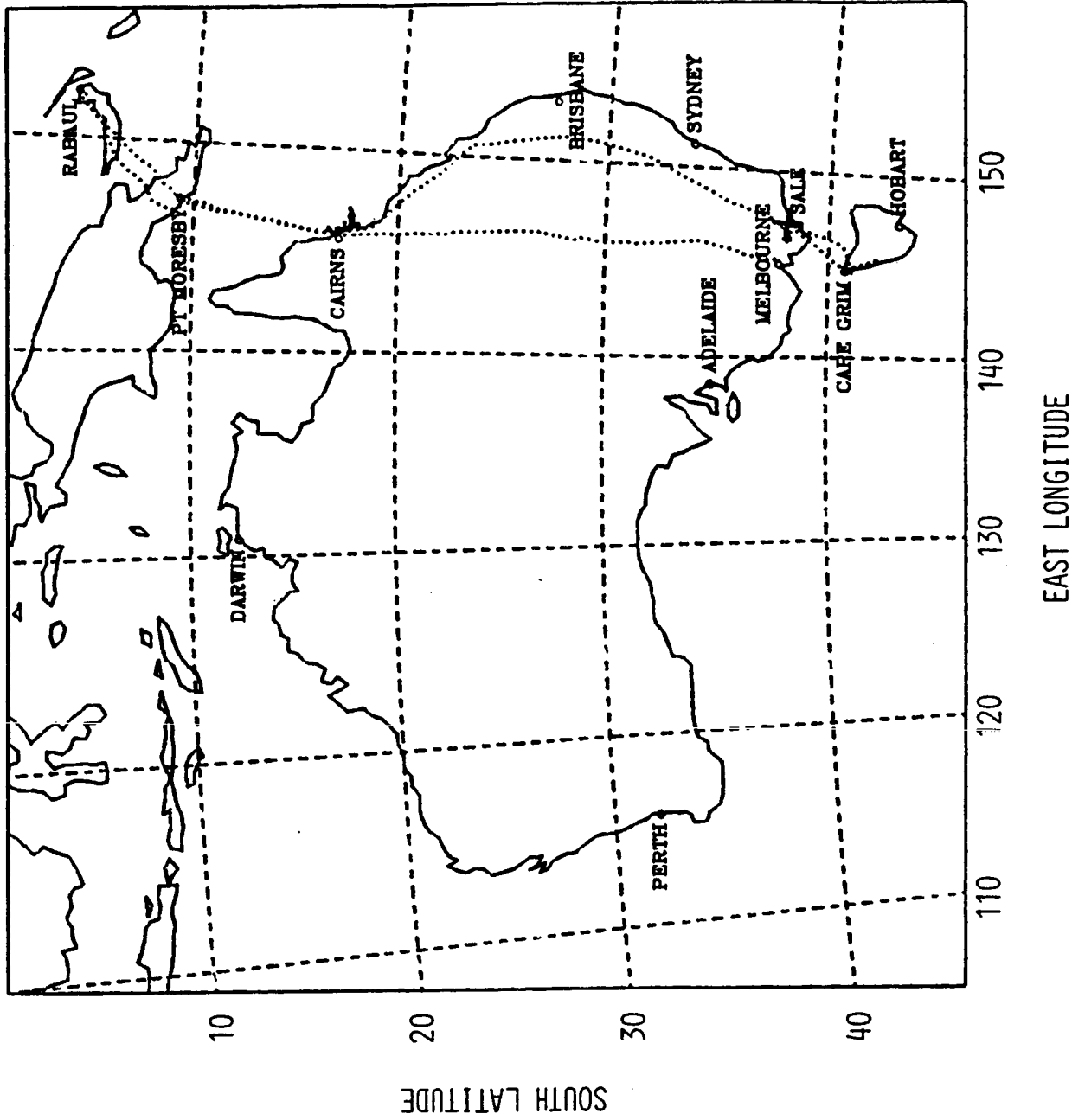


Figure 1. Map of Australia and New Guinea showing principal experiment sites at Sale and Cairns and flight tracks.

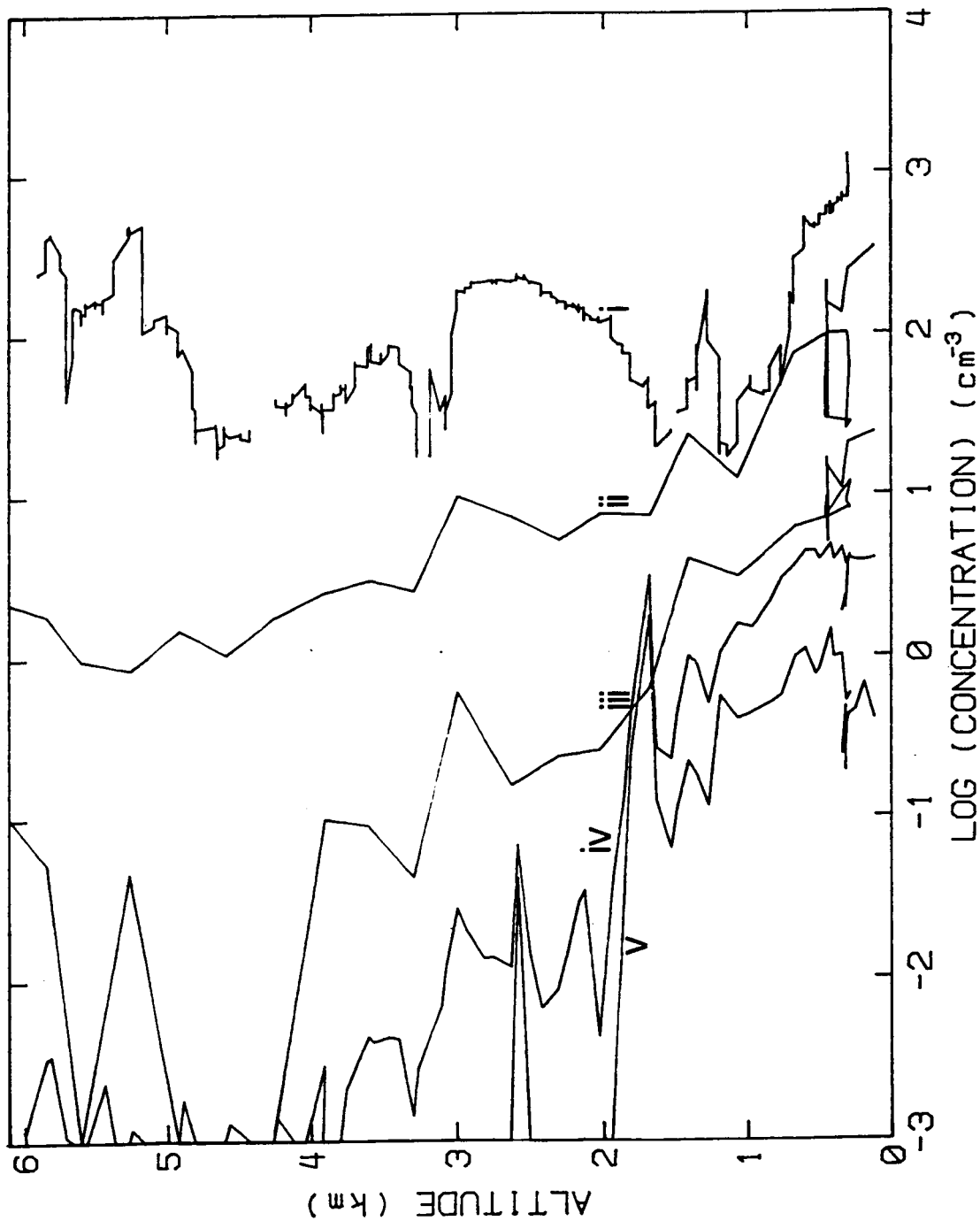


Figure 2. Sale May 29, 1986 (descent). Concentration profiles of CN (GE counter, $r > \text{apx. } 0.002\mu\text{m}$), particles with $r > 0.06\mu\text{m}$ and $0.13\mu\text{m}$ (ASASP) and $0.2\mu\text{m}$ and $0.5\mu\text{m}$ (Climet), profiles (i) to (v) respectively.

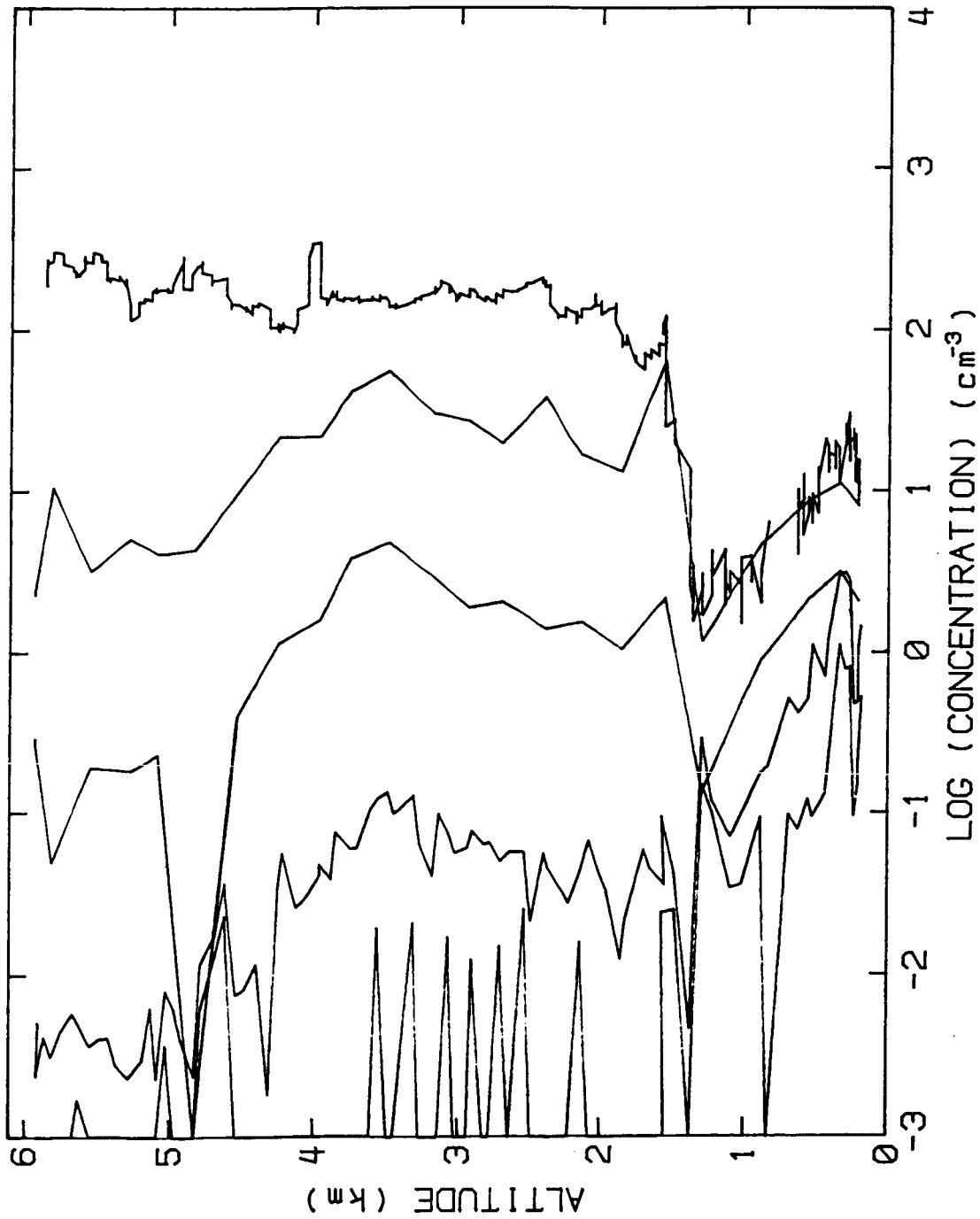


Figure 3. Cape Grim May 30, 1986 (descent), same size limits as Fig.2. These profiles and those in Fig.1 show two orders of magnitude change in concentration in the 3.5-4km altitude region over a 1 day period.

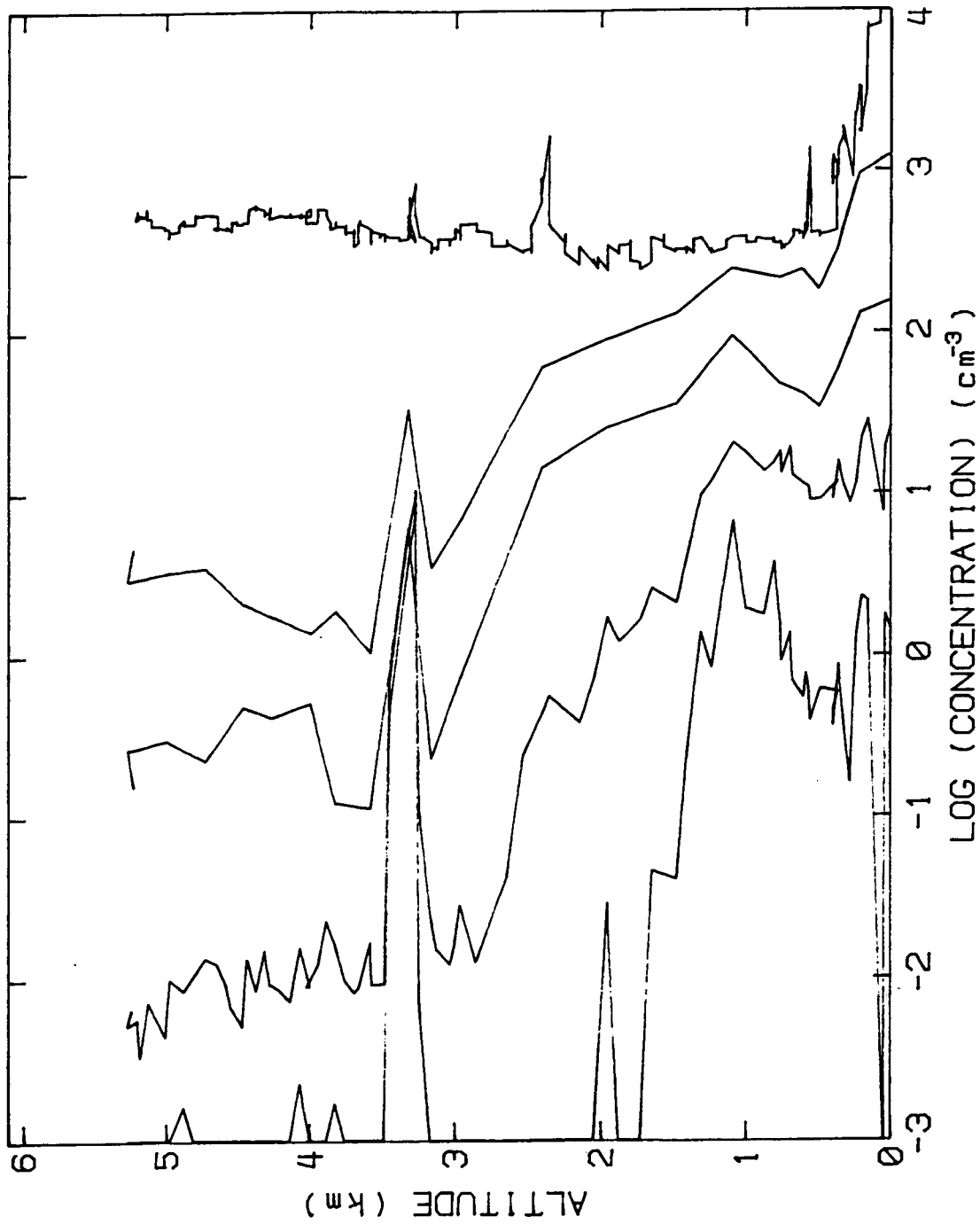


Figure 4. Rabaul June 4 1986, early afternoon (descent), same size limits as Fig.2. The peak at 3.3km is a cloud layer, local smoke was obvious near ground level.

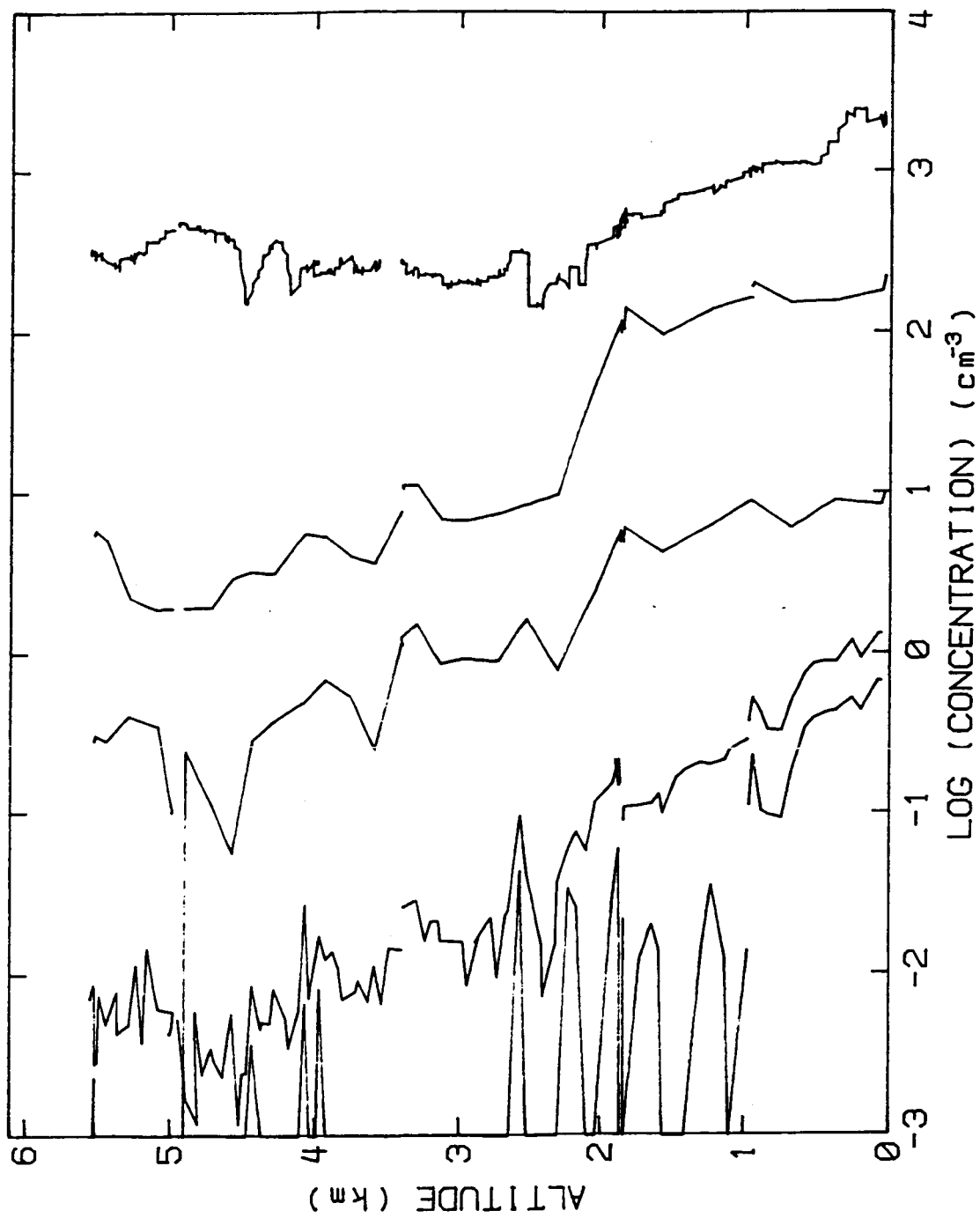


Figure 5. Cowley Beach (near Cairns) June 10 1986 (ascent), same size limits as Fig.2. This is a typical example of the Cairns profiles.

ORIGINAL PAGE IS
OF POOR QUALITY

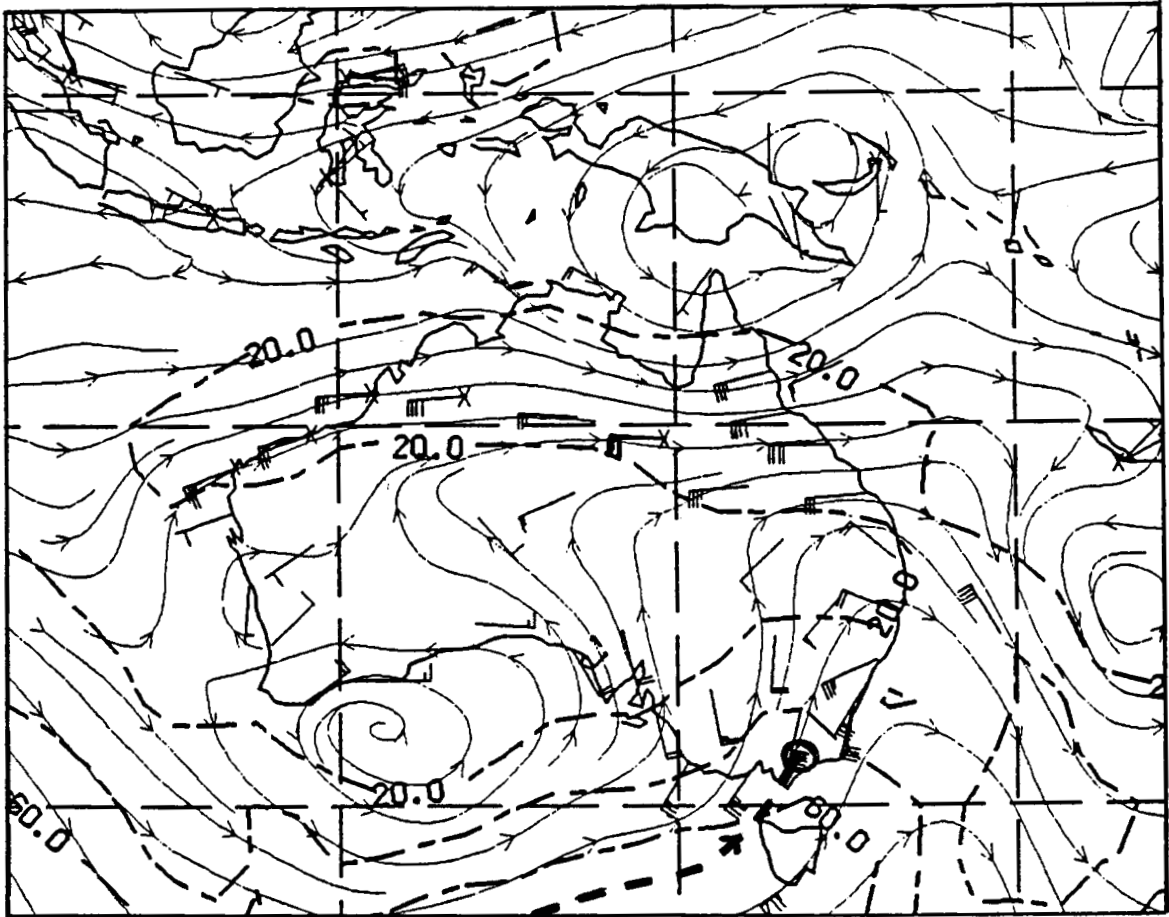


Figure 6. Stream analysis for 2300Z (1100, May 29 1986 local time) at 500 HPa. Sale is circled and the stream from the Southern Ocean passing over Sale is indicated by the dashed line.

ORIGINAL PAGE IS
OF POOR QUALITY

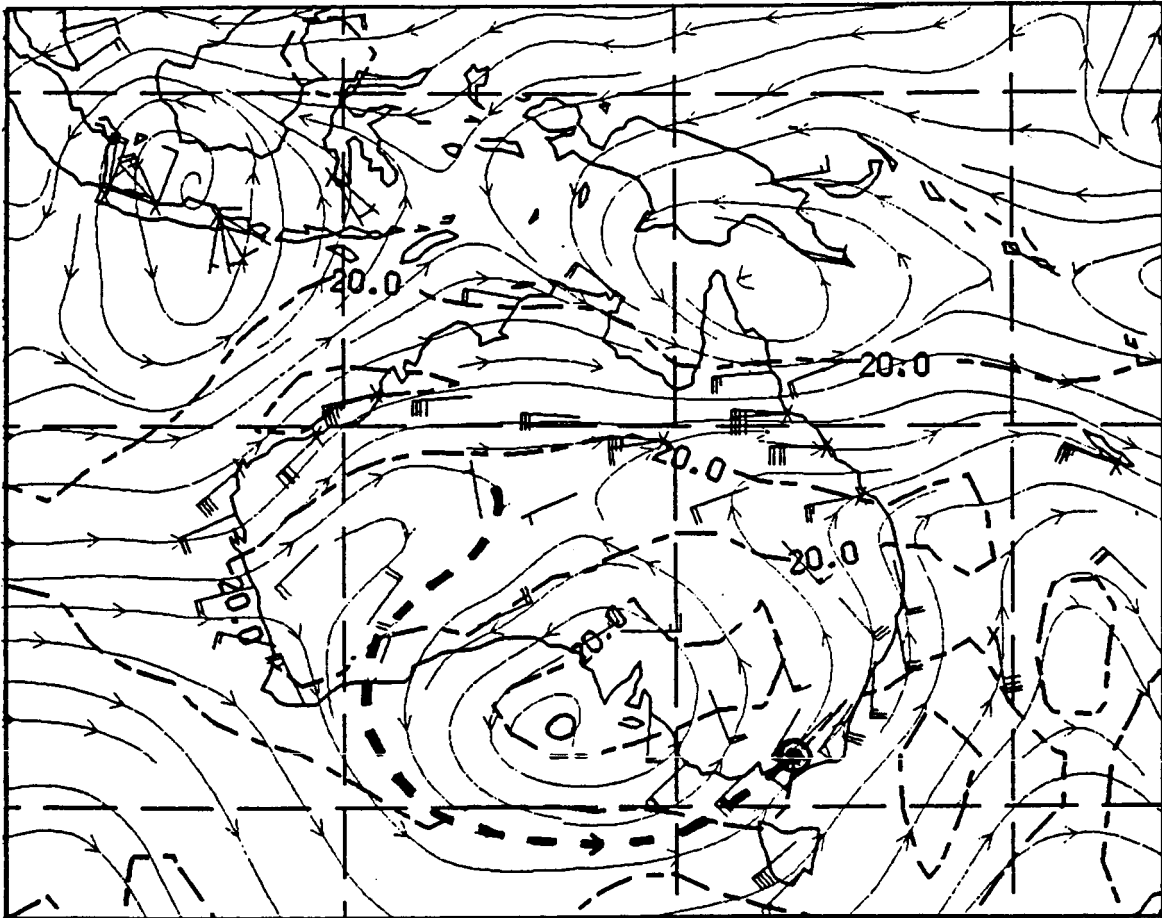


Figure 7. Stream analysis for 2300Z (1100, May 30 1986 local time) at 500 HPa. Sale is circled and the dashed line indicates the stream line for air passing over Sale. This indicates a trajectory recently passing over central Australia.

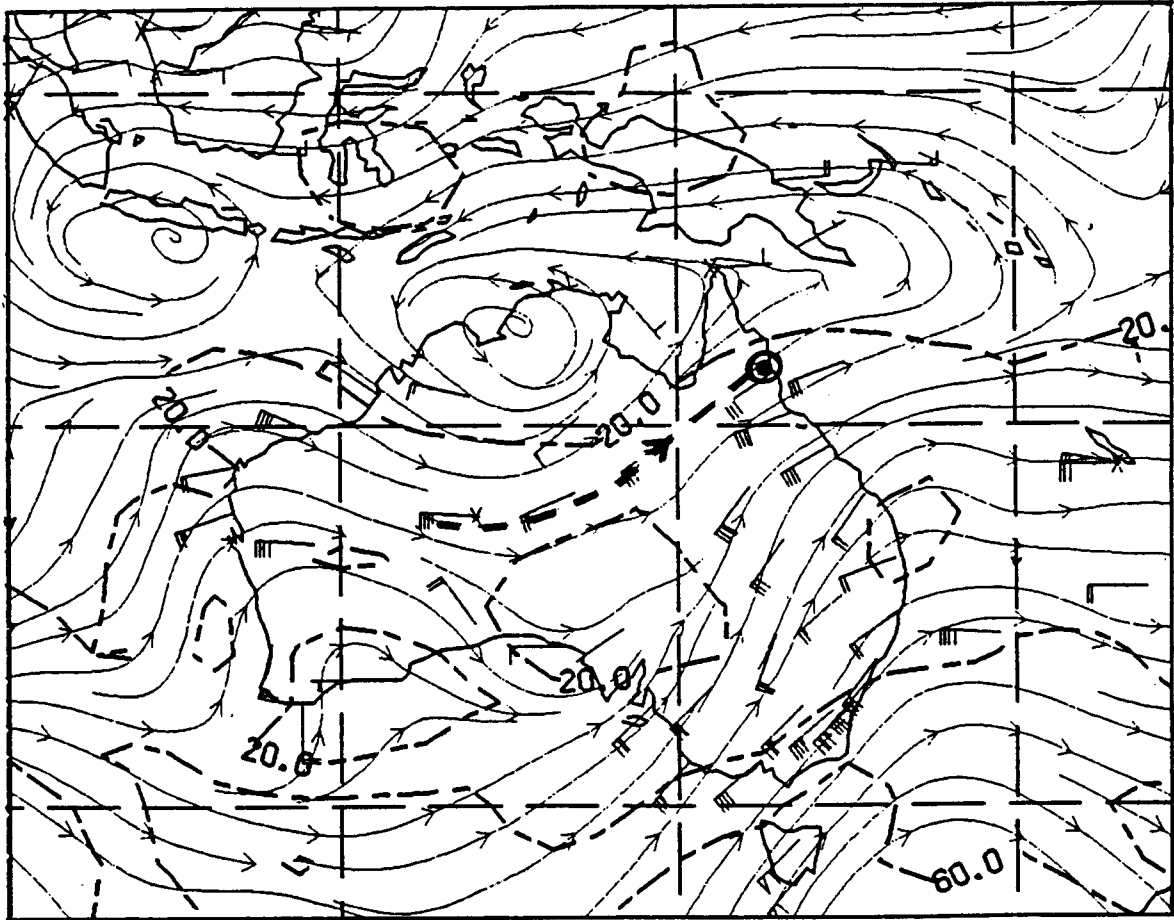


Figure 8. Stream analysis for 2300Z (1100, June 10 1986 local time) at 500 HPa. Cairns is circled and the stream passing over Cairns is indicated by a dashed line.

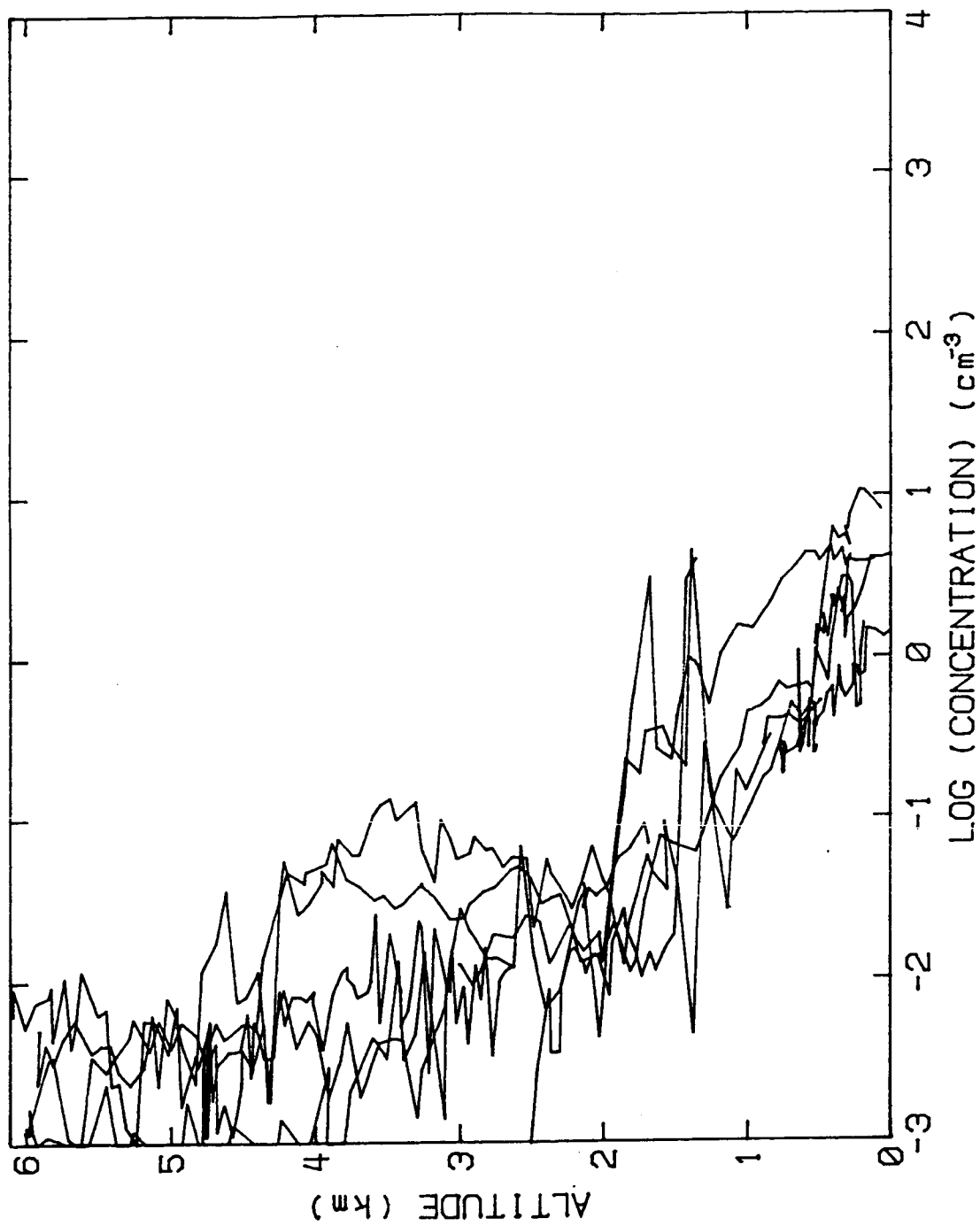


Figure 9. Profiles of the concentration of particles with $r > 0.2 \mu\text{m}$ (Climet channel 2+) in the vicinity of Sale-Cape Grim for May 26-June 1 1986. The enhancement of concentrations at about 3.5km followed the reversion to a continental trajectory after a period of oceanic trajectories.

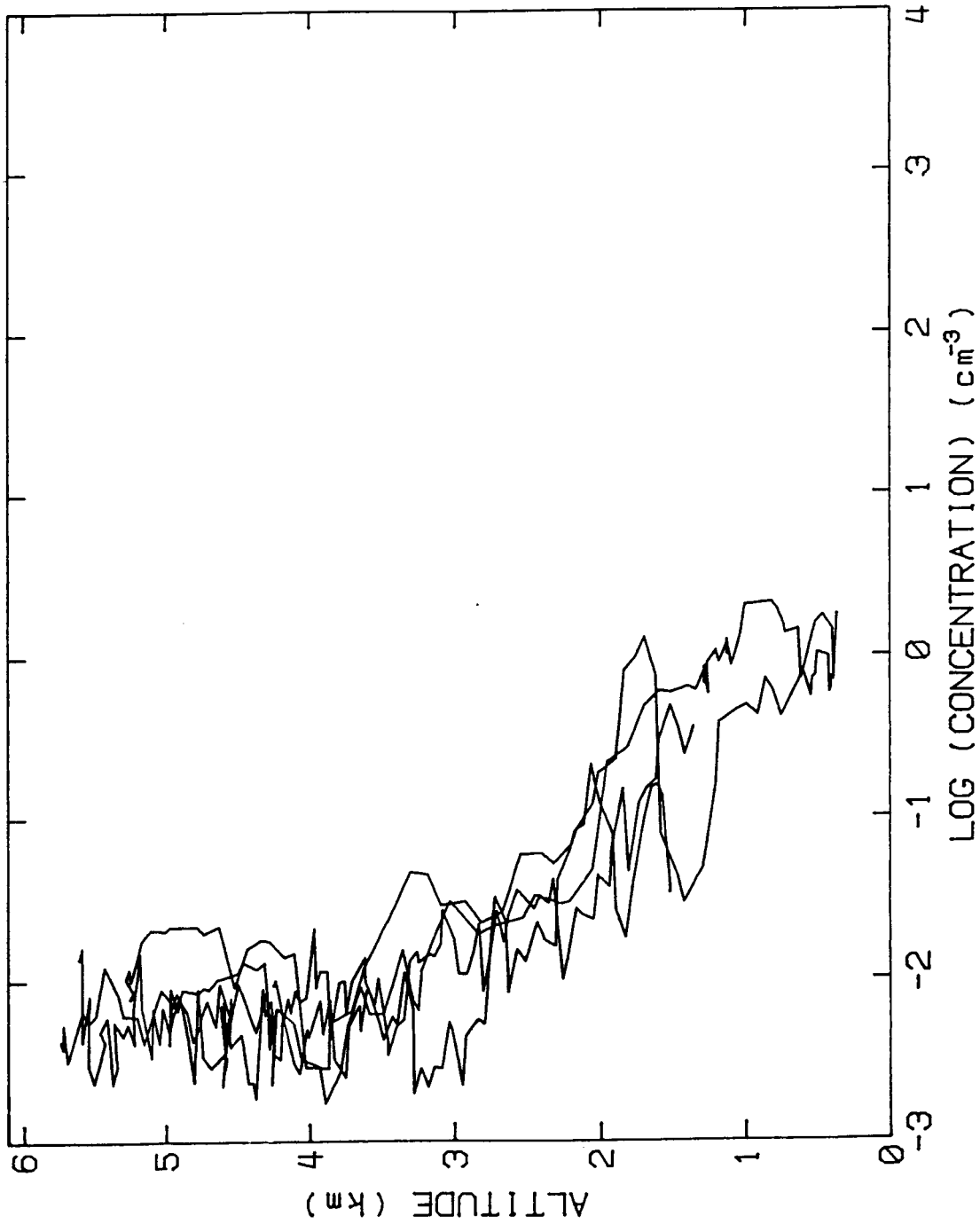


Figure 10. Profiles of the concentration of particles with $r > 0.2 \mu\text{m}$ (Climet channel 2+) for soundings in central New South Wales made during transit flights on June 1 and June 11 1986. These profiles are very similar to those from Cairns.

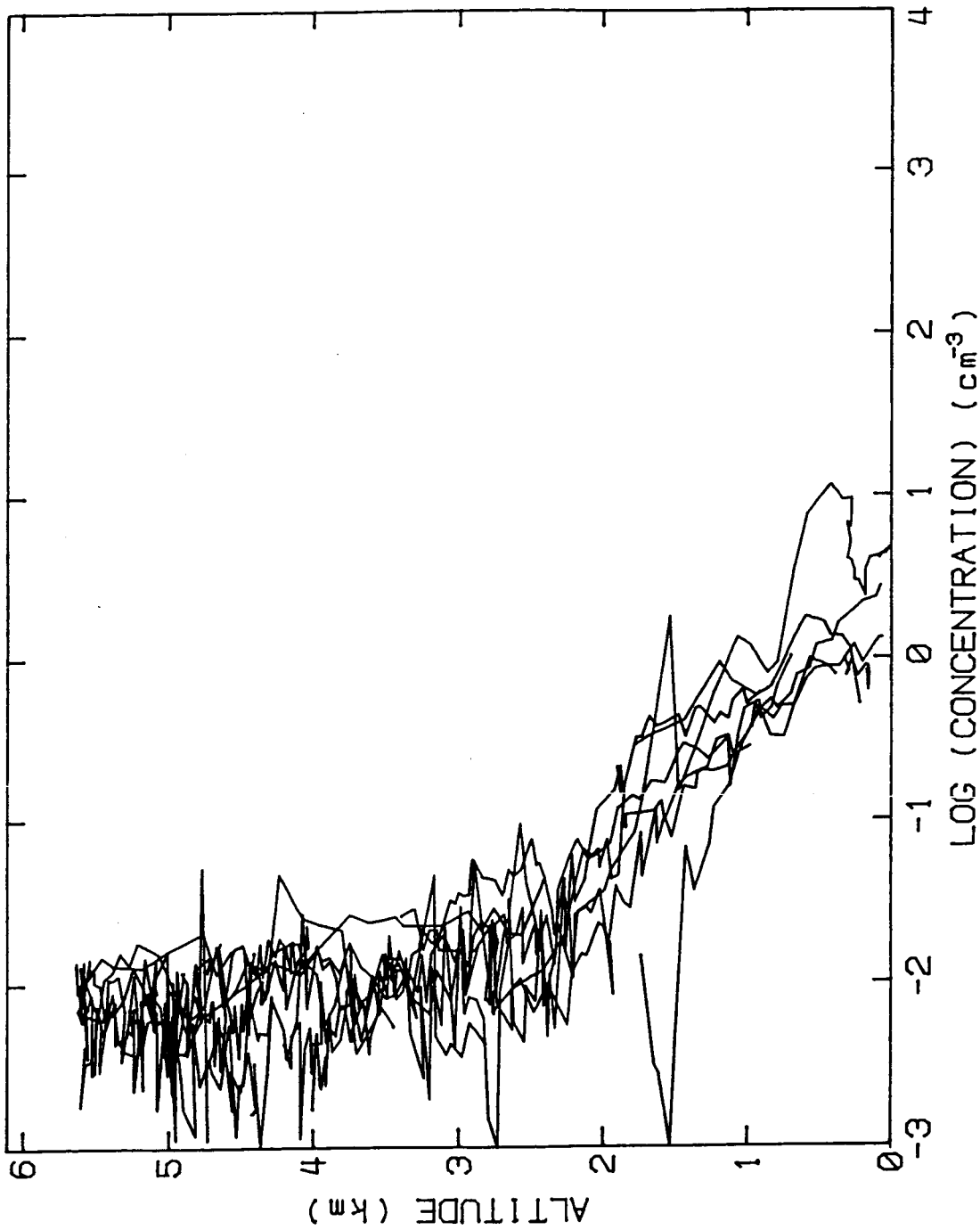


Figure 11. Profiles of the concentration of particles with $r > 0.2 \mu\text{m}$ (Climet channel 2+) for soundings in the Cairns-Cowley Beach area, June 2 to June 11 1986.

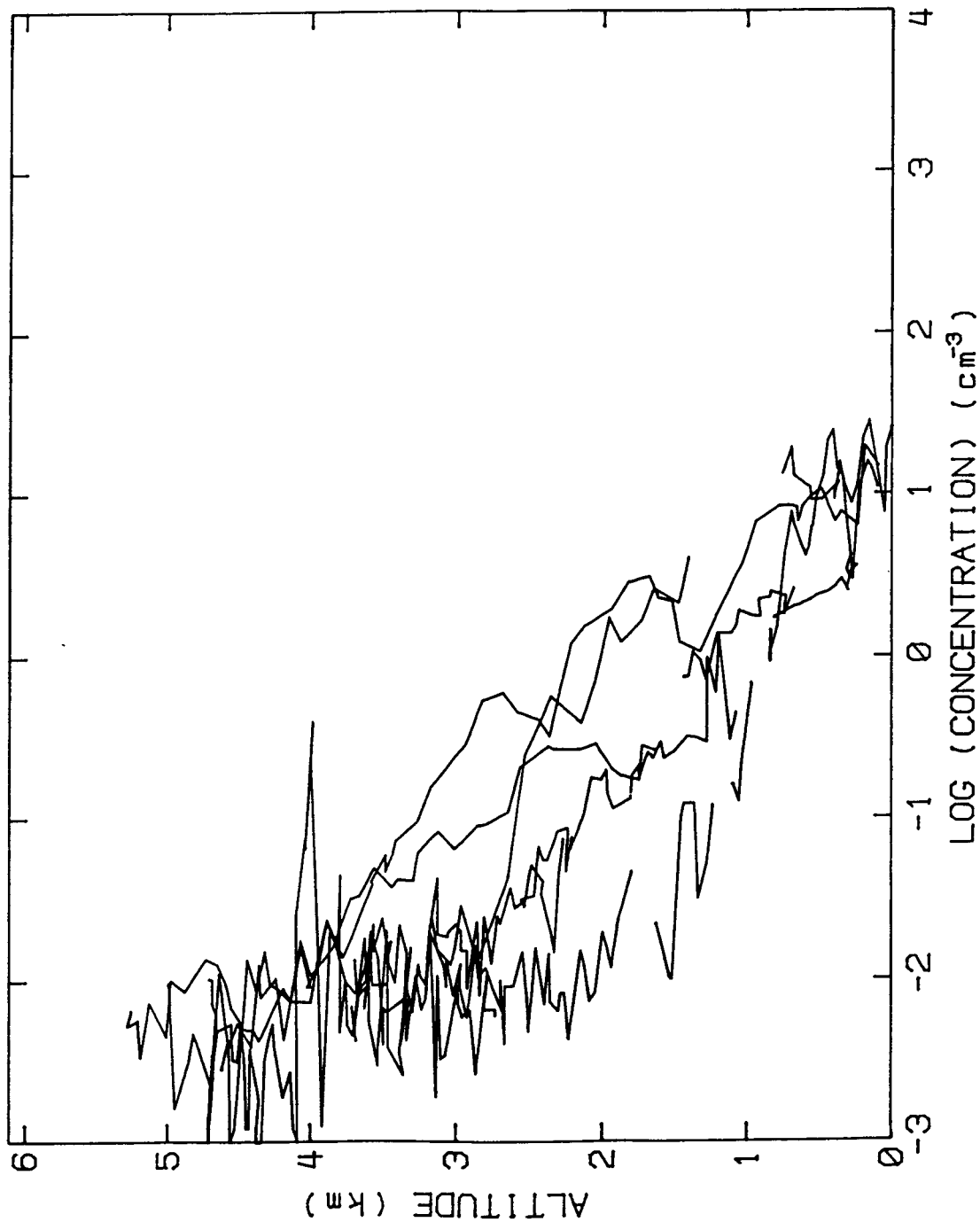


Figure 12. Profiles of the concentration of particles with $r > 0.2 \mu\text{m}$ (Climet channel 2+) for soundings made in New Guinea June 5 and June 7 1986. The profile with the minimum concentrations below 3km was obtained near Rabaul at around 9 AM. The other soundings were taken around midday.

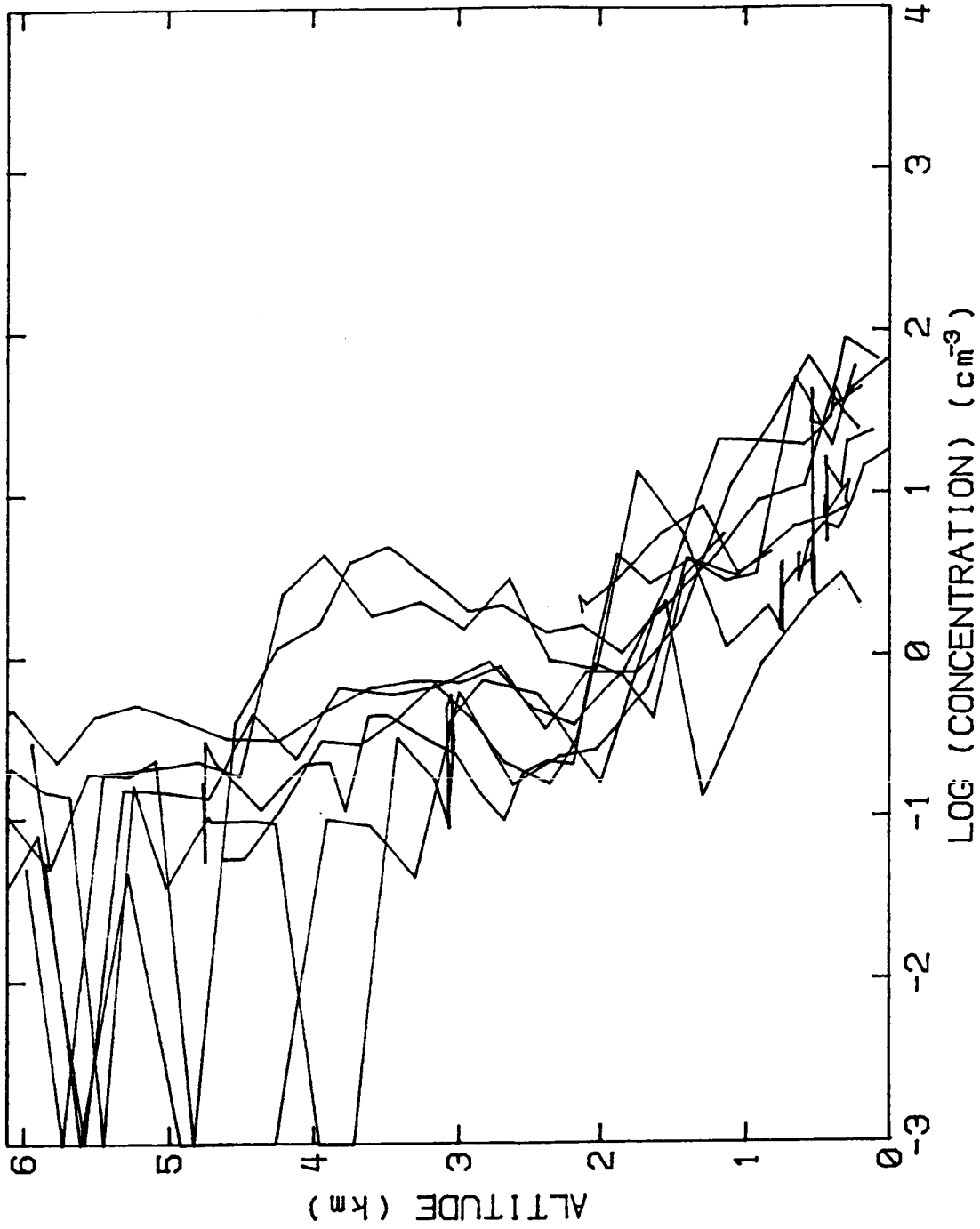


Figure 13. Concentration profiles for particles with $r > 0.13 \mu\text{m}$ (ASASP) from Sale-Cape Grim soundings May 26-June 1 1986. Corresponds with Climet soundings in Fig. 9.

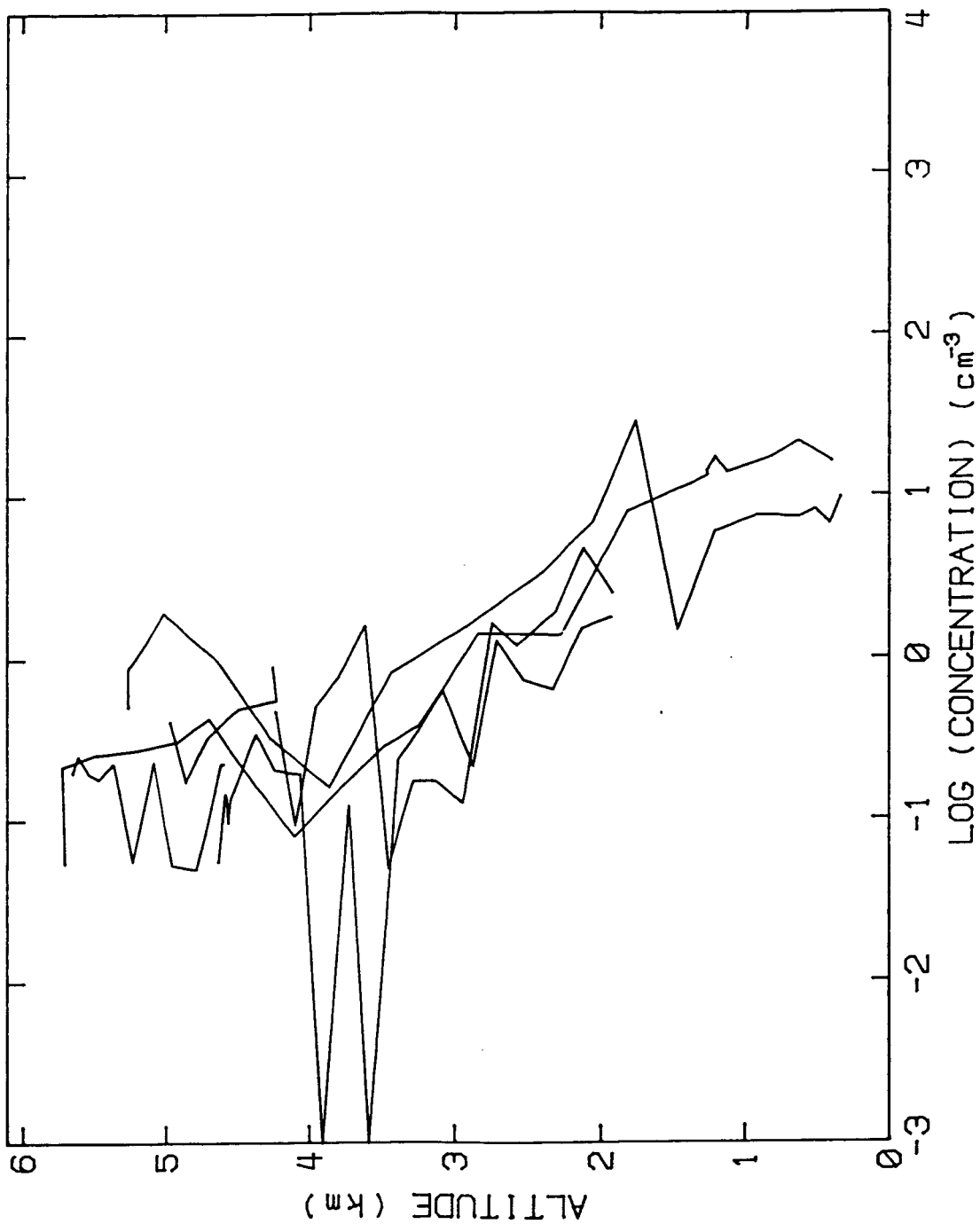


Figure 14. Concentration profiles for particles with $r > 0.13 \mu\text{m}$ (ASASP) for central New South Wales soundings on June 1 and June 11 1986, Corresponds with Climet data in Fig. 10.

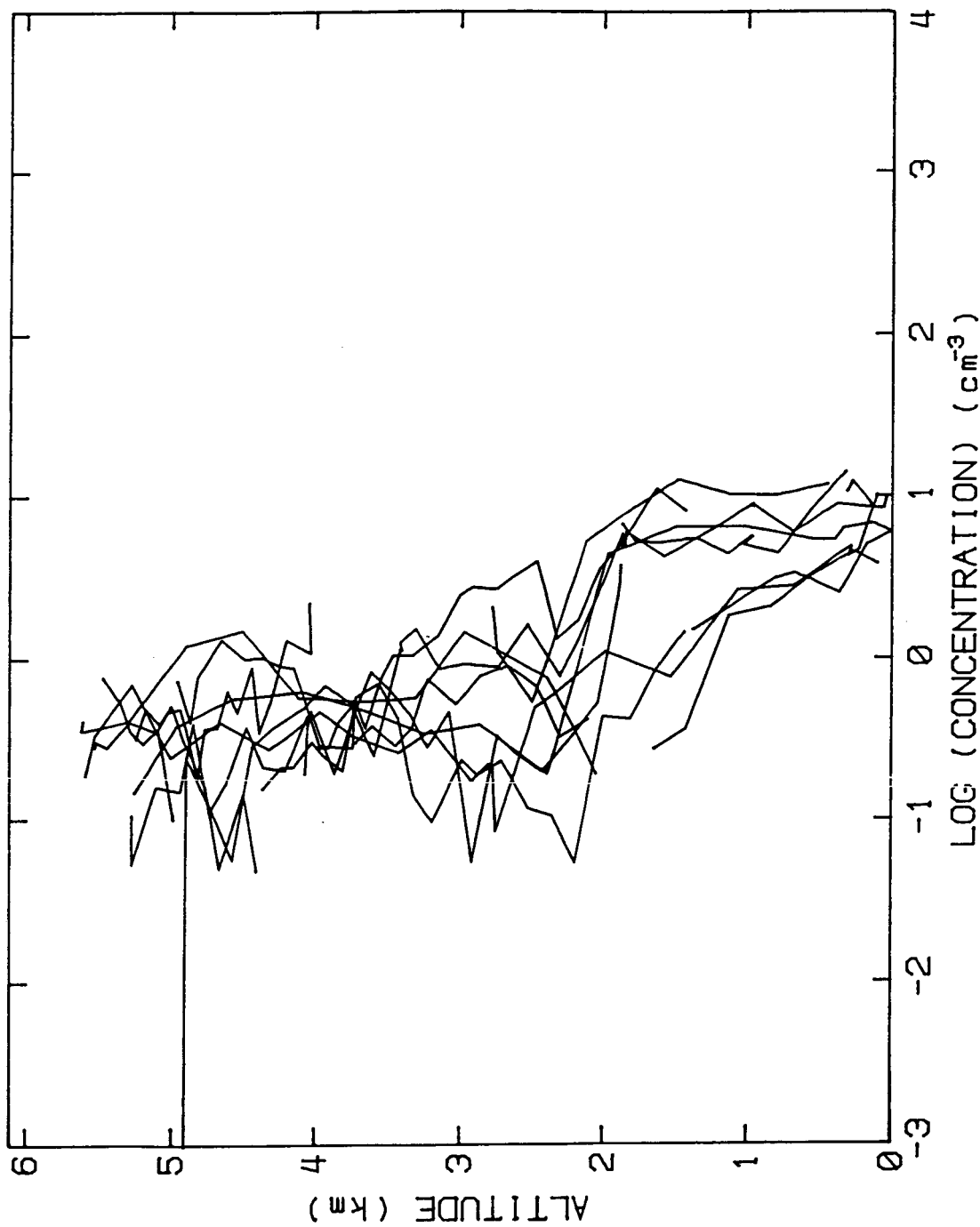


Figure 15. Concentration profiles for particles with $r > 0.13 \mu\text{m}$ (ASASP) for Cairns-Cowley Beach soundings June 2-June 11 1986. Corresponds with Climet soundings in Fig. 11.

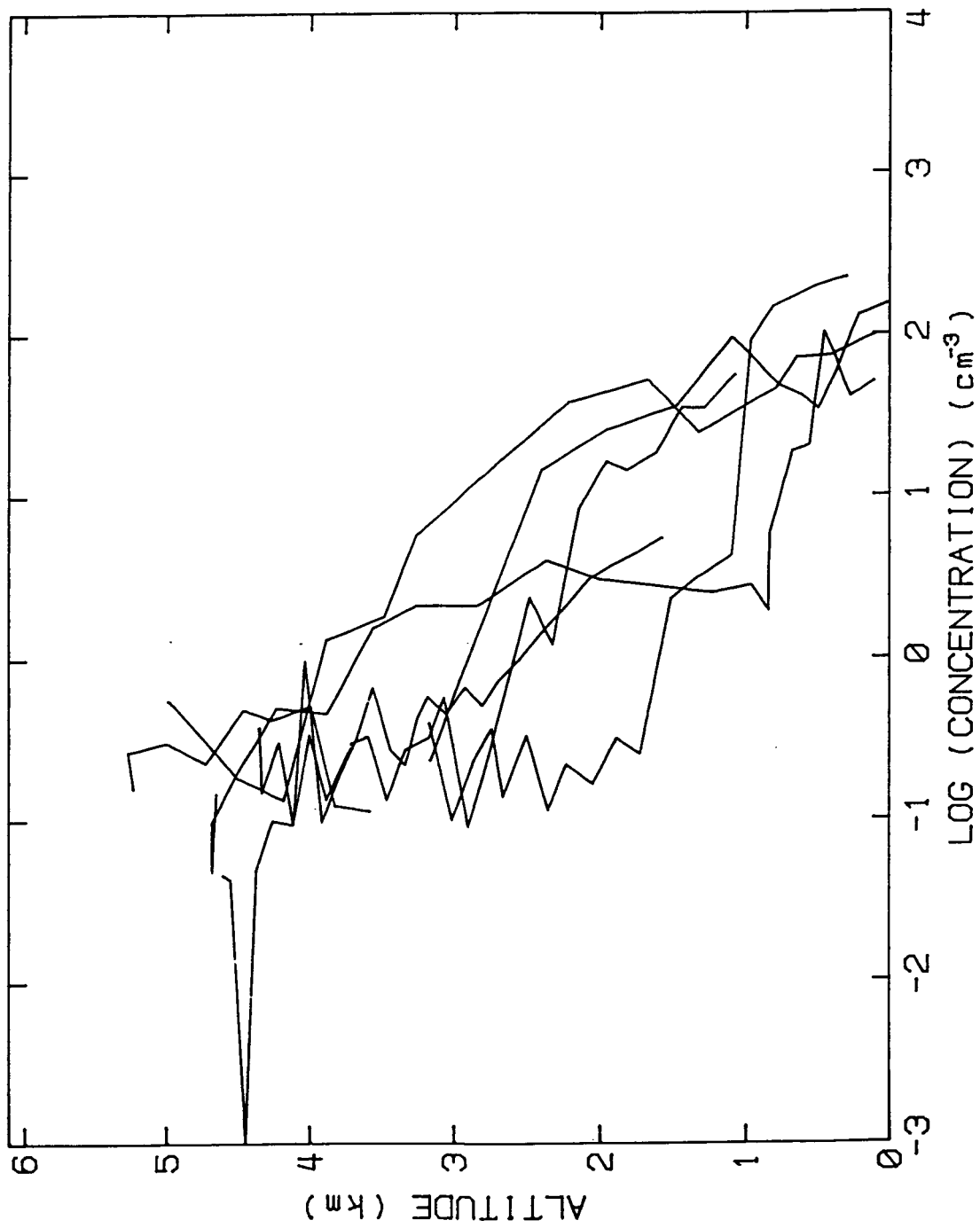


Figure 16. Concentration profiles for particles with $r > 0.13 \mu\text{m}$ (ASASP) for soundings in Papua New Guinea June 5-June 7 1986. Corresponds with Climet soundings in Fig. 12.

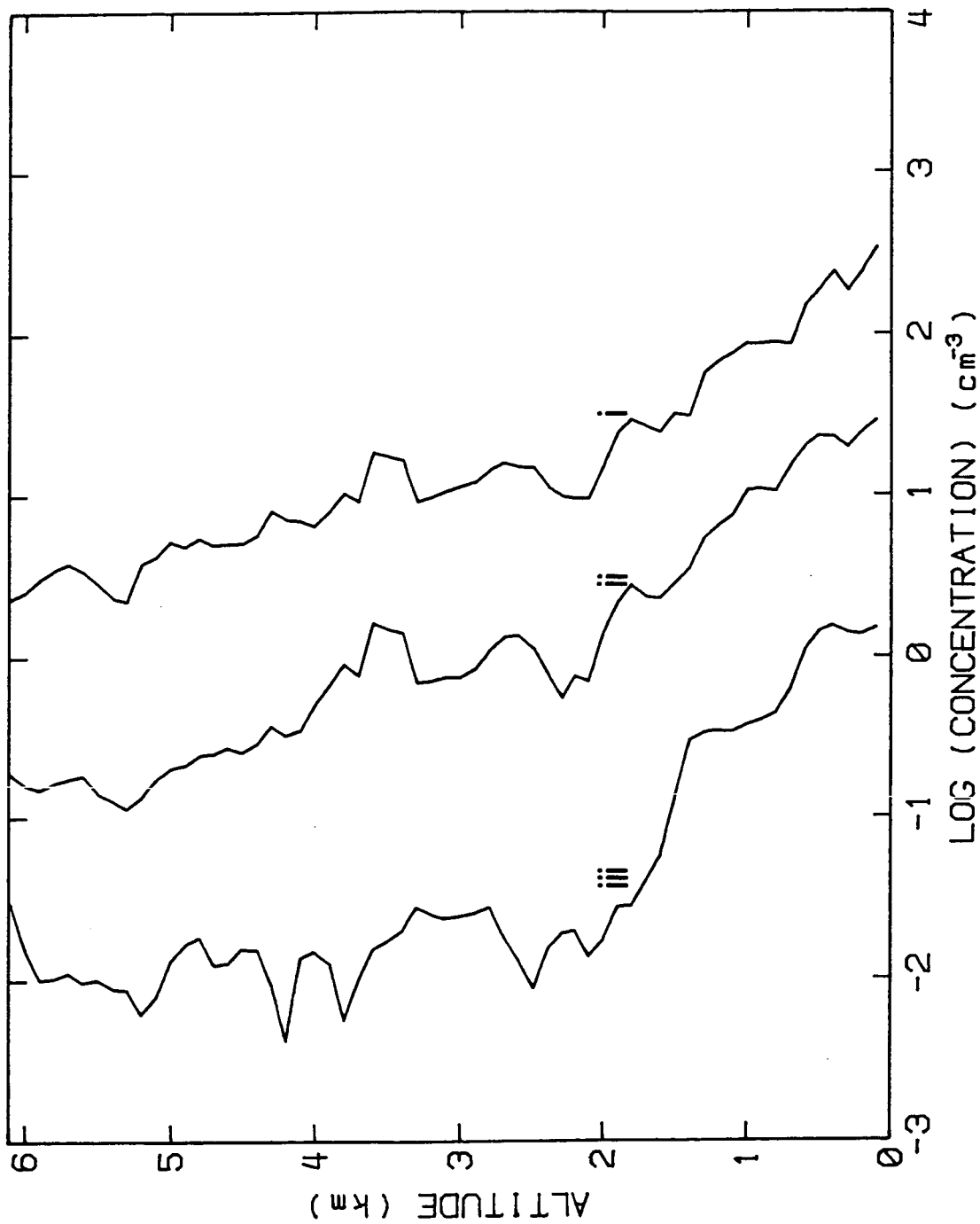


Figure 17. Sale May 25-June 1 1986. Mean concentration profiles from ASASP for particles with radii larger than (i) 0.06 μ m, (ii) 0.13 μ m, and (iii) 0.25 μ m in the boundary layer, 0.3 μ m in the free troposphere.

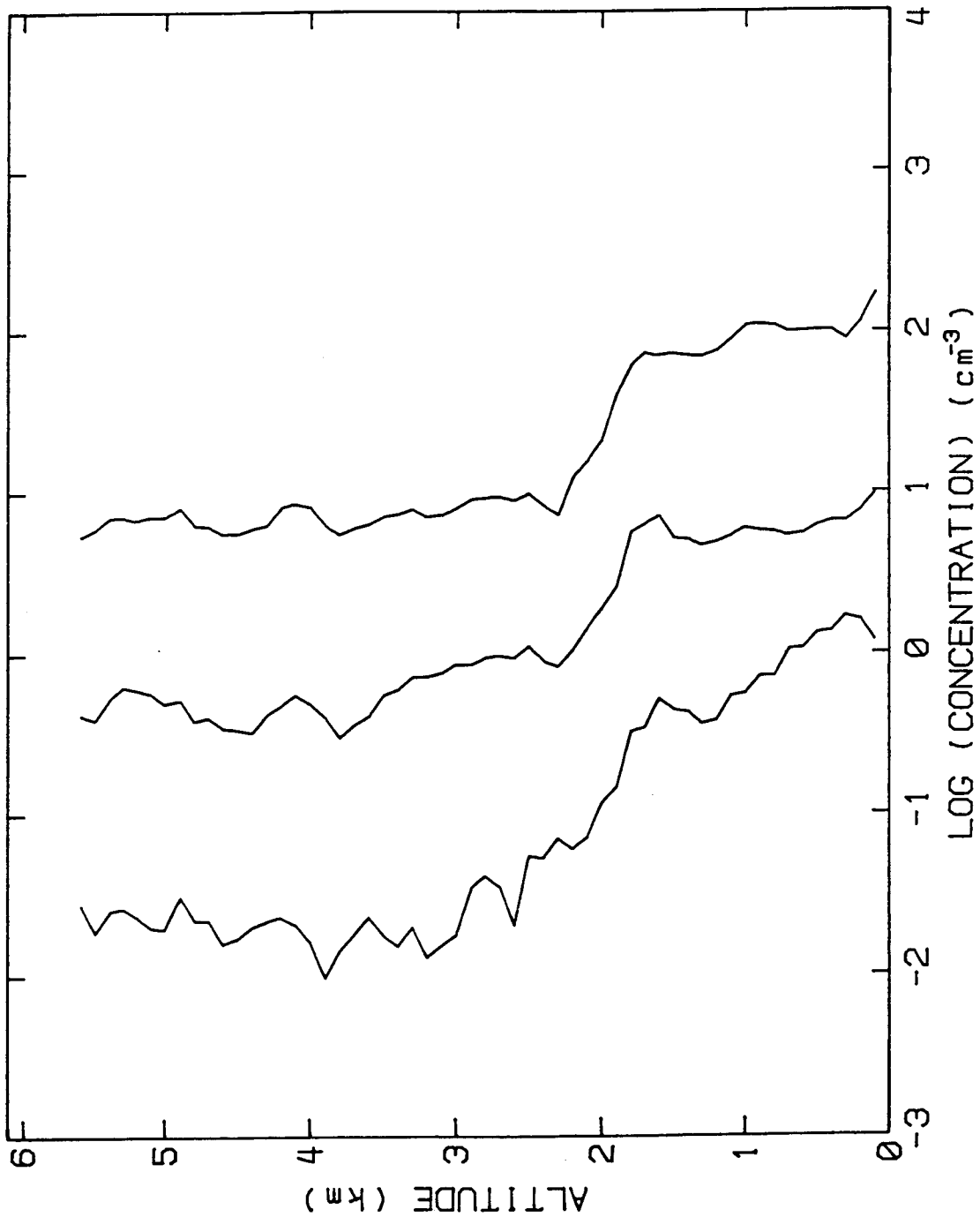


Figure 18. Cairns-Cowley Beach June 2-June 11 1986. Mean concentration profiles, same size limits as Fig. 17.

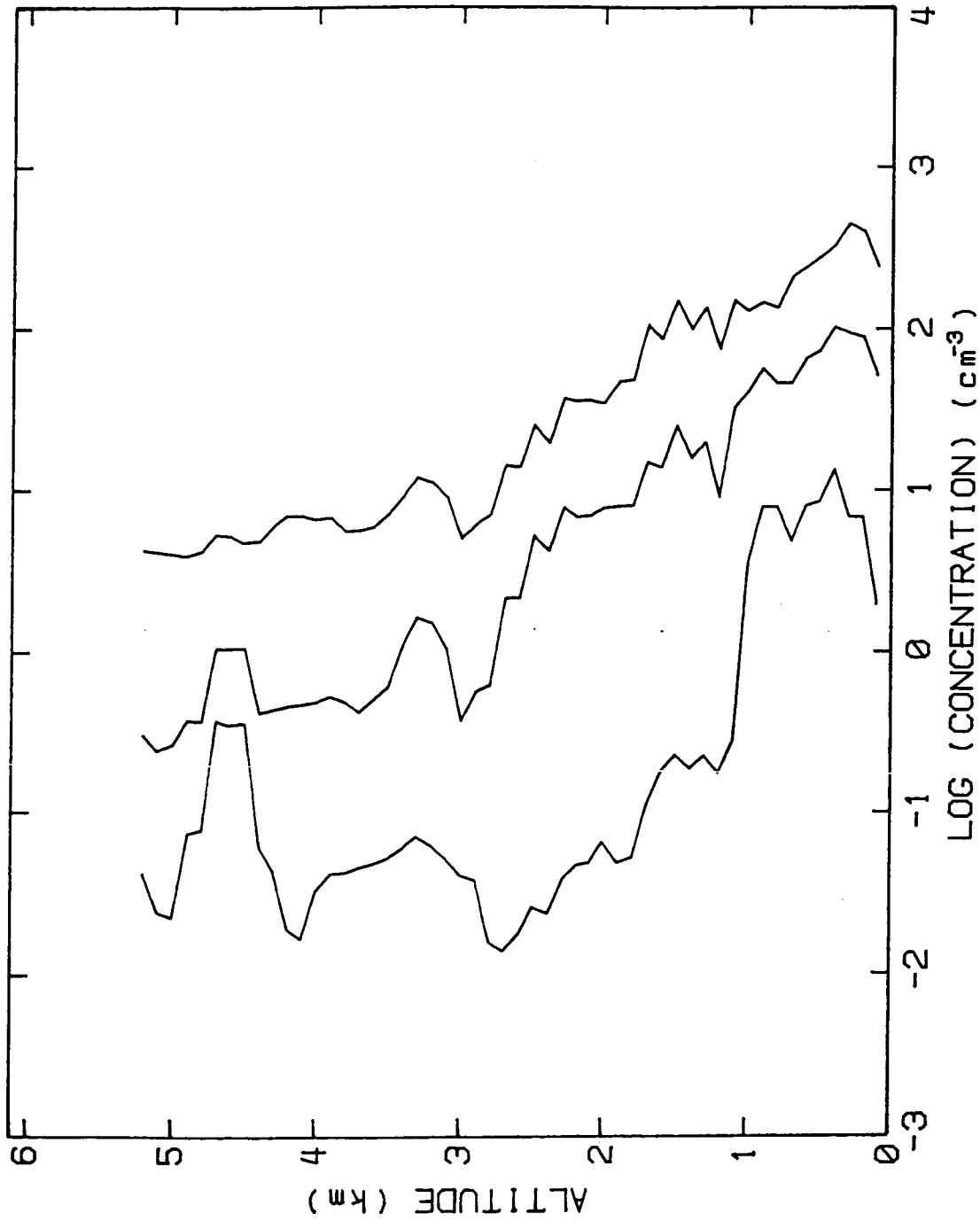
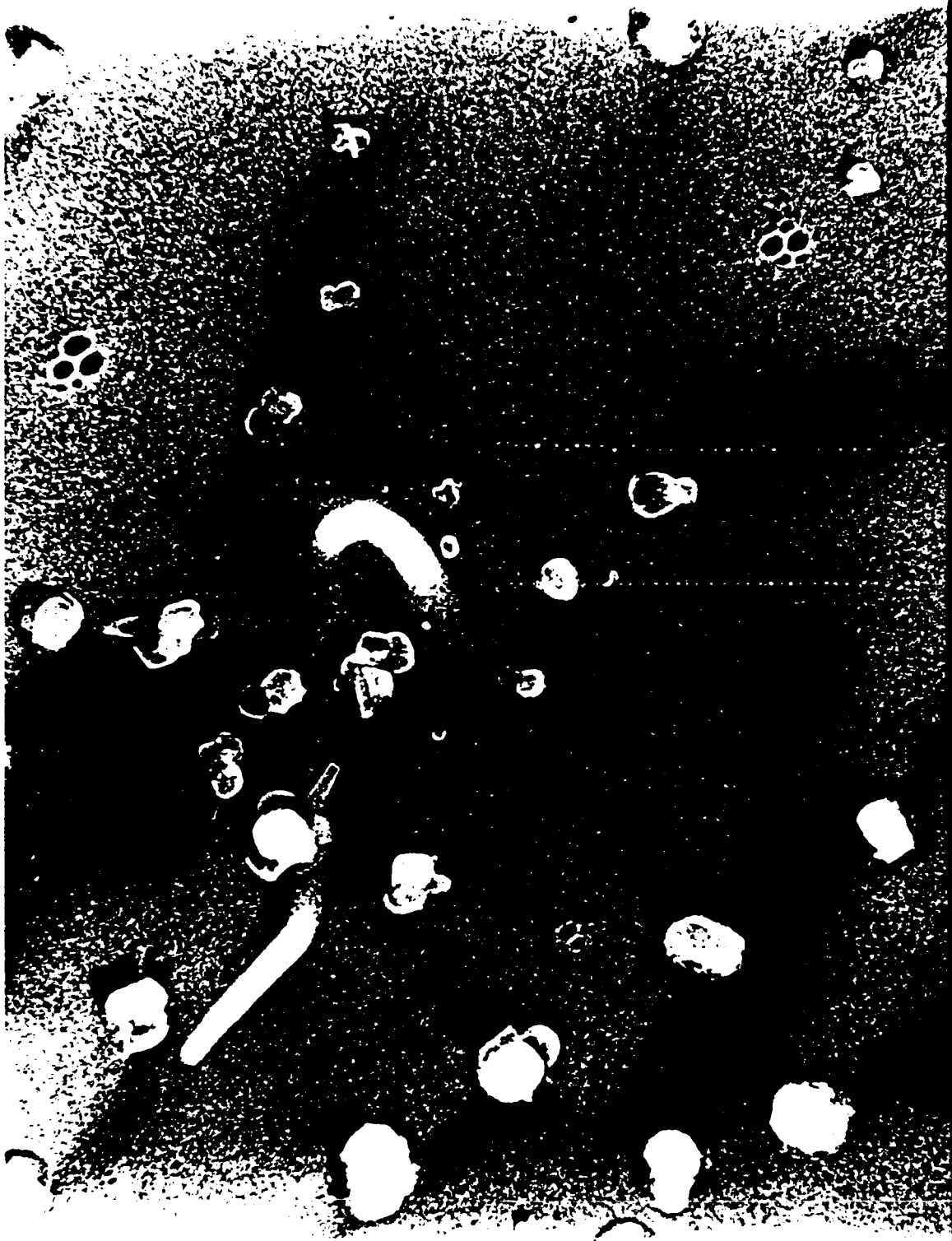


Figure 19. Papua New Guinea June 5-June 7 1986. Mean concentration profiles, same size limits as Fig. 17.



ORIGINAL PAGE IS
OF POOR QUALITY

35KW X2200 2547 10.00 CLOO

Figure 20. Transmission microscopy image of particle field from collection at 1.7km near Cowley Beach in maritime air stream. Sea salt particles are rectangular with low debris rings surrounding them.

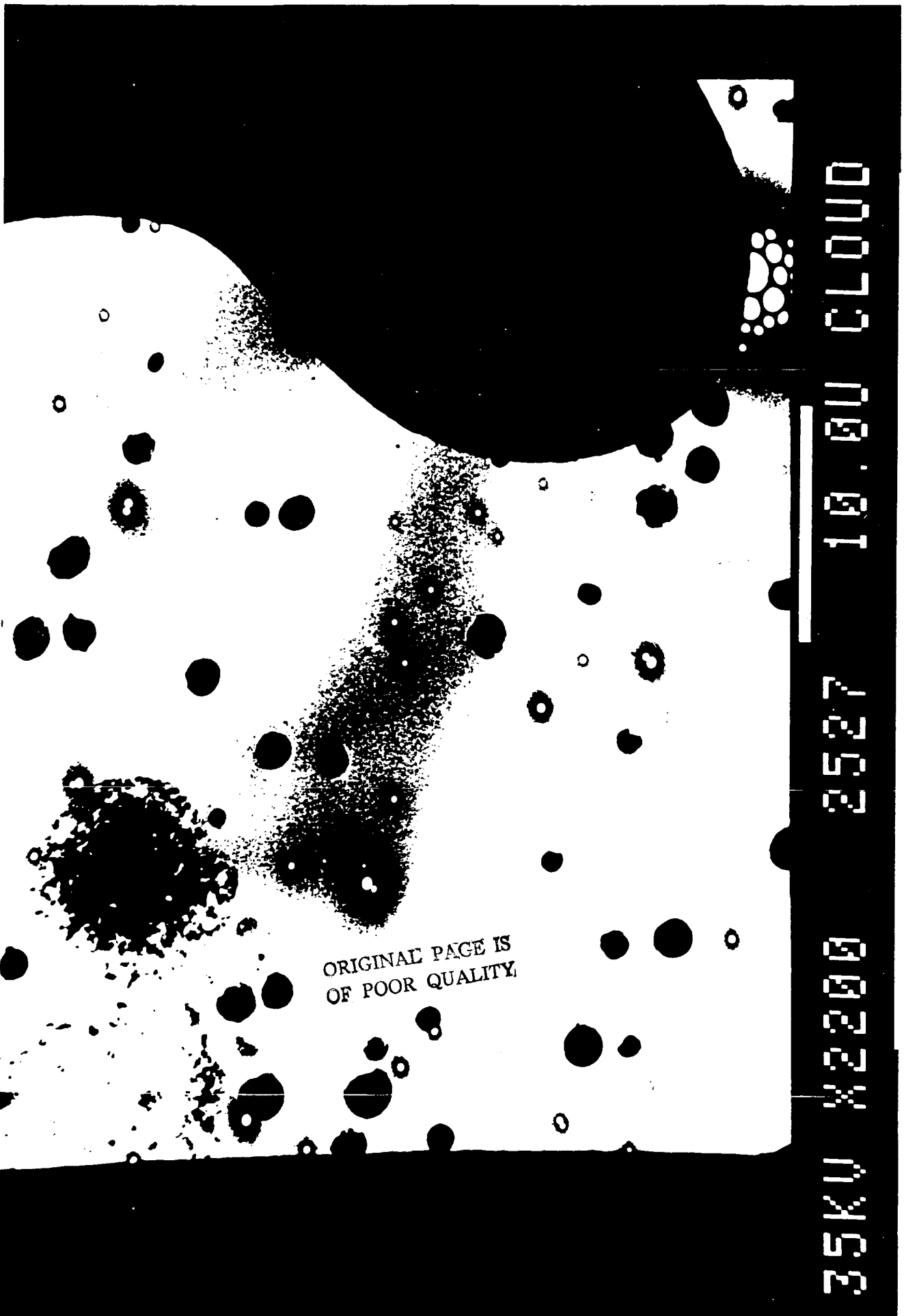
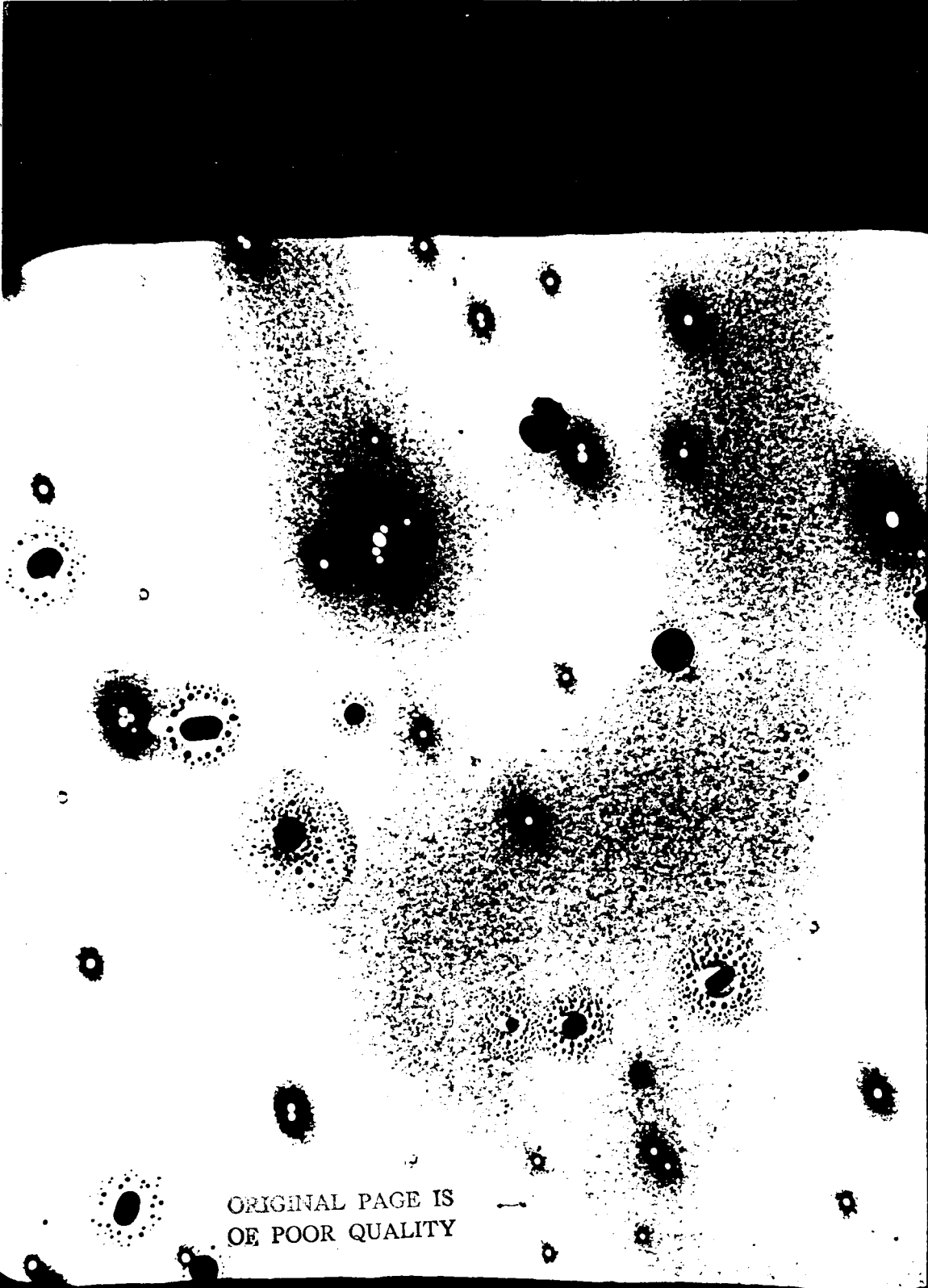


Figure 21. Transmission microscopy image showing a carbon (?) particle cluster collected at 900m in a maritime airstream near Cairns.



ORIGINAL PAGE IS
OF POOR QUALITY

35KU W2200 2485 10.00 CLOO

Figure 22. Transmission microscopy image showing a particle field from a collection at 6km near Cairns. Note that most particles have a sulfate morphology of a central cap-shaped particle (or ammonium sulfate bar) surrounded by droplet rings.

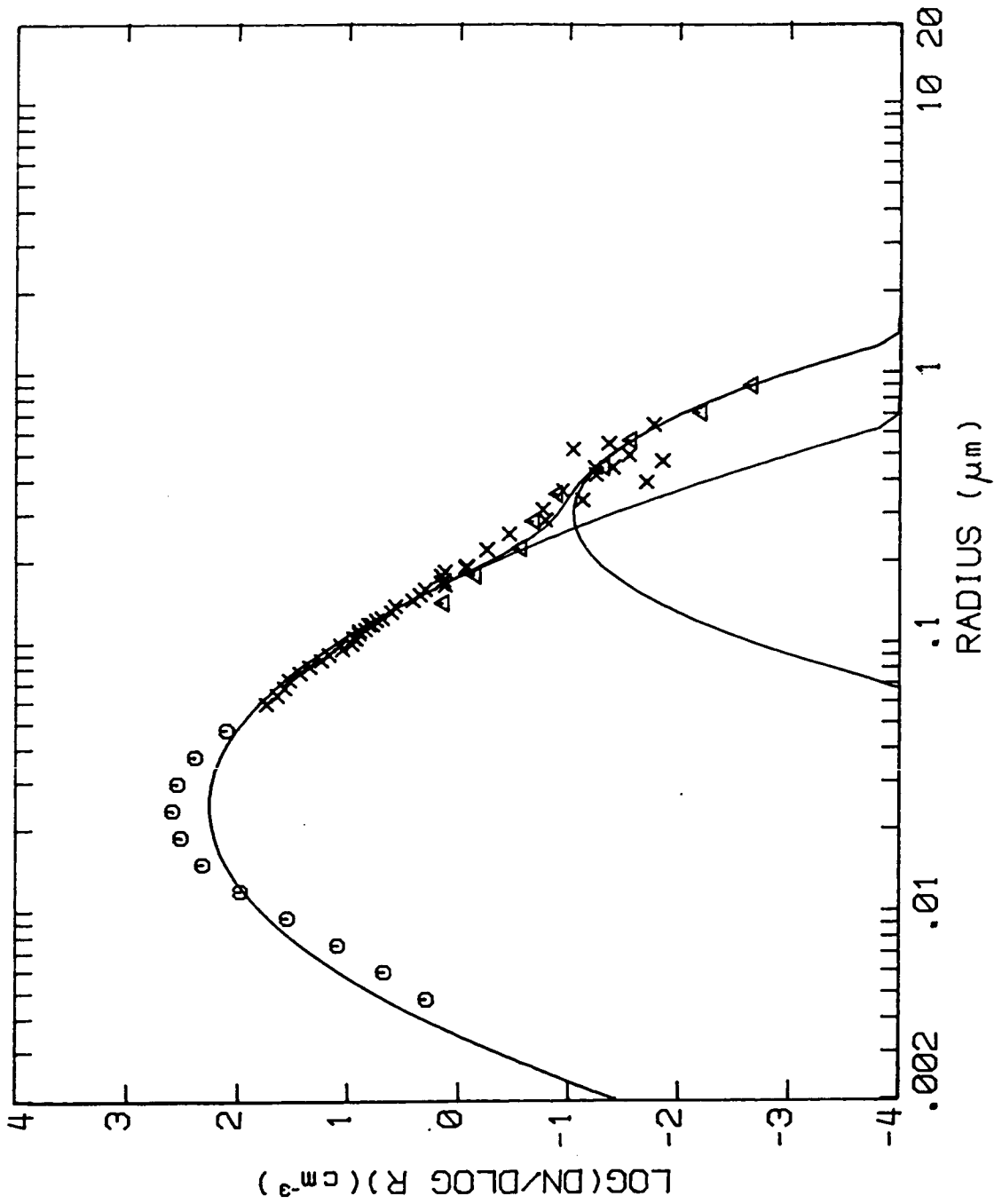


Figure 23. Mean size distribution data used to fit analytic distribution function for Cairns, altitudes 3.5-6km. Circles are GE diffusion battery, crosses ASAP, triangles impactor. The two fitted distribution modes and combined distribution function are also given.

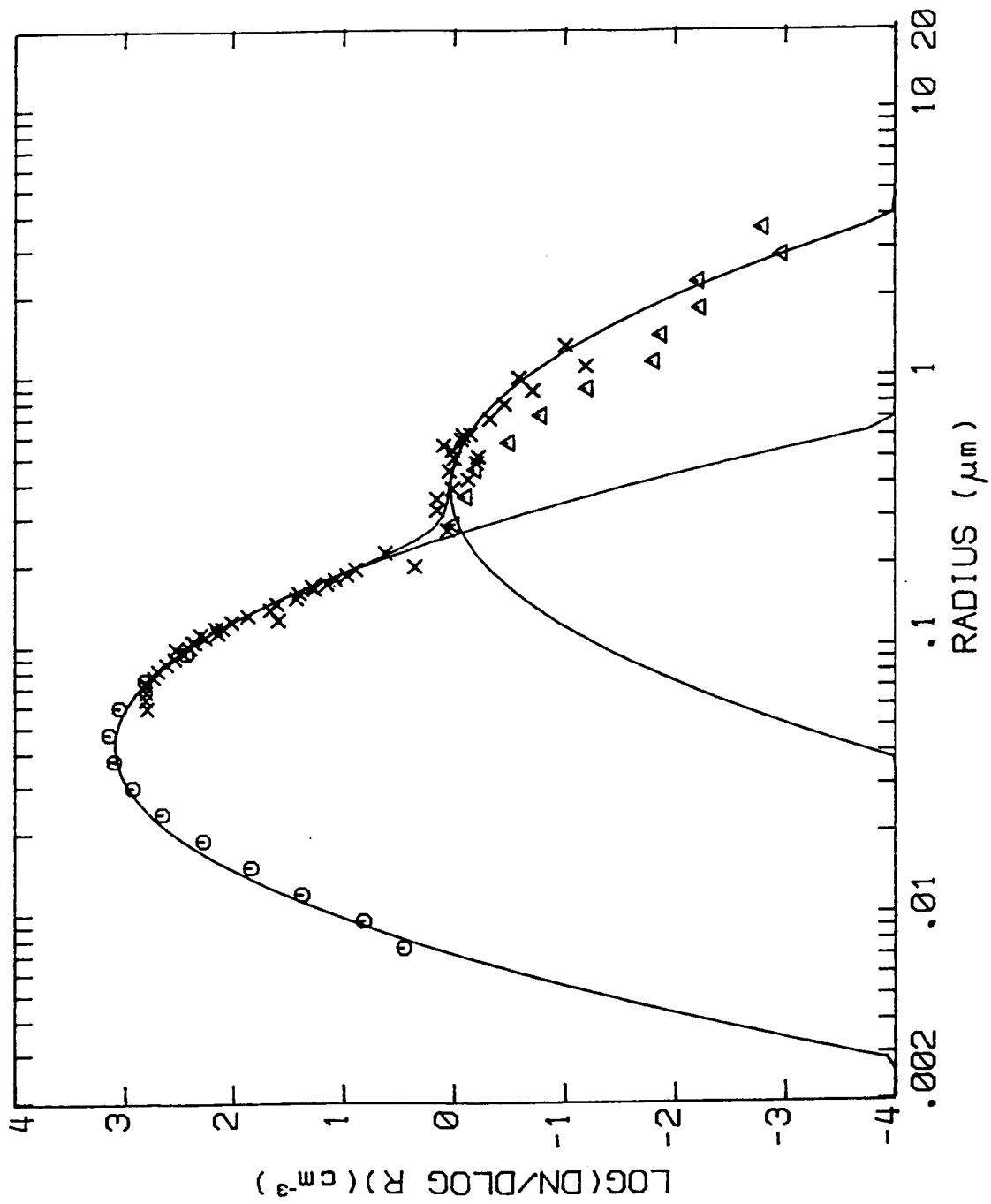


Figure 24. Same as Fig. 23 but for Cairns 0.76km-2.3km altitudes.

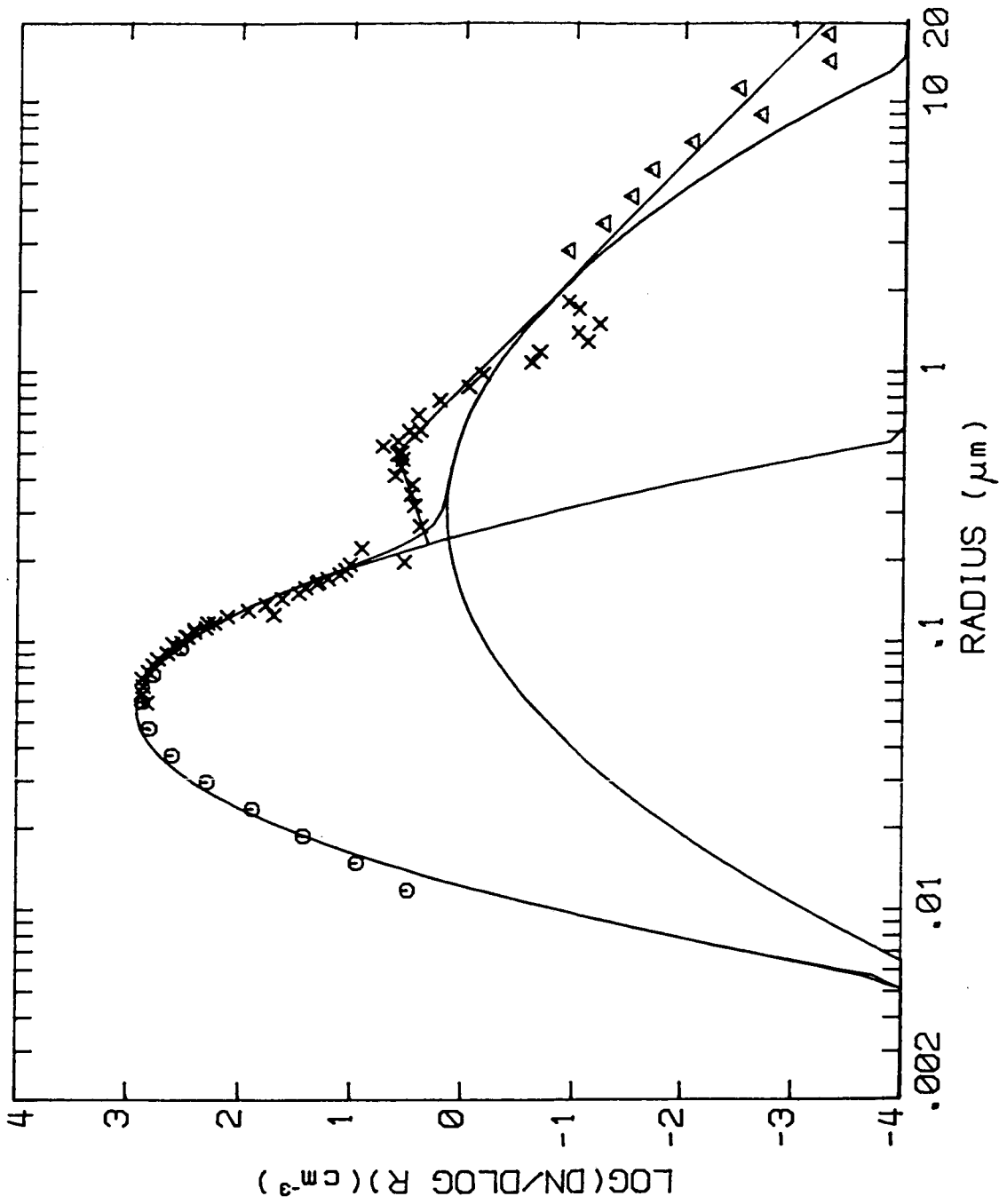


Figure 25. Same as Fig. 23 but for Cairns 0-.76km. As well the alternative power law distributions for large particles are shown.

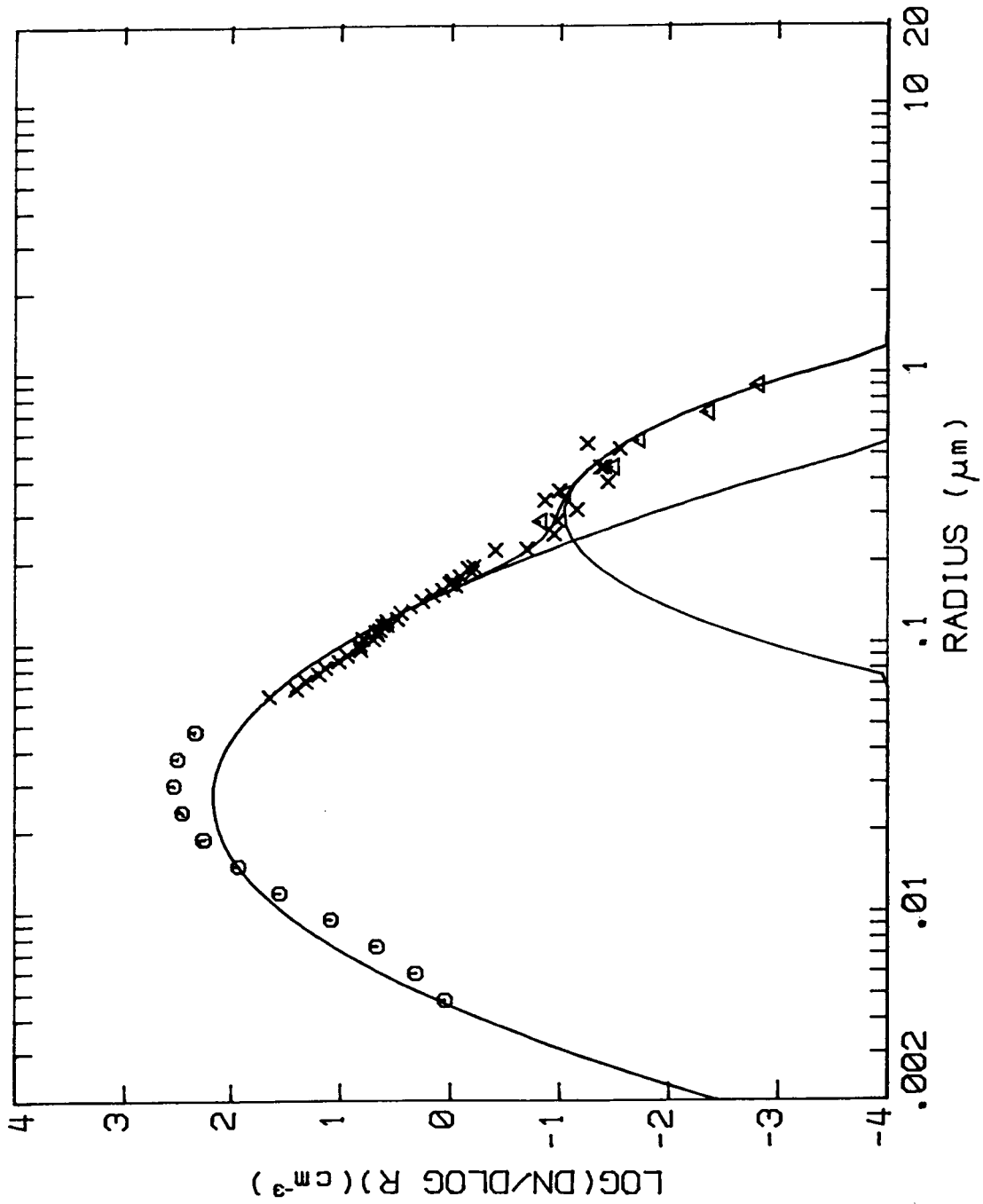


Figure 26. Same as Fig. 23 but for Sale 3.5km-6.1km.

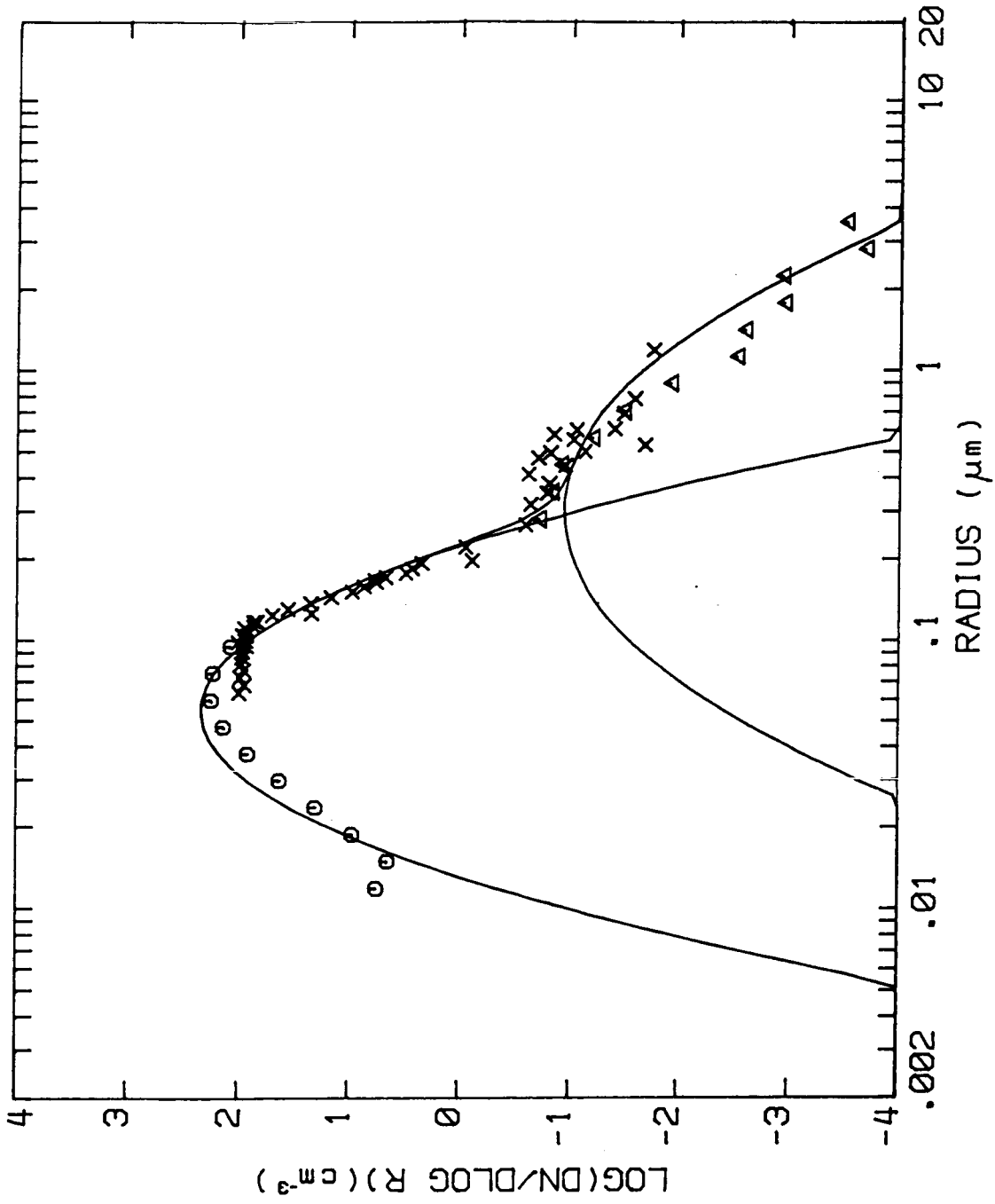


Figure 27. Same as Fig. 23 but for Sale 0.76km-2.3km.

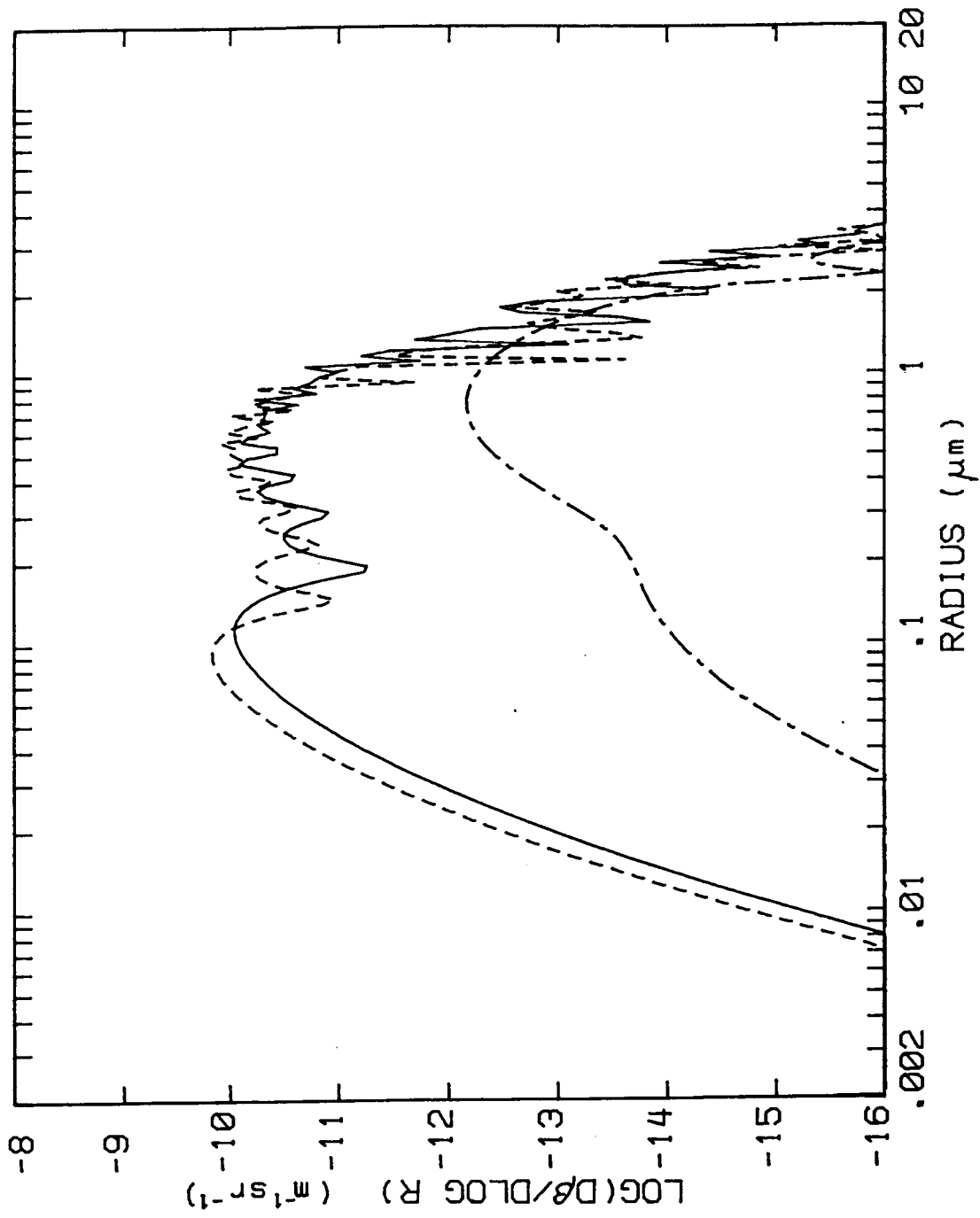


Figure 28. Cairns 3.5km-6km backscatter coefficient distributions calculated from the size distribution in Fig. 24. The short dashed line is for a wavelength of 0.532 μ m, the solid line 0.693 μ m and the dot-dashed line 10.6 μ m.

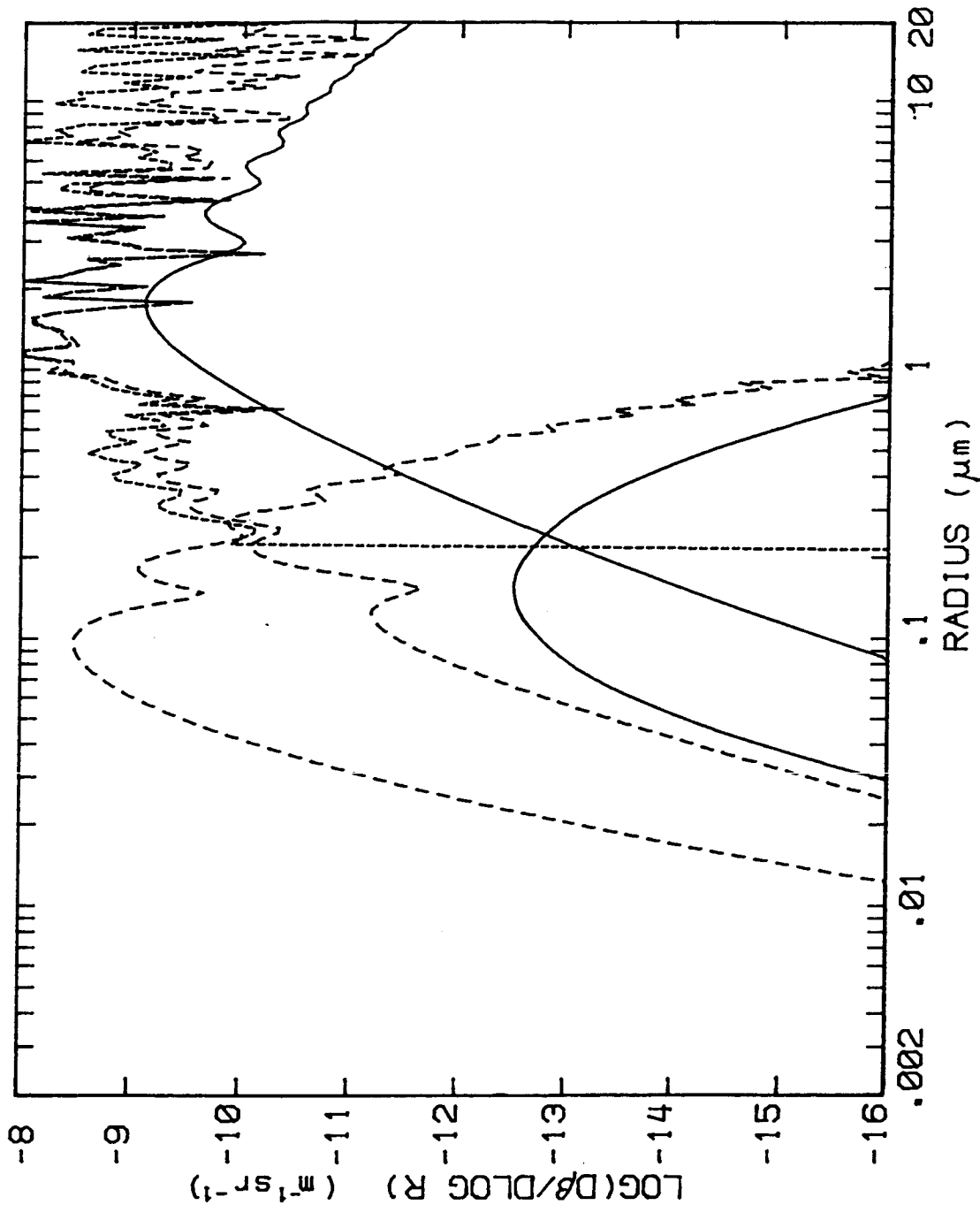


Figure 29. Cairns 0-.76km backscatter coefficient distributions calculated from the size distributions in Fig. 25. The two aerosol modes are plotted separately. The dashed line is for a wavelength of 0.532 μ m the solid line 10.6 μ m (log normal distns.). The short dashed line is the 0.532 μ m backscatter distribution for the power law distribution.

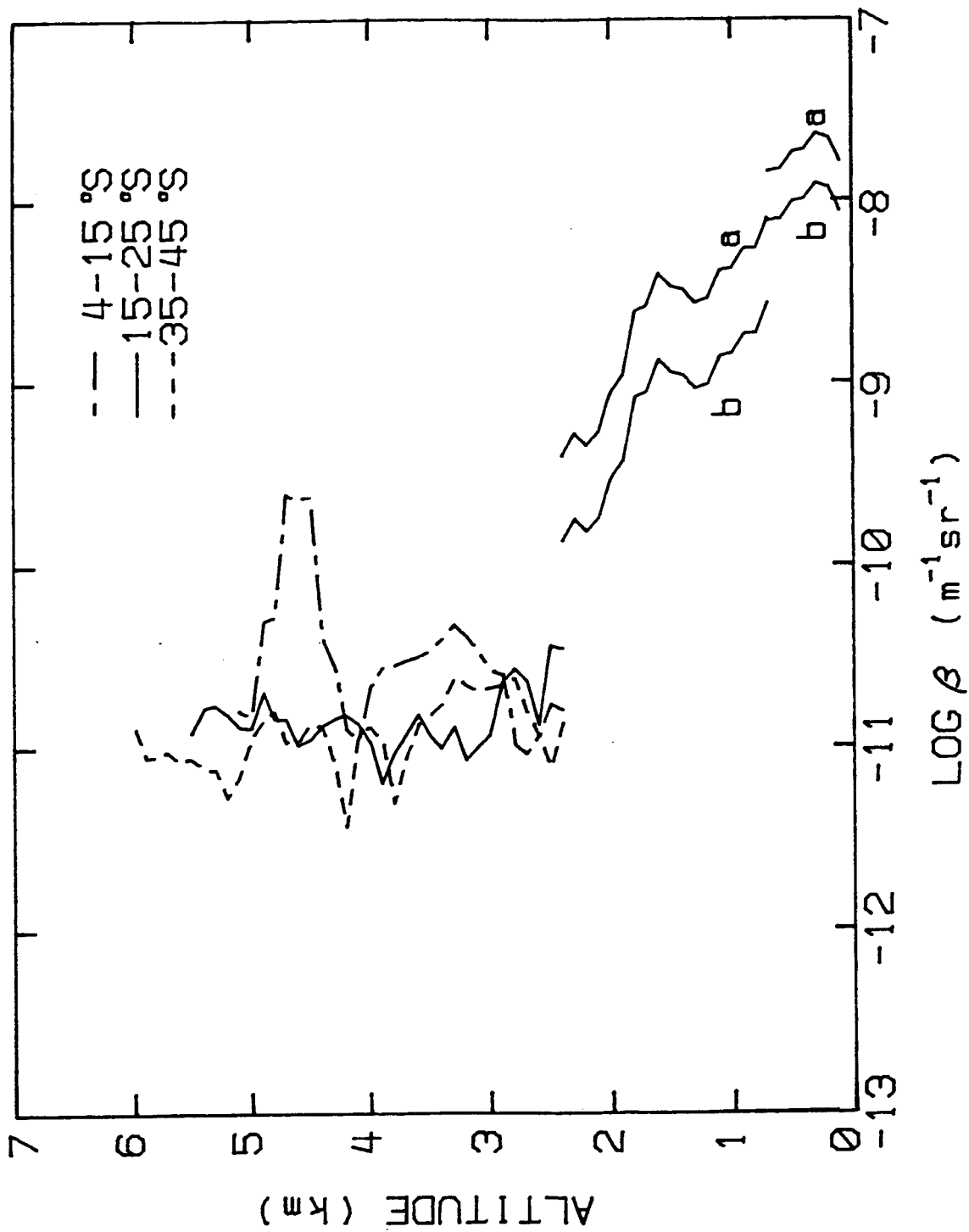


Figure 30. Profiles of calculated 10.6 μ m backscatter coefficient as a function of altitude in three latitude ranges. Profile (a) used the refractive index of water and (b) a "maritime" value (see text).

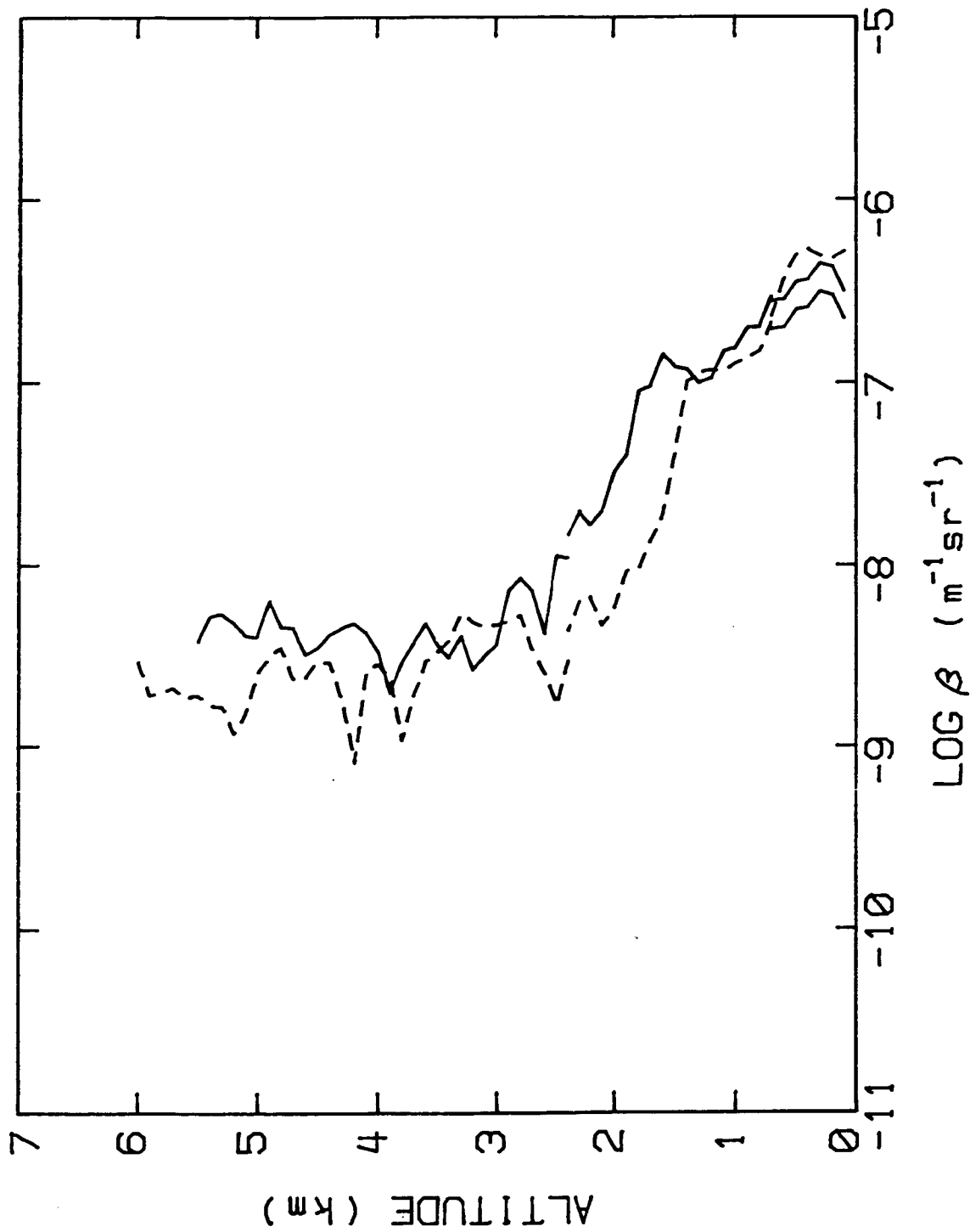


Figure 31. Profiles of calculated backscatter coefficient for 0.532 μm at Cairns (solid line) and 0.693 μm at Sale (dashed line). Profiles derived from model size distributions and the mean ASASP concentration profiles for particles with $r > 0.25\mu\text{m}$.

APPENDIX B

AUSTRALIAN AEROSOL BACKSCATTER AT 10.6 MICRONS
USING AN AIRBORNE CW CO₂ COHERENT LIDAR

Michael J. Kavaya¹
R. Milton Huffaker¹
John L. Gras²
Edward C. Russell¹
William D. Jones³

1. Coherent Technologies, Inc.
3300 Mitchell Lane, Suite 330
Boulder, CO 80301 USA
2. CSIRO Division of Atmospheric Research
Private Mail Bag #1
Aspendale, Australia
3. Guidance, Control, and Optical Systems Division (EE23)
Information and Electronics Systems Laboratory
NASA-Marshall Space Flight Center
Huntsville, AL 35812 USA

1. Introduction

NASA is planning a space-based Laser Atmospheric Wind Sounder (LAWS) to measure global wind velocity profiles. One of the most important design issues will be the values of aerosol backscatter coefficient on which to base the LAWS system design. The most uncertain region of the globe is the low latitude southern hemisphere where aerosol backscatter is expected to be at near minimal values. In order to obtain aerosol backscatter values and to assist in resolving this issue, NASA/CSIRO conducted an experiment in 1986 with ground and airborne lidars combined with an extensive set of aerosol sampling equipment on a CSIRO F-27 aircraft.

A joint NASA/CSIRO flight experiment was conducted in Australia during 25 May to 11 June 1986 to determine the aerosol backscatter at the 0.532, 0.694 and 10.591 μm laser wavelengths. The ground-based 0.532 μm doubled Nd:YAG lidar was based at Cowley Beach, Australia; the ground-based 0.694 μm ruby lidar was based at Sale, Australia; and the 10.591 μm coherent continuous-wave (CW) CO_2 lidar was mounted in the CSIRO F-27 aircraft. Aerosol equipment was also mounted in the aircraft which determined the aerosol number density, size distribution, and species. Comparison measurements of aerosol backscatter were made between the airborne CW CO_2 lidar and (1) the ruby lidar at Sale, Australia, and (2) the doubled Nd:YAG lidar at Cowley Beach, Australia. Several special flights were conducted by the F-27 aircraft for just the CW CO_2 lidar and aerosol sampling measurements.

The CW CO_2 coherent lidar was developed by NASA-MSFC and was operated by William D. Jones of NASA-MSFC during the flight. Jones coordinated the installation of the CW lidar on the F-27 aircraft, operated the lidar during the experiment, and guided the analysis of the data. The lidar operated successfully for the duration of the experiment from 25 May to 11 June 1986. Figure 1 shows the aircraft flight track and CW CO_2 lidar measurement path. The Cowley Beach location is located just south of Cairns. Measurements were made from 0 - 7 km altitude, from 5° S to 42° S latitude, and from 145° E to 153° E longitude. A total of 60 flight hours were accumulated during the 2.5 weeks of the experiment. The "cloud-free" lidar data spans about 23 hours as shown in Figure 2. Measurements with the CW CO_2 lidar in the free troposphere gave a backscatter coefficient of $1-2 \times 10^{-11} \text{ m}^{-1} \text{ sr}^{-1}$ at 10.6 μm although the accuracy and sensitivity of the instrument were marginal at this level.

It is recommended that more experimental data be taken in this region, that the lidar be upgraded in laser power in order to increase system sensitivity, and that the CW lidar data calibration methodology in both the volume mode and single particle mode, be reviewed and improved.

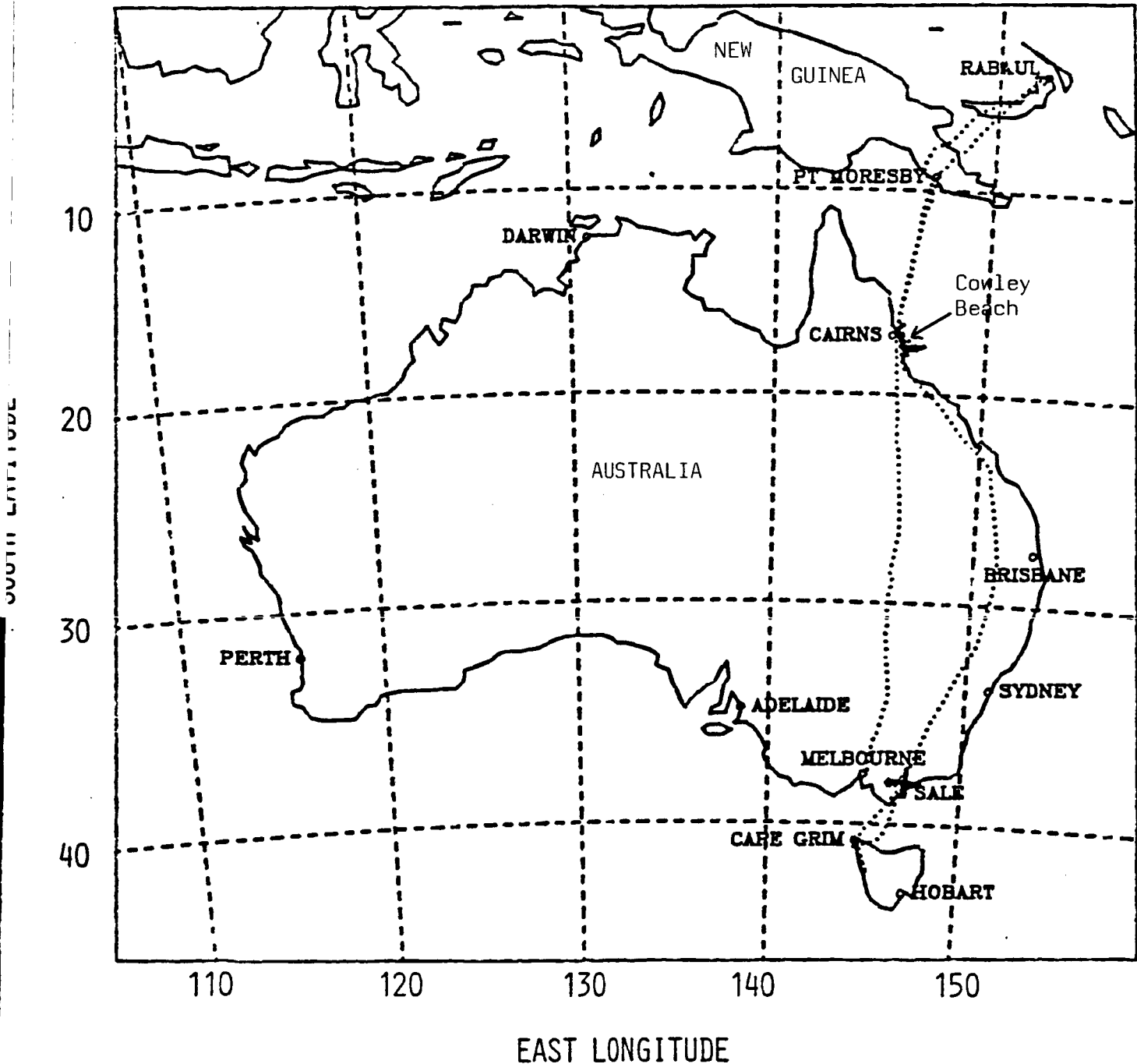


Figure 1. Flight track of CSIRO F-27 Aircraft.

HISTOGRAM PLOT OF AIRCRAFT ALTITUDE

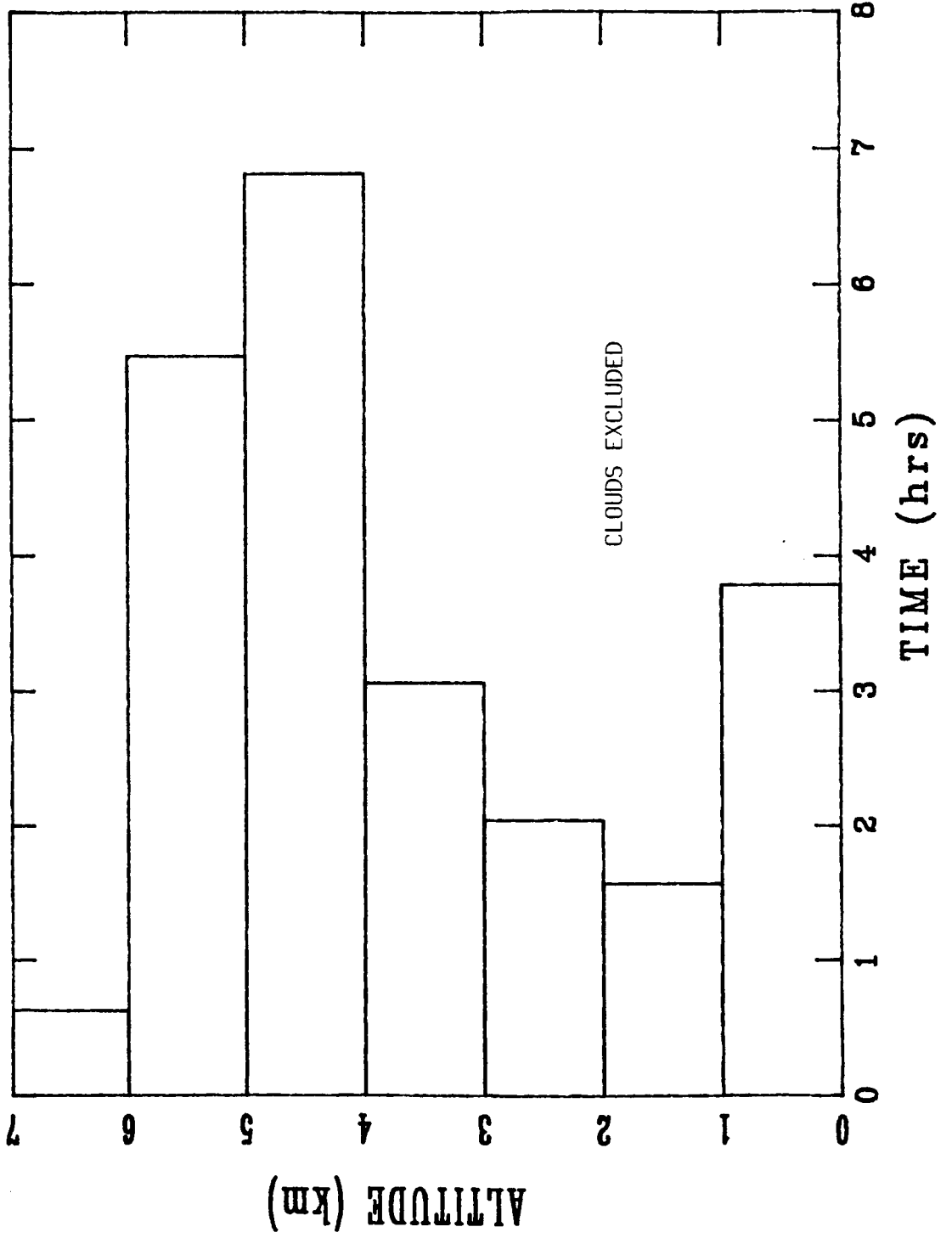


Figure 2. Histogram of altitude of CW lidar data.

2. Description of the CW CO₂ Lidar

A simplified optical layout of the CW CO₂ lidar system is shown in Figure 3. Detailed descriptions of the lidar system are presented in References 1 and 2, and a photograph of the lidar is shown in Figure 4. The lidar uses a 10.6 μm CO₂ laser with a typical output power of 7 W. A Mach-Zehnder interferometer is used to separate the laser beam into a transmitted and a reference beam. The transmitted beam is directed into a 15-cm off-axis telescope which is used to both expand the transmitted beam and to collect the backscattered, Doppler-shifted laser radiation. Focus adjustment of the telescope is possible, varying from 10 m to infinity. A focal range of 10 m was primarily used for this measurement program, except at low altitudes where the laser beam was collimated.

The expanded beam from the telescope is directed into the atmosphere by using two flat mirrors. The second mirror is able to oscillate about its vertical axis, thus changing the angle between the lidar line-of-sight and the aircraft flight direction. By oscillating between two angles during flight, the aerosol signal is shifted into and out of the pass-band of the processing electronics, due to the different Doppler frequency shifts. The processor bandpass filter can be tuned to allow a broad range of aircraft speeds. For this measurement program, the two angles were $+17.44^\circ$ (where 0° would be perpendicular to the aircraft velocity vector) for the data (or signal+noise) position, and $+14.12^\circ$ for the noise (out of pass-band) position.

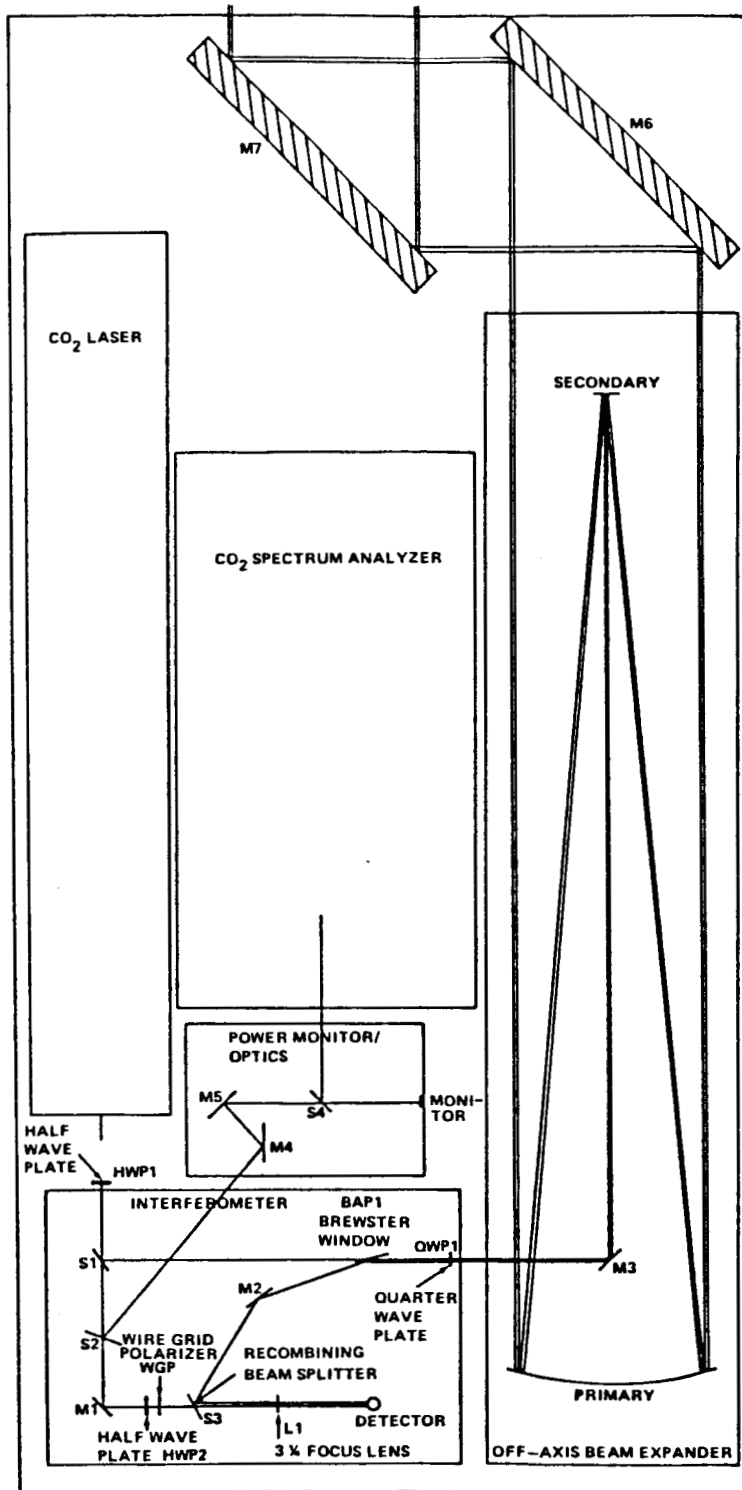


Figure 3. Optical Layout of the CW CO₂ Lidar System

ORIGINAL PAGE IS
OF POOR QUALITY

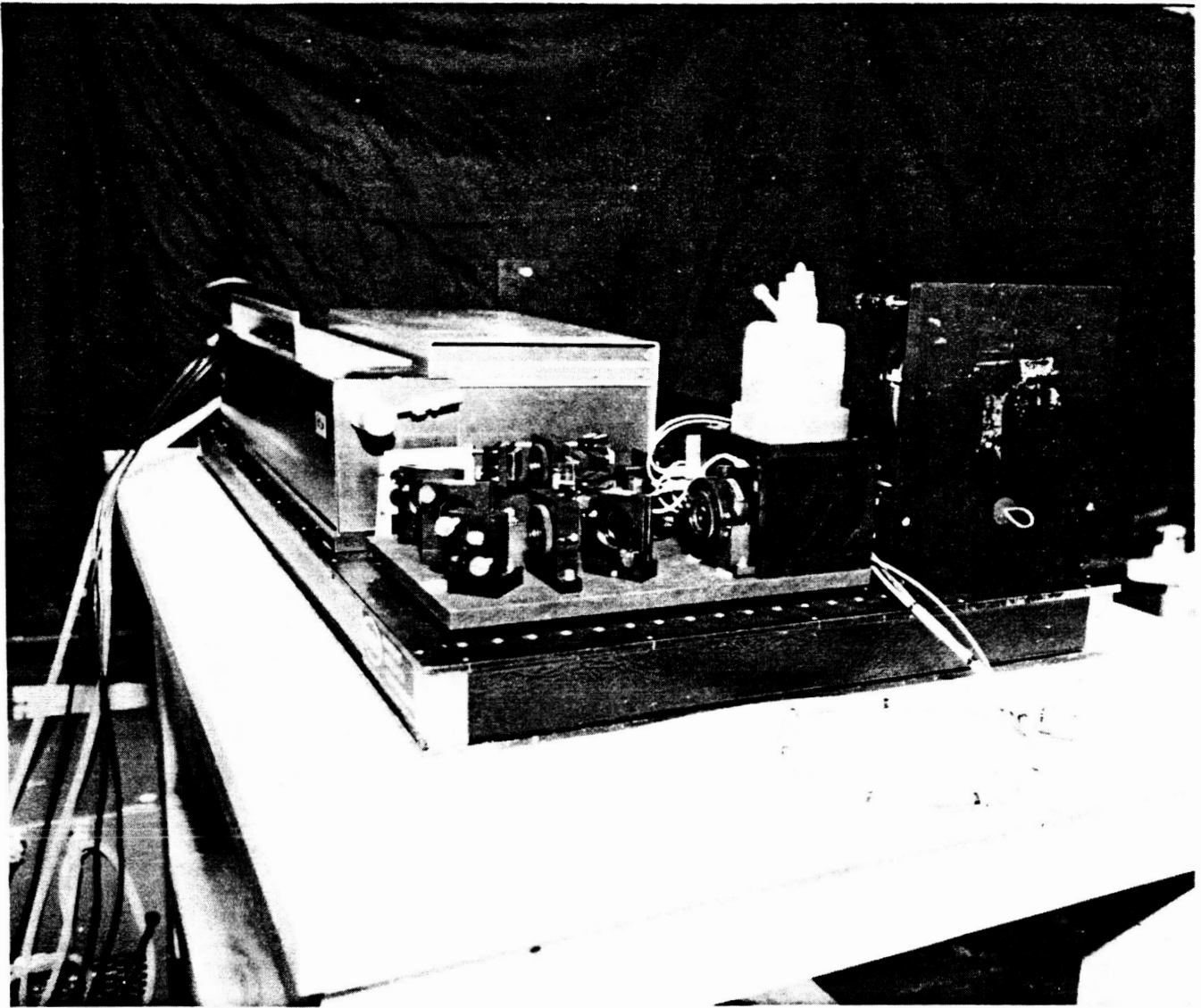


Figure 4. Focused Coherent Lidar System

3. Theory of CW Lidar Backscatter Measurements

3.1 Volume Mode

When a focused CW lidar is detecting backscatter from a target of "infinite" extent (e.g. aerosol particles in the atmosphere), the theoretical signal-to-noise ratio (SNR) is given by:^{2,3}

$$\text{SNR}_{\text{VM}} = \frac{P_T}{h\nu B} \frac{\eta\beta\lambda}{2} \left[\frac{\pi}{2} + \tan^{-1} \left[\frac{\pi R^2}{\lambda f} \right] \right], \quad (1)$$

where VM stands for volume mode, P_T [W] is the transmitted power, $h = 6.6262 \cdot 10^{-34}$ [Js] = Planck's constant, ν is the laser frequency [Hz], B is the electronic bandwidth [Hz], η is the optics and detector efficiency, β is the atmospheric aerosol backscatter coefficient [$\text{m}^{-1} \text{sr}^{-1}$], $\lambda = c/\nu$ is the laser wavelength [m], $c = 2.9979 \cdot 10^8$ [m s^{-1}] is the velocity of light, f is the focal range of the telescope [m], and R is the e^{-2} (13.5%) intensity radius of the transmitted Gaussian beam [m]. In Eq. (1), the Gaussian beam is assumed untruncated and monochromatic in a coaxial system, atmospheric extinction and refractive turbulence effects are neglected, the local oscillator (LO) beam for heterodyne detection is assumed to be a Gaussian plane wave, square-law detection and shot-noise-limited detection are assumed, and other sources of received power such as molecular backscatter are neglected. Dickson⁴ has shown that the effects of beam truncation are only negligible if the minimum physical lens or mirror radius is at least $2R$ (i.e. $e^{-8} \approx 0.034\%$). The factor 2 in the denominator of Eq. (1) is due to an assumed photoconductive detector. It should be removed for a photovoltaic detector, which is the type employed in the MSFC CW lidar.

For a given set of system parameters, Eq. (1) may be written

$$\text{SNR}_{\text{VM}} = K \beta, \quad (2)$$

where K [m sr] is a system constant. If K can be determined, then β can be found once SNR_{VM} is determined from measurements. Since the MSFC CW lidar alternately measures signal plus noise (S+N) and noise (N) through its angular Dicke switching, SNR_{VM} is computed as

$$\text{SNR}_{\text{VM}} = \frac{S+N}{N} - 1. \quad (3)$$

A second technique for determining β employs a hard calibration target.¹ A plane rotating target with a known bidirectional reflectance-distribution function (BRDF) f_r [sr⁻¹] is placed at the beam's focus. The measured SNR is given by

$$\text{SNR}_{\text{HT}} = G f_r, \quad (4)$$

where HT stands for hard target, G [sr] is a system constant, and where f_r depends on the illuminating and detected polarization of light and is assumed constant over the illumination and detection solid angles. The target is then removed and the aerosol backscatter SNR is given by

$$\text{SNR}_{\text{VM}} = G \Delta L \beta, \quad (5)$$

where ΔL [m] is defined as the range interval from which 50% of the detected heterodyne signal is returned:¹

$$\Delta L = \frac{\lambda f^2}{R^2}. \quad (6)$$

Eqs. (4) and (5) are then used to solve for backscatter:

$$\beta_{\text{VM}} = \frac{\text{SNR}_{\text{VM}}}{\text{SNR}_{\text{HT}}} \frac{f_r}{\Delta L}. \quad (7)$$

The advantage of the second technique is that the system constant G cancels and therefore many difficult to measure parameters of the system (especially η) are not needed, as they are when using the first technique. Disadvantages of the second technique include the wide dynamic range of signals from aerosol particles and hard targets, and the difficulty of accurately knowing f_r .⁵ The second technique was used in deriving the volume mode backscatter coefficient for all the Australian data.

Lawrence et al⁶ give without derivation ΔL for untruncated Gaussian beams as

$$\Delta L = \frac{2\lambda L f}{\pi R^2} = \frac{0.64 \lambda L f}{R^2}, \quad (8)$$

where $L \sim f$ in the strong focusing regime, and Post et al⁷ increased ΔL by a factor of 2.2 or

$$\Delta L = \frac{1.4 \lambda f^2}{R^2}, \quad (9)$$

due to the assumption that the primary mirror truncates the Gaussian beam at the e^{-2} intensity points. Eq. (6) is clearly bounded by Eqs. (8) and (9). However, both Ref. 6 and Ref. 7 define ΔL as the distance between the points where the SNR drops to one half of its maximum value at the focus. This is not necessarily the same as the definition in Eq. (5). In addition, the definition in Eq. (5) appears to include an intrinsic factor of 2 error for SNR_{VM} since only 50% of the returned energy is included. Using intermediate results in Ref. 6, we have derived⁸

$$\Delta L = \frac{0.49 \lambda f^2}{R^2} \quad (10)$$

for untruncated Gaussian beams, a tight focus ($\pi R^2 \gg \lambda f$), and for the ΔL definition of References 6 and 7. (For the MSFC CW lidar, $\pi R^2 / (\lambda f) \cong 167 \gg 1$.) Eq. (10) should be compared to Eq. (8), and is smaller by a factor of 1.31.

However, the definition of ΔL by Jones et al¹ in Eq. (5) is more fundamental to the calibration of backscatter. We may start with Eq. (26) of Ref. 3 which gives the SNR of a CW lidar focused at range f and detecting aerosol backscatter starting at range L_1 and ending at range L_2 :

$$\begin{aligned} \text{SNR}_{\text{VM}}(L_1, L_2) = & \frac{P_T}{h\nu B} \frac{\eta\beta\lambda}{2} \left[\tan^{-1} \left[\frac{\lambda L_2}{\pi R^2} - \frac{\pi R^2}{\lambda f} \left[1 - \frac{L_2}{f} \right] \right] \right. \\ & \left. - \tan^{-1} \left[\frac{\lambda L_1}{\pi R^2} - \frac{\pi R^2}{\lambda f} \left[1 - \frac{L_1}{f} \right] \right] \right]. \quad (11) \end{aligned}$$

Eq. (11) reduces to Eq. (1) when $L_1 = 0$ and $L_2 = \infty$, i.e. an infinite target. We now ask the question: "For what path length $\Delta L = 2\epsilon$ centered at $z = f$ will a fraction α of the total signal of Eq. (1) be obtained?" The equation to be solved for ϵ is:

$$\begin{aligned}
& \tan^{-1} \left[\frac{\lambda(f+\epsilon)}{\pi R^2} - \frac{\pi R^2}{\lambda f} \left[1 - \frac{f+\epsilon}{f} \right] \right] \\
& - \tan^{-1} \left[\frac{\lambda(f-\epsilon)}{\pi R^2} - \frac{\pi R^2}{\lambda f} \left[1 - \frac{f-\epsilon}{f} \right] \right] \\
& = \alpha \left[\frac{\pi}{2} + \tan^{-1} \left[\frac{\pi R^2}{\lambda f} \right] \right], \tag{12}
\end{aligned}$$

where $0 < \alpha < 1$ and $\epsilon > 0$. As it stands, this equation must be solved numerically for specific cases. If we again assume a tight focus, $\pi R^2 \gg \lambda f$, and also that $\pi R^2 \gg \lambda(f+\epsilon)$, then Eq. (12) becomes

$$2 \tan^{-1} \left[\frac{\pi R^2 \epsilon}{\lambda f^2} \right] = \alpha \left[\frac{\pi}{2} + \tan^{-1} \left[\frac{\pi R^2}{\lambda f} \right] \right]. \tag{13}$$

We now assume that $(\pi R^2 \epsilon)/(\lambda f^2) < 1$. Since the second \tan^{-1} argument is much greater than 1, two different series expansions of \tan^{-1} must be employed. Keeping only the lower power terms of quantities less than 1, we find⁸

$$\Delta L = 2\epsilon \approx \frac{\alpha \lambda f^2}{R^2}. \tag{14}$$

Since the length ΔL only includes a fraction α of the return signal, it should be multiplied by $1/\alpha$ to represent 100% of the returned signal. This cancels α in Eq. (14) and yields

$$\text{SNR}_{\text{VM}} = G \frac{\lambda f^2}{R^2} \beta, \tag{15}$$

which is identical to Eqs. (5) and (6). Therefore Eqs. (5) and (6) are correct, but ΔL is adjusted to account for 100%, not 50%, of the detected signal, as it should be. There is no intrinsic factor of 2 error. Returning to our two assumed inequalities for ϵ , and using Eq. (14), we find that they require $\alpha < 2\pi R^4/(\lambda^2 f^2) \approx 17724$ and $\alpha > 2/\pi = 0.64$, which is quite reasonable.

3.2 Single Particle Mode

A third technique for determining β is called the single particle mode.^{1,2,9-12} The lidar system is focused to a short range (tight focus) and the detected signal is examined for the signature of individual aerosol particles passing through the transmitted beam. If the lidar is airborne and

its beam is perpendicular to the aircraft velocity, then the particles may be assumed to pass through the beam perpendicular to the optical axis. Since the lidar beam has a Gaussian intensity profile, the aerosol particle signature is expected to have a Gaussian shape. Each particle's signature will depend on its backscatter cross-section, σ [$\text{m}^2/\text{particle}$], and on its path of penetration through the beam, i.e. its position both along the optical axis and transverse to the optical axis. A measurement of the peak of a particle's signature does not alone yield the backscatter cross-section.

The number of peak signals of value S is given by

$$N(S) = L \int_{\sigma_{\min}}^{\infty} A(S, \sigma) N(\sigma) d\sigma, \quad (16)$$

where L [m] is the length of the flight path, σ_{\min} is the minimum cross-section which can yield the peak signal value S , $A(S, \sigma)$ [m^2] is the projected area, on a plane perpendicular to the particle trajectories, of the beam volume which yields a peak signal value of S for a particle cross-section of σ , and $N(\sigma)$ [particles/ $\text{m}^3\text{-m}^2$] is the number of particles with cross-section σ per unit volume per unit σ increment. The lidar signal processor determines the peak height of each pulse which meets shape and width criteria and forms a histogram of counts vs peak height S . A large number of particles are typically used for each measurement, so that a uniform spatial distribution of particle trajectories utilizing all particle sizes can be assumed. Typically, this number is 10^4 . If L and $A(S, \sigma)$ are known, then $N(\sigma)$ may be found iteratively until a calculated histogram $N(S)$ matches the measured histogram. Values for $A(S, \sigma)$ are determined by spatial mapping of the system's sensitive volume.¹³ To retrieve $N(\sigma)$, the following algorithm is followed:

1. A physically reasonable model for the aerosol cross-section density $N(\sigma)$ is postulated.
2. The parameters of the model are postulated.
3. For the chosen model and its parameters, the expected histogram $N(S)$ is computed using Eq. (16) and the measured system sensitivity profiles.
4. The calculated histogram is compared to the measured histogram in a least mean square sense.

5. The parameters of the cross-section density are adjusted.

6. Steps 3-5 are repeated until a satisfactory match of histograms is achieved.

The single particle mode (SPM) backscatter coefficient, β_{SPM} [$\text{m}^{-1}\text{sr}^{-1}$ particle $^{-1}$], is then computed as

$$\beta_{\text{SPM}} = \frac{1}{4\pi} \int_0^{\infty} \sigma N(\sigma) d\sigma . \quad (17)$$

The factor of 4π [sr] is apparently introduced by assuming that the particle scatter is isotropic.

4. Data Analysis Procedures

Coherent Technologies, Inc. (CTI) received four magnetic tapes from W.D. Jones of NASA-MSFC which contained: 1) the FORTRAN source code of the MSFC program for analyzing the CW lidar data, 2) a calibration data file used by the FORTRAN program in calculating the volume mode backscatter, and 3) the flight data obtained during the Australian measurements. (Problems were encountered with the calibration data file, but a second copy sent via modem worked fine.) Much of the FORTRAN code had to be adapted and/or rewritten to allow it to run on our Digital Equipment Corporation MicroVax II computer. All flight data files were combined into a single flight database. This file was written as an unformatted, direct access file for rapid access of data records based on date and time. Comparison runs were done at MSFC and CTI on selected data, showing near identical results, and confirming the adaptation of the code to the MicroVax II computer.

The FORTRAN program was found to process the alternating data records (S+N) and noise records (N) in pairs. The data were collected with a 0.5 Hz switching rate, so that nominally 1 s data records are interleaved with 1 s noise records (i.e. a 2 s period). (Apparently the software does not allow a new record to start if the operator is in the process of entering a comment from the terminal. This potential bug should be investigated.) The processing of each record produced a single integer for volume mode backscatter V [counts] (32 bits) and an array (histogram) of integers S_i [counts] representing the number of single particle events which had a peak height in bin i of a 256-bin, 16-bit (0 to 65535) pulse height analyzer. The histogram included only particle

events which passed certain shape and width criteria. This testing is designed to eliminate, for example, multiple particle events and noise events. The number of counts in each of the bins was then summed for the data record (D) and for the noise record (N). The difference in these sums for record pair j was

$$ISUM_j = \sum_i S_{ij}^D - \sum_i S_{ij}^N . \quad (18)$$

$ISUM_j$ was summed for each record pair j and the sum after k record pairs was compared to an input single particle net count threshold NPART:

$$ISUM_k = \sum_{j=1}^k ISUM_j \geq NPART ? \quad (19)$$

Typical values for NPART appeared from the code to be 1000 or 10,000. Only when Eq. (19) was true did the signal processor calculate β_{VM} and β_{SPM} .

From this description, it is seen that the flight length and measurement time (spatial and temporal resolution) for calculating β_{VM} and β_{SPM} were entirely determined by the threshold on the SPM counts. Running the program produced highly variable spatial and temporal integration intervals for the β calculations. Furthermore, the processing often produced negative values of β_{VM} , while β_{SPM} was always positive. This occurred in low signal regions where S+N and N values were nearly equal. The FORTRAN program discarded these negative β_{VM} values, which presumably biased the overall volume mode backscatter results to higher values.

An example of the output values for 25 May 1986 is shown in Figure 5. Note that the time interval between calculated values of β is highly variable. Also, several calculations of β_{SPM} do not have a corresponding β_{VM} plotted. These represent occurrences of negative values of β_{VM} .

A perplexing result seen in Figure 5 is that the values of β_{SPM} were typically larger than the values of β_{VM} by factors of 40-90. This was quite consistent throughout the data. Earlier comparisons² also showed $\beta_{SPM} > \beta_{VM}$, but with only a factor of 4 difference. No explanation had been found.

In an effort to resolve the discrepancy and to improve the data analysis procedures and outputs, several changes were made to the FORTRAN code by CTI personnel:

1. The single particle net count threshold, NPART, was implemented as an input variable.
2. A negative particle net count cutoff was implemented. Occasionally the particle count difference between a data (S+N) record and its associated noise (N) record shows a large negative excursion. A value of $ISUM_k$ below -1000 causes the program to reset $ISUM_k$ to 0.
3. A cutoff for the elapsed time between records was implemented. If the time difference between two data records is greater than 60 s, the value of $ISUM_k$ is reset to 0. This prevented data that occurs before and after a period when the lidar is off from being combined into an estimate of β .
4. A cloud filter option was implemented. A flag was written to a data-noise record pair if the measurement was taken in a cloud. This was determined manually by comparing the single particle bin counts with the flight log from Dr. J.L. Gras. When anomalously high particle counts (especially in the high peak signal bins) occurred concurrently with reports of cloud occurrence in the flight log, the flag was set true. (In particular, bins 190, 192, and 256 often had high counts and were closely monitored. Bin 256 would contain the A/D output of 255 = 1111 1111B and represents all high peak signal values. Similarly, bin 192 would contain 1011 1111B and bin 190 would contain 1011 1101B. Perhaps bits 2 and 7 were often misread as 0 when they were actually 1.) During execution of the program, the user may choose to include or exclude "cloud" record pairs.

Five new data fields were also written to each record:

1. Cloud flag. This was described above in (4).
2. Altitude. Altitude as a function of time was computed for each day from data supplied to CTI by Dr. Gras. An altitude value was interpolated for each record by using

$$ALT = 146.2 [1 - (SP/QNH)^{0.1902}], \quad (20)$$

where ALT is altitude [kft], SP is static pressure [mbar], and QNH is sea level pressure [mbar]. Altitude data were entered directly from the flight log for 4 June 1986 from 1105 - 1218 hours due to a gap in Dr. Gras' data. (1 kft = 304.8 m; 1 atm = 1013 mbar.)

3. Latitude. Values as a function of time for each day were hand entered from the flight log supplied by W.D. Jones.
4. Longitude. Same as latitude.
5. TAS. True airspeed values were calculated for each record from data

supplied by Dr. Gras using

$$\text{TAS} = [2170 (273.15 + T) \text{ DP/SP}]^{0.5}, \quad (21)$$

where TAS is true airspeed [kt], T is corrected reverse flow temperature [K], and DP is differential pressure [mbar]. (1 knot = 6080 ft/hr = 1.151 mi/hr = 0.514 m/s.) The TAS had been permanently set at 170 knots in the code.

As an example of the usefulness of these changes, Figure 6 again shows the 25 May 1986 plot of β_{VM} vs time. The altitude of the CSIRO F-27 aircraft is also plotted vs time. "Cloud" record pairs were excluded, and a value of 1000 was used for NPART. (Recall that NPART still affects the timing of the β_{VM} calculations even if β_{SPM} is not desired.) The horizontal line segments near $\log(\beta) = -5.5$ represent the time intervals that the CW lidar was taking measurements. The calculated values of β_{VM} are plotted as horizontal line segments of varying length. The line segments indicate the time required to make that measurement of β_{VM} . Note that there are several times when the lidar is on, but that no value for β_{VM} is plotted. This can be due to 1) negative values of β_{VM} , 2) ISUM was reset to zero due to reaching the negative threshold or elapsed time threshold, or 3) ISUM never reached the value of NPART due to very clean air. The last possibility is the most probable since the trend of decreasing β_{VM} with increasing altitude is evident.

Although these changes to the program were very useful in reducing and plotting the data, the large differences between β_{VM} and β_{SPM} still remained. Several investigations such as varying the value of NPART were tried with no improvement. After several discussions with Bill Jones, we decided to concentrate solely on the volume mode backscatter coefficient. Plots were made of β_{VM} and aircraft altitude vs time for the remaining 14 days of measurements (in addition to 25 May 1986 in Figure 6) and these are given in the next section.

At this stage, negative values of β_{VM} still occurred and simply were not plotted. We investigated whether the data (S+N) and noise (N) records could get out of sync with the processing program, or be reversed in order, but no consistent pattern in the negative β_{VM} records supported this hypothesis. When cumulative probability plots were desired, as will be shown in the next section, it was not clear whether to include the effect of the negative β_{VM} values (which shifted positive β_{VM} values to higher cumulative probability

values) or to exclude them. We calculated the standard deviation σ_{β} using all the β_{VM} values and then tried excluding β_{VM} values (outliers) that were smaller than $\bar{\beta}_{VM} - A \sigma_{\beta}$, but it was hard to justify a particular value of A.

The negative values of β_{VM} appeared to indicate a problem with establishing the instrument zero for these flights. In addition, the instrumental zero offset appeared to be time-varying. This is plausible due to the Dicke switching technique employed to zero the CW lidar. This technique assumes that angle tuning of the laser beam will result in either all of the return signal energy or none of it being passed by the detection bandpass filter. However, previous flights of the CW lidar took place on board the now destroyed NASA CV-990 aircraft. The speed of the CSIRO F-27 aircraft was much less than the NASA CV-990 (170 vs 390 knots), and the lidar system position in the F-27 prevented a larger Dicke switching angle deviation (than in the CV-990) from being used. These two effects combined to cause a much closer spacing of the return signal spectrum positions. (The angles in the CV-990 were 7.98° and 4.65° for a differential Doppler shift of 2.18 MHz. In the F-27, the angles, given in Section 2, produced a differential Doppler shift of 920 kHz. The processor bandwidth was 800 kHz wide.) In addition, there was no automatic transmission of true airspeed (TAS) data to the lidar in the F-27, as there was in the CV-990, forcing the operator to manually tune the center frequency of the bandpass filter. (The center frequency is tunable from 2.5 to 7 MHz.) These effects all increased the probability that the aerosol backscatter was not fully transmitted by the bandpass filter in the "on" or "data" position, and that it was not fully blocked in the "off" or "noise" position. A time-varying zero offset would also be likely.

In order to investigate this hypothesis, a set of time intervals representing constant altitude flight of the F-27 was selected from the flight database. Rather than accumulate data-noise record pairs until $ISUM_k \geq NPART$, values of β_{VM} were calculated for each data-noise record pair. Therefore a varying number of β_{VM} calculations occurred in each time interval. For each time interval a mean value, $\bar{\beta}_{VM}$, was calculated. In order to examine only low backscatter flight segments, the value $\bar{\beta}_{VM}$ was rejected if the value of $ISUM_k$, with k records in that time interval, was larger than 100. Both positive and negative values of $\bar{\beta}_{VM}$ were accepted. (The mean altitude value for each time interval was also computed for later use.) Figure 7 shows a histogram of the

calculated values of $\bar{\beta}_{VM}$. Note the negative mean value of these calculated values, and that their standard deviation equals $2.28 \cdot 10^{-11} \text{ m}^{-1}\text{sr}^{-1}$. Using the same set of time intervals, the whole process was repeated, except that data records were skipped, and β_{VM} was calculated from noise-noise record pairs. The resulting histogram is shown in Figure 8, using the same time intervals that passed the $ISUM_k$ test for the data-noise record pairs. The noise-noise standard deviation was $3.14 \cdot 10^{-11} \text{ m}^{-1}\text{sr}^{-1}$. Since approximately twice as many values of β_{VM} were calculated in the data-noise case as in the noise-noise case for each time interval, we should scale the noise-noise standard deviation by $\sqrt{2}$:

$$\sigma_{eq} = 3.14 \cdot 10^{-11} / \sqrt{2} = 2.22 \cdot 10^{-11} \text{ m}^{-1}\text{sr}^{-1}, \quad (22)$$

which is very close to $2.28 \cdot 10^{-11}$ found from the data-noise pairs. It appears for this test case of time intervals, and for $ISUM_k < 100$, that the backscatter signal is completely overwhelmed by the noise (actually the time-varying instrument zero). This is supported by the positive mean value in Figure 8.

Since the standard deviation of the calculated values of $\bar{\beta}_{VM}$ in the noise-noise case, adjusted for the greater number of data-noise pairs, is approximately $2 \cdot 10^{-11} \text{ m}^{-1}\text{sr}^{-1}$, this value should be used for the overall instrument sensitivity during the Australian flight program. It is conceivable that the instrument zero fluctuations were smaller (or larger) during specific portions of the flight program. It is highly recommended that this limiting factor on instrument sensitivity be investigated and improved for future flights.

25 MAY 1986

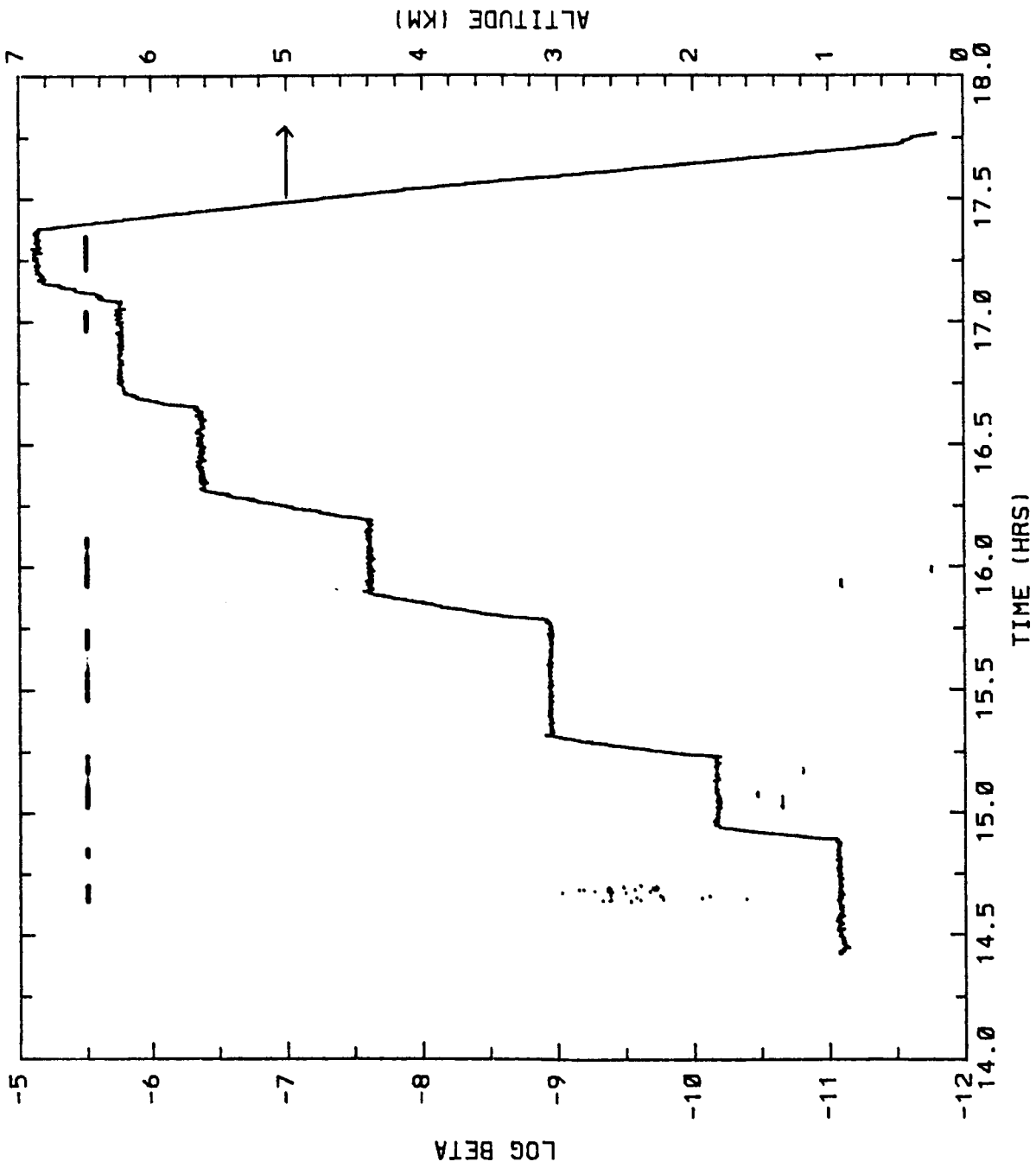


Figure 6. Volume mode backscatter and altitude vs time with clouds excluded.

HISTOGRAM PLOT OF BETA DISTRIBUTION

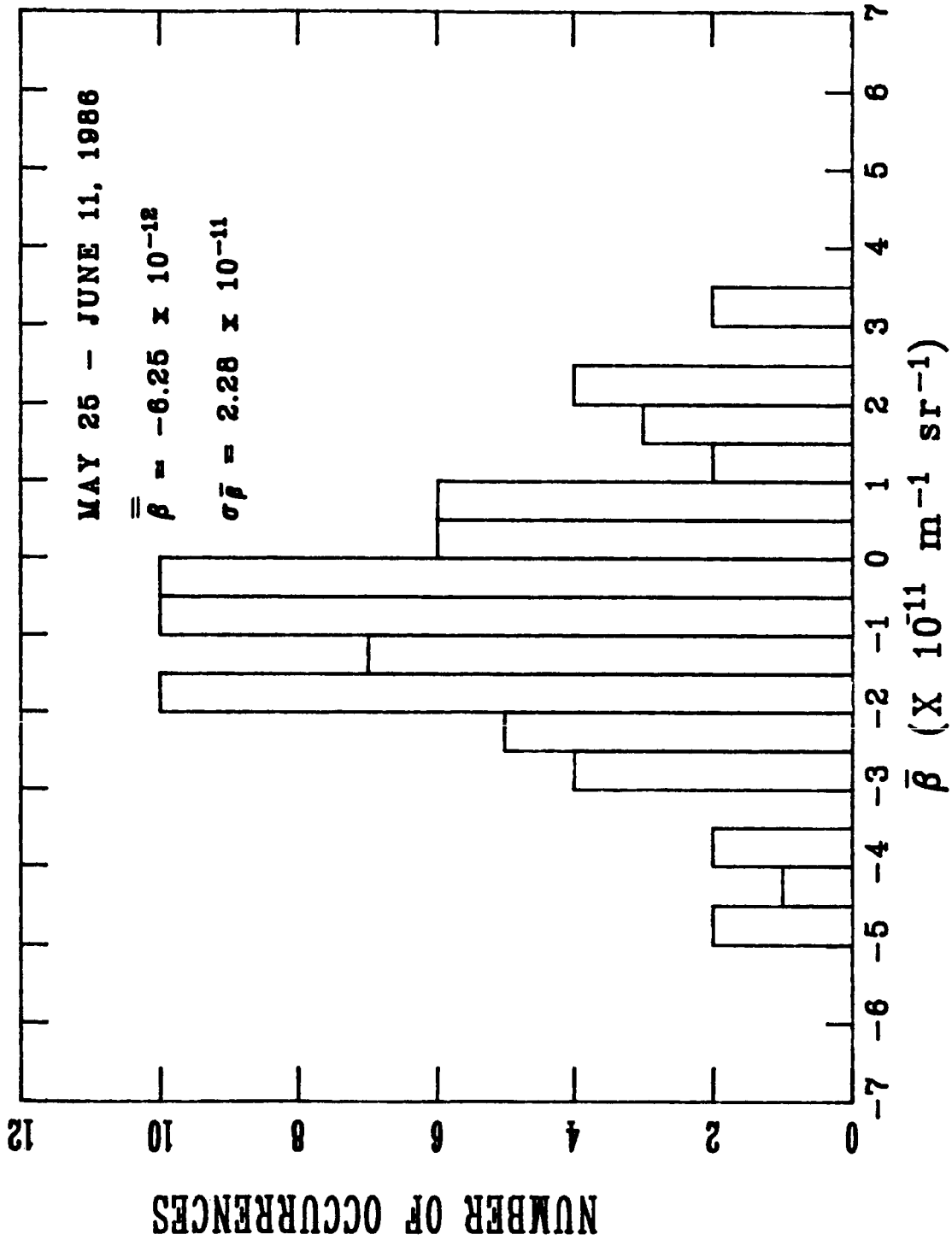


Figure 7. Histogram of calculated values using data-noise record pairs.

HISTOGRAM PLOT OF NOISE DISTRIBUTION

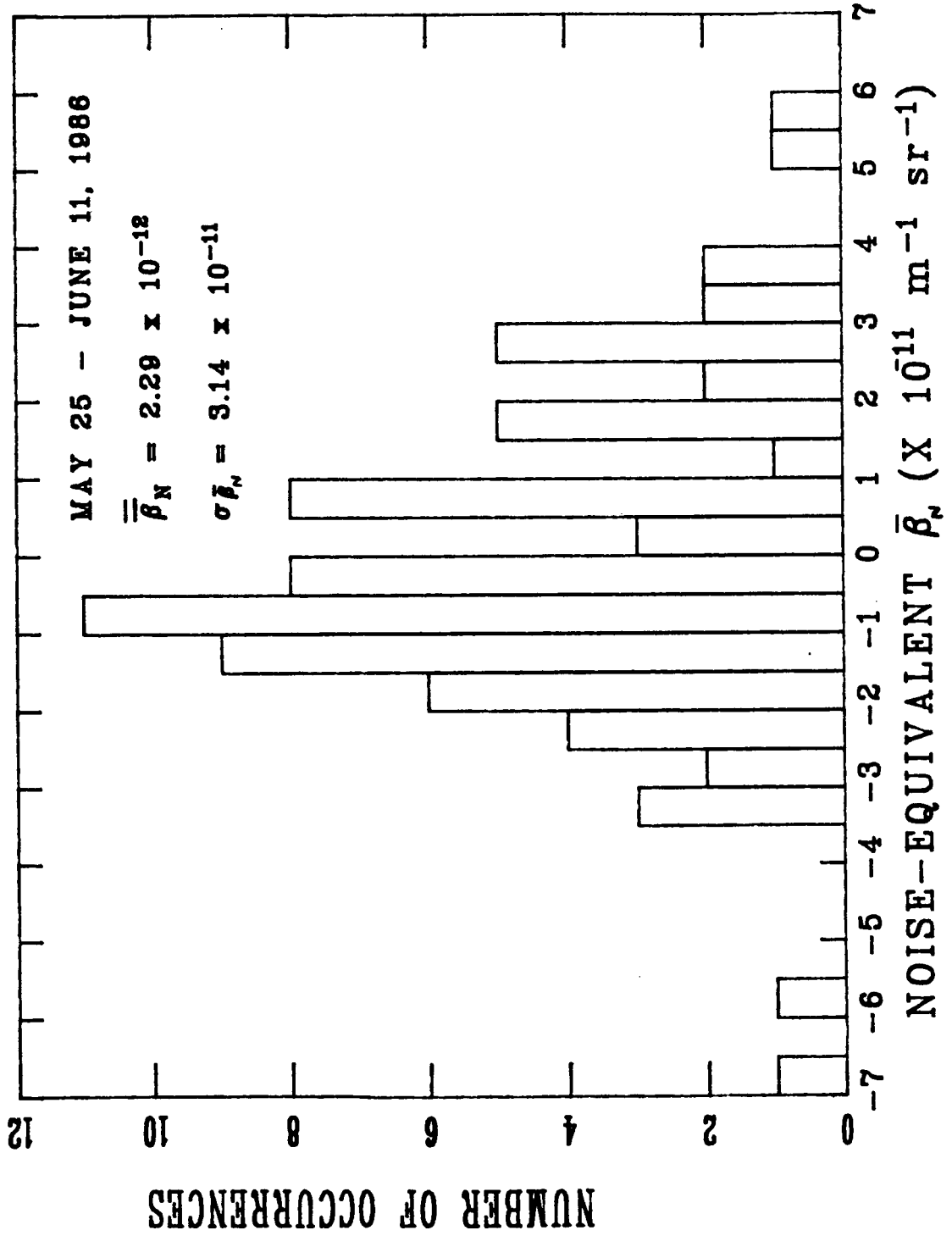


Figure 8. Histogram of calculated values using noise-noise record pairs.

5. Measurement Results

As discussed in the last section, plots identical to Figure 6 were made for the other days of the flight program. These are shown in Figures 9-22. Recall that "cloud" record-pairs are excluded, NPART = 1000, negative values of β_{VM} are thrown away, the length of each β_{VM} horizontal line segment shows over what period of time it is calculated, and the horizontal line segments near $\log(\beta) = -5.5$ show when the CW lidar was taking measurements. Figure 23 gives the geometric mean backscatter coefficient vs altitude for the entire flight program.

Figure 24 shows all of the calculated "cloud-free" backscatter values from the entire measurement program plotted vs altitude. Error bars equal to $\pm 1 \sigma_{eq} = \pm 2.22 \cdot 10^{-11} \text{ m}^{-1}\text{sr}^{-1}$ are plotted on each point. The right-hand error bar can be seen for many points that are not plotted, which results if $\beta_{VM} < 10^{-13}$, including the negative values of β_{VM} . (The length of the constant value error bars depends on the absolute position on the $\log \beta$ plot.) The values of β_{VM} that are clearly above the instrument sensitivity occur below 2 km and also near 4.5 km. Figures 25 and 26 show the data from Figure 24 divided into 0-25 S and 25-45 S latitude bands. Figure 27 shows the cumulative probability plot of "cloud-free" β_{VM} for the whole measurement program, but only for altitudes between 3 and 7 km. The median value of β_{VM} is $3 \cdot 10^{-11} \text{ m}^{-1}\text{sr}^{-1}$. Finally, Figure 28 shows the cumulative probability divided into four latitude bands. The median values of β_{VM} differ by about an order of magnitude, with the largest value and the greatest variability (slope) occurring in the 0-15 S latitude band.

6. Conclusions

The MSFC CW CO₂ lidar was adapted for the CSIRO F-27 airplane, shipped to Australia, and used successfully to measure aerosol backscatter at $\lambda = 10.6 \text{ }\mu\text{m}$ during a 2.5-week measurement program in May-June 1986. The lidar data and data analysis FORTRAN program were transferred to Coherent Technologies, Inc. CTI personnel implemented several improvements to the code for reducing and displaying the lidar data. An instrument zero offset problem was identified that was time varying and that was likely aggravated due to several aspects of the F-27 aircraft. Several suggestions for improving instrument calibration and sensitivity were made. The Australian backscatter data were presented as a function of time, altitude, latitude, and statistical parameters.

26 MAY 1986

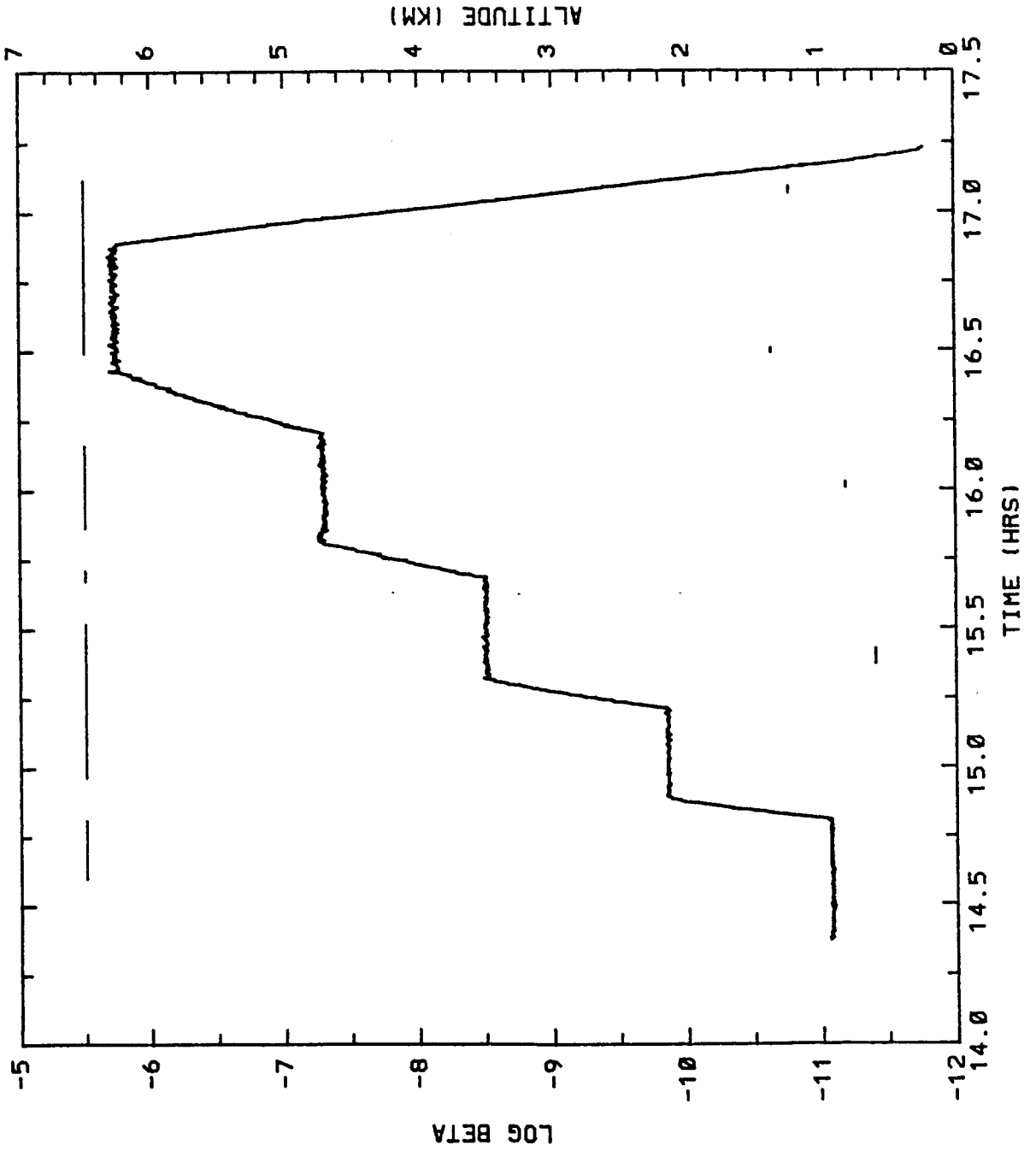


Figure 9. Volume mode backscatter and altitude vs time with clouds excluded.

C-2

NASA CW CO₂ LIDAR AEROSOL BACKSCATTER, AIRCRAFT
ALTITUDE AND INSTRUMENT STATUS

27 MAY 1986

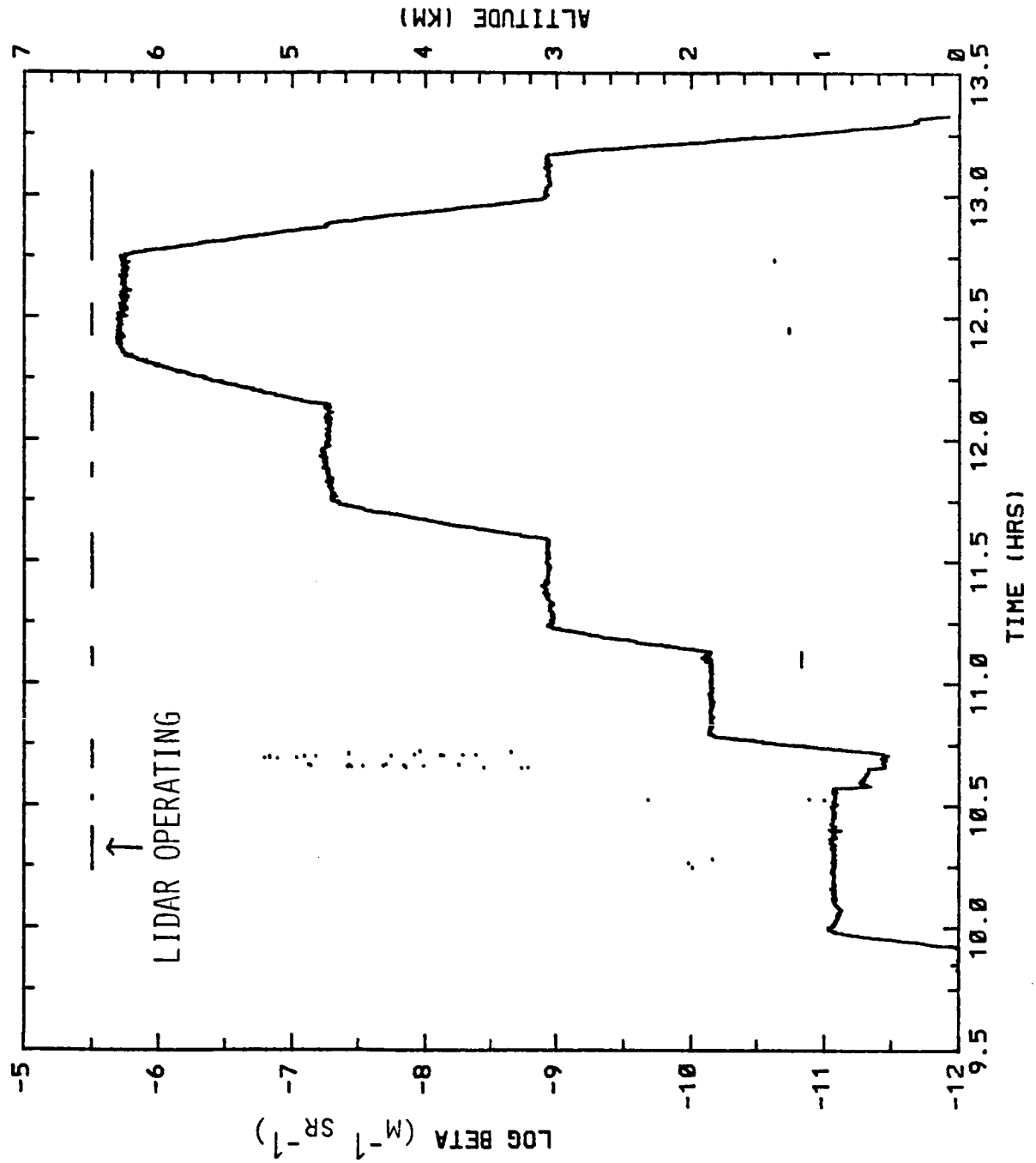


Figure 10. Volume mode backscatter and altitude vs time with clouds excluded.

29 MAY 1986

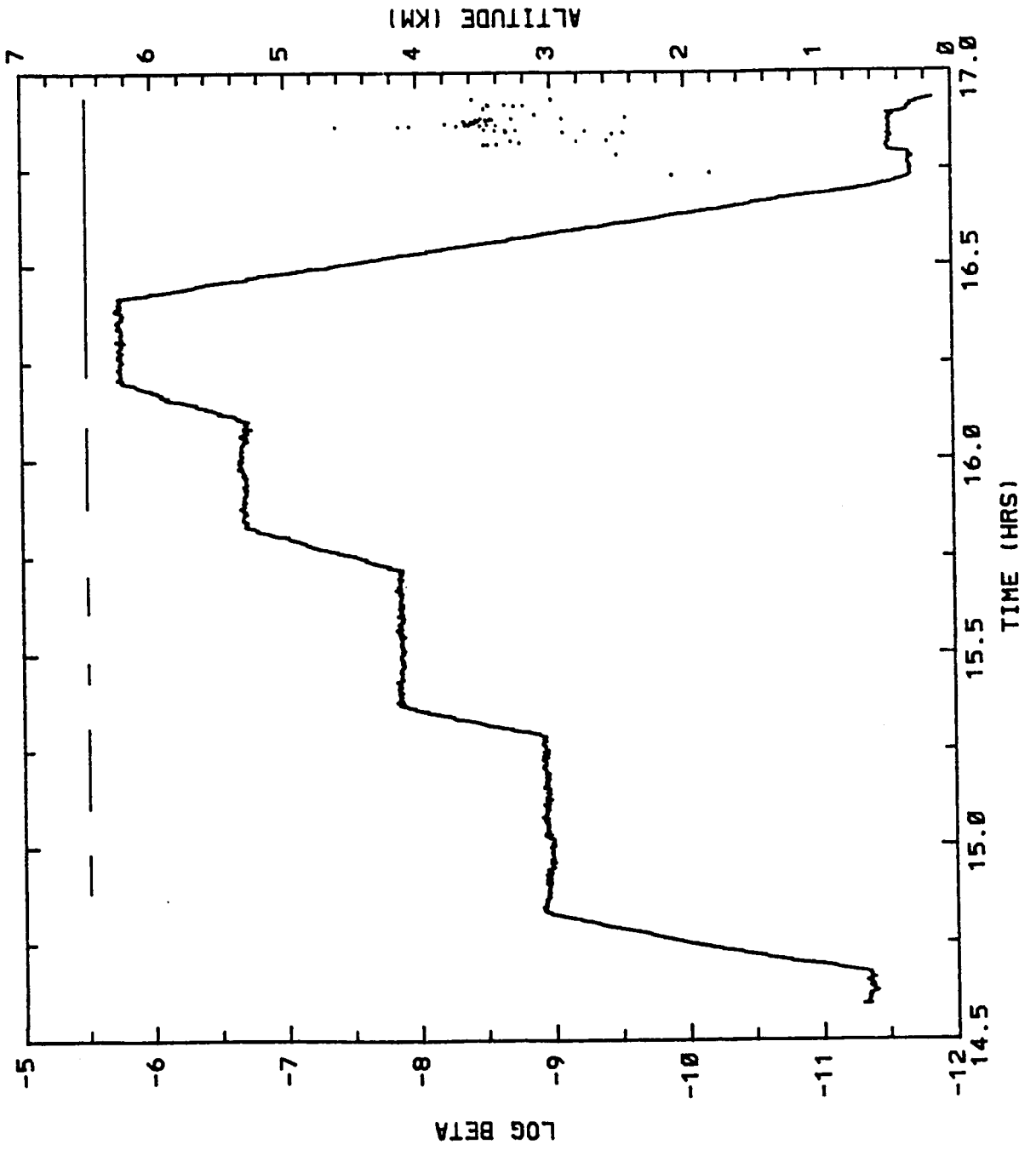


Figure 11. Volume mode backscatter and altitude vs time with clouds excluded.

NASA CW CO₂ LIDAR AEROSOL BACKSCATTER. AIRCRAFT
ALTITUDE AND INSTRUMENT STATUS

30 MAY 1986

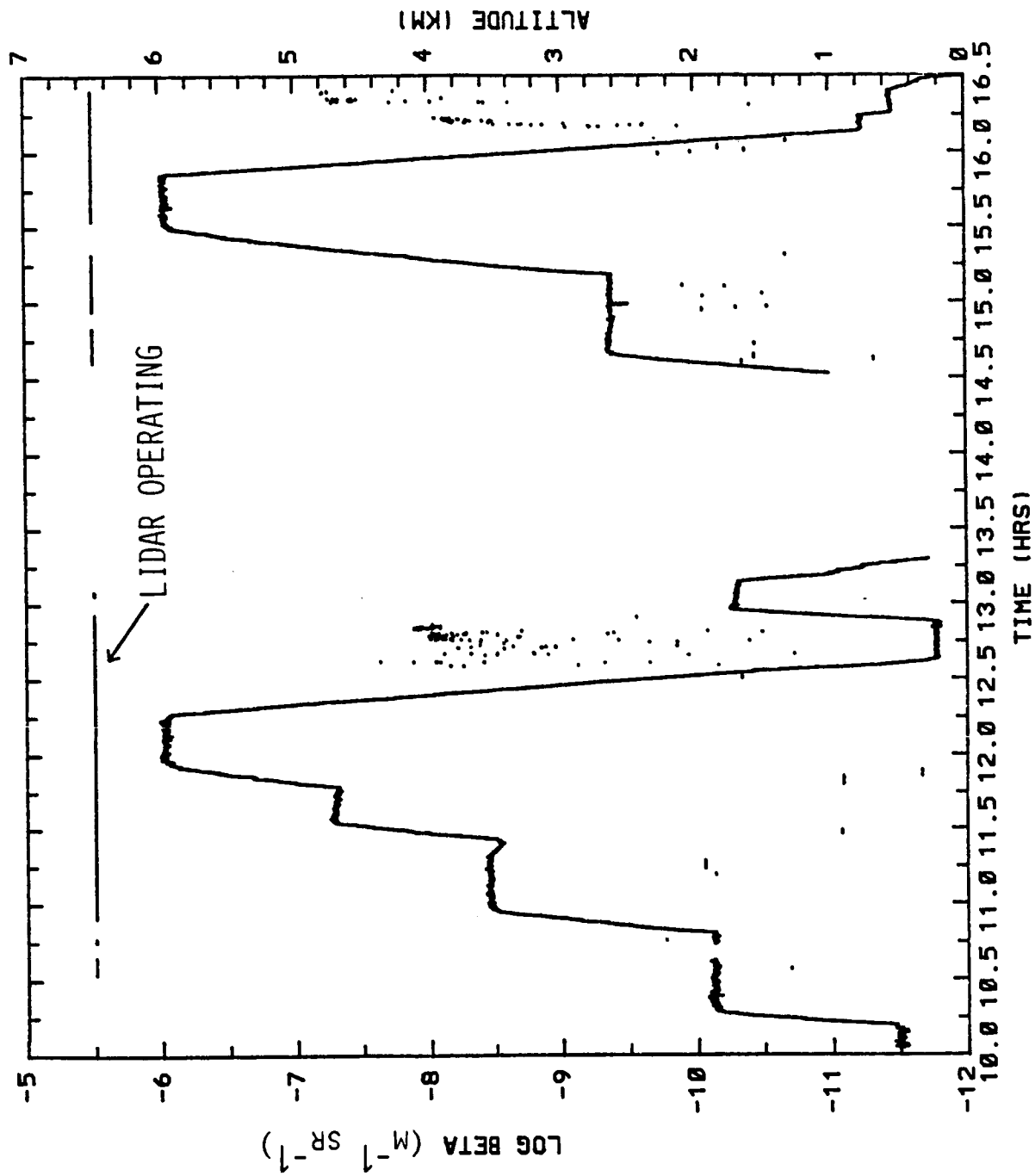


Figure 12. Volume mode backscatter and altitude vs time with clouds excluded.

31 MAY 1986

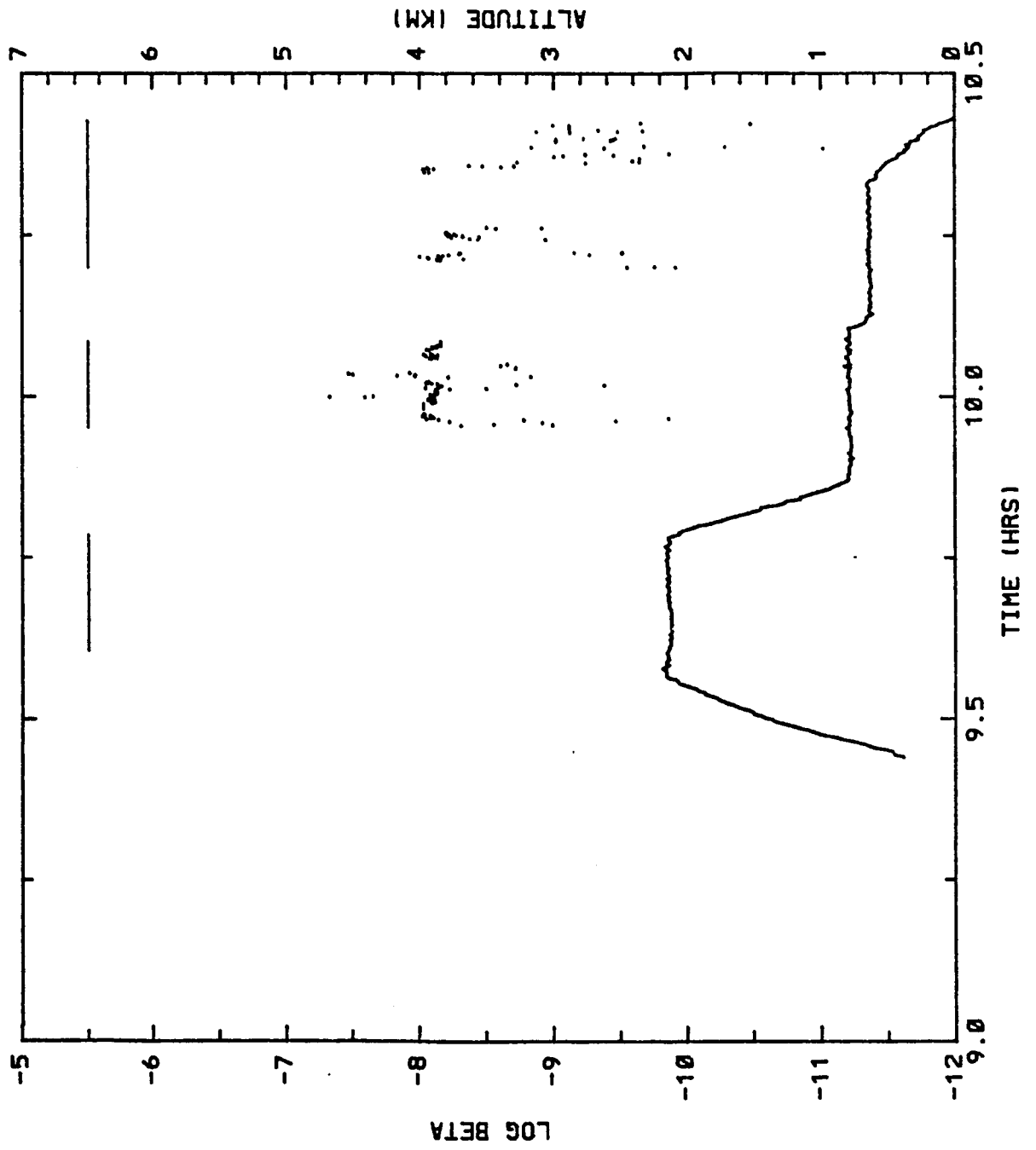


Figure 13. Volume mode backscatter and altitude vs time with clouds excluded.

1 JUNE 1986

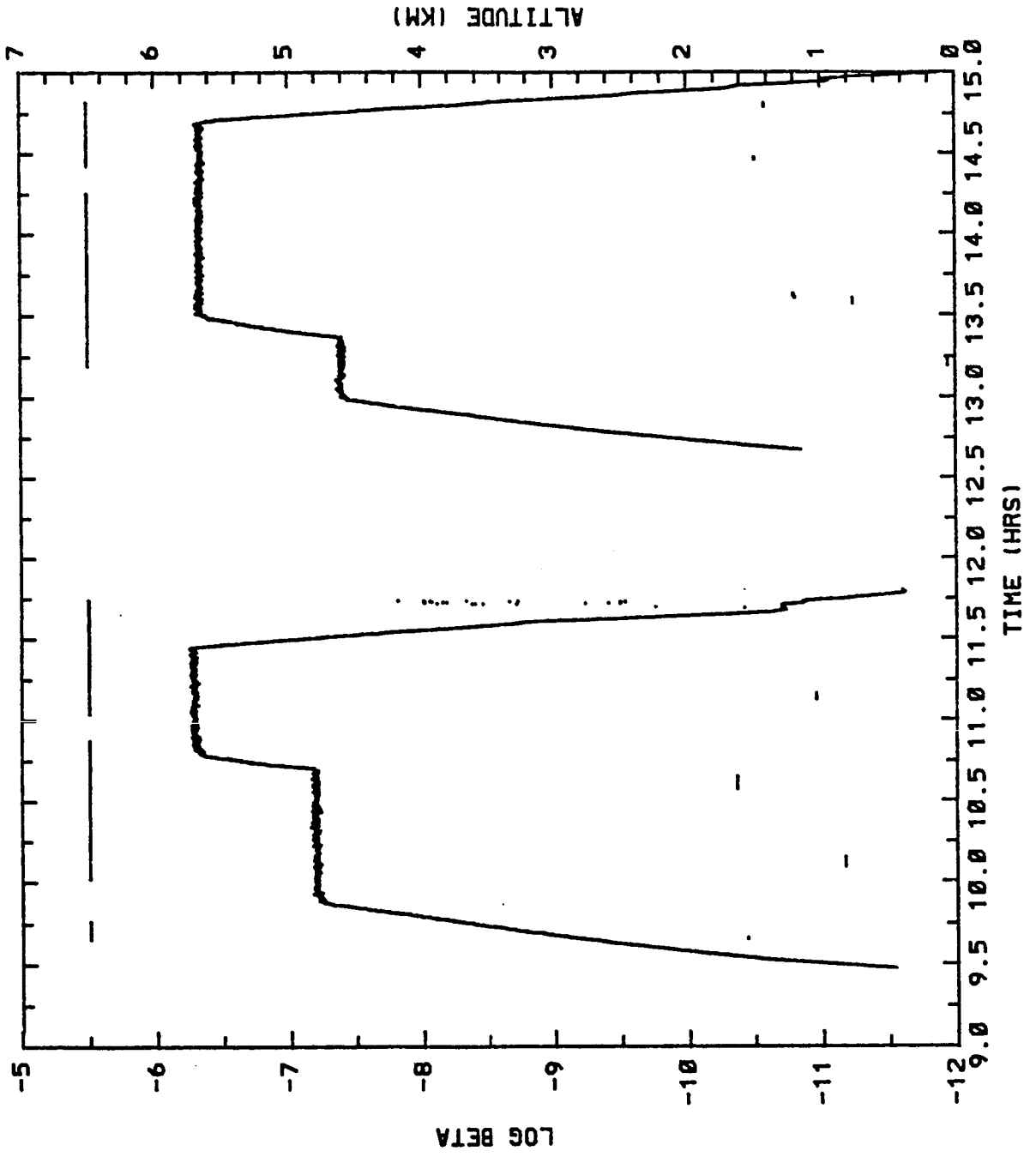


Figure 14. Volume mode backscatter and altitude vs time with clouds excluded.

2 JUNE 1986

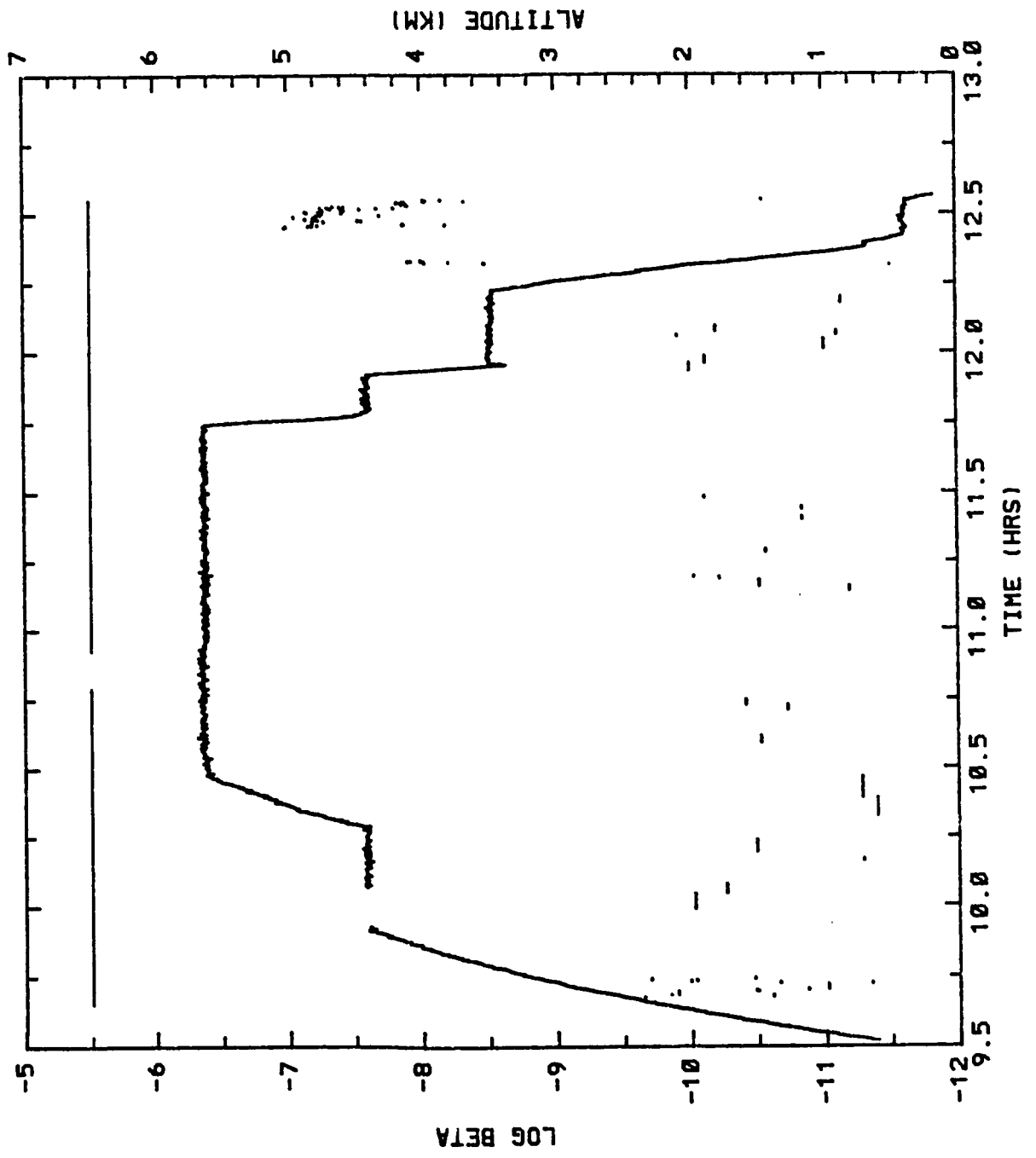


Figure 15. Volume mode backscatter and altitude vs time with clouds excluded.

4 JUNE 1986

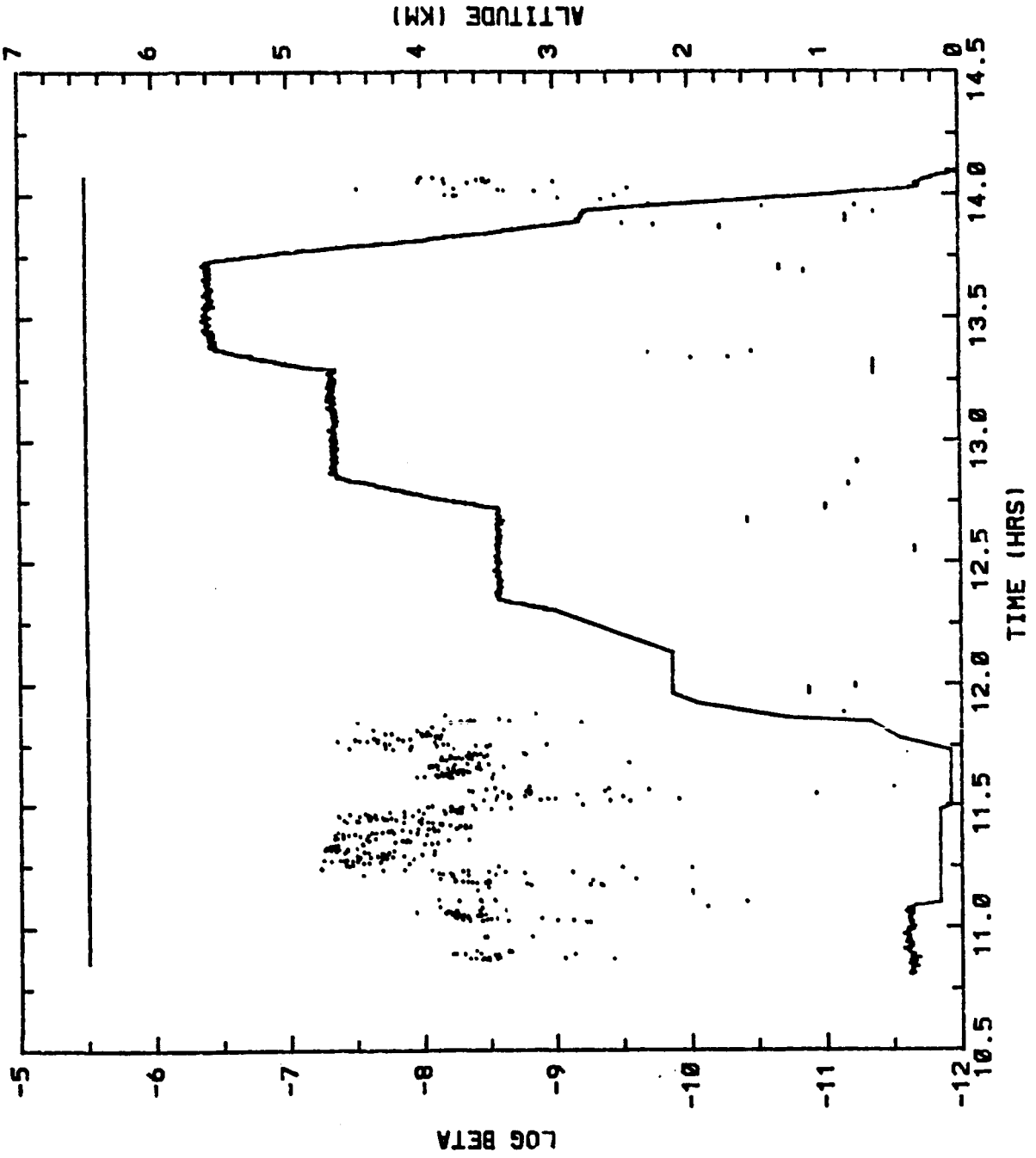


Figure 16. Volume mode backscatter and altitude vs time with clouds excluded.

NASA CW CO₂ LIDAR AEROSOL BACKSCATTER, AIRCRAFT
ALTITUDE AND INSTRUMENT STATUS

5 JUNE 1986

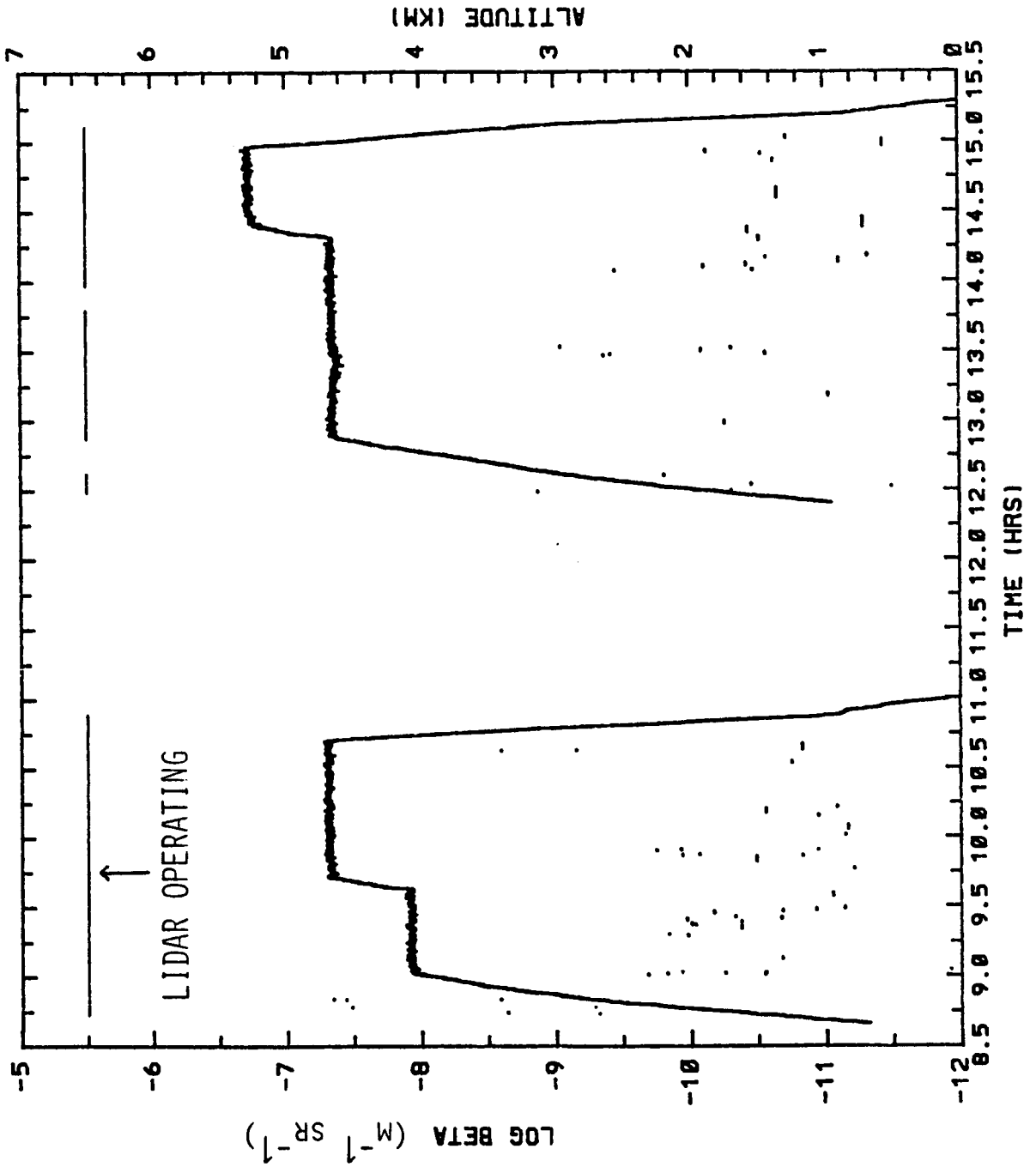


Figure 17. Volume mode backscatter and altitude vs time with clouds excluded.

7 JUNE 1986

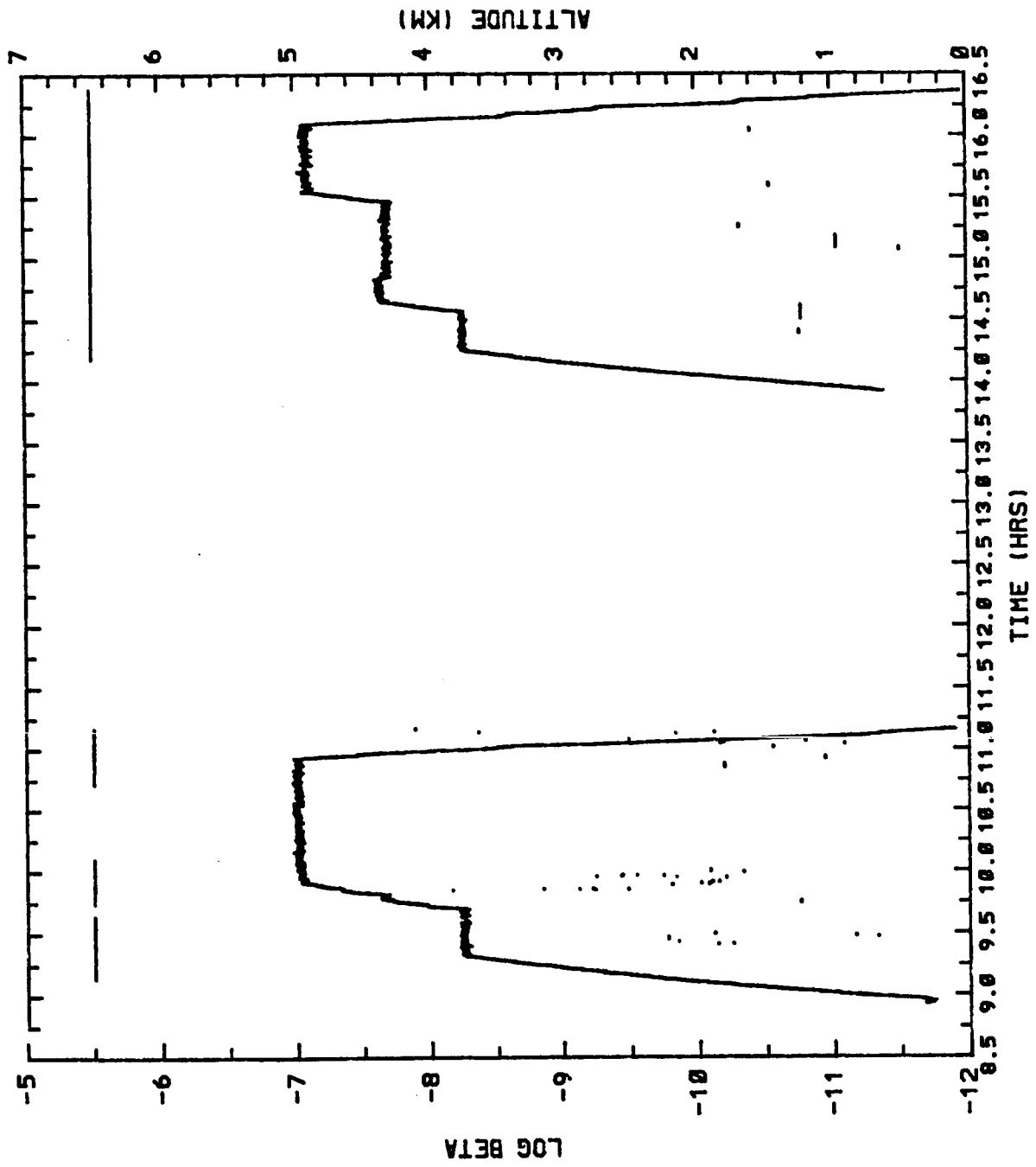


Figure 18. Volume mode backscatter and altitude vs time with clouds excluded.

8 JUNE 1986

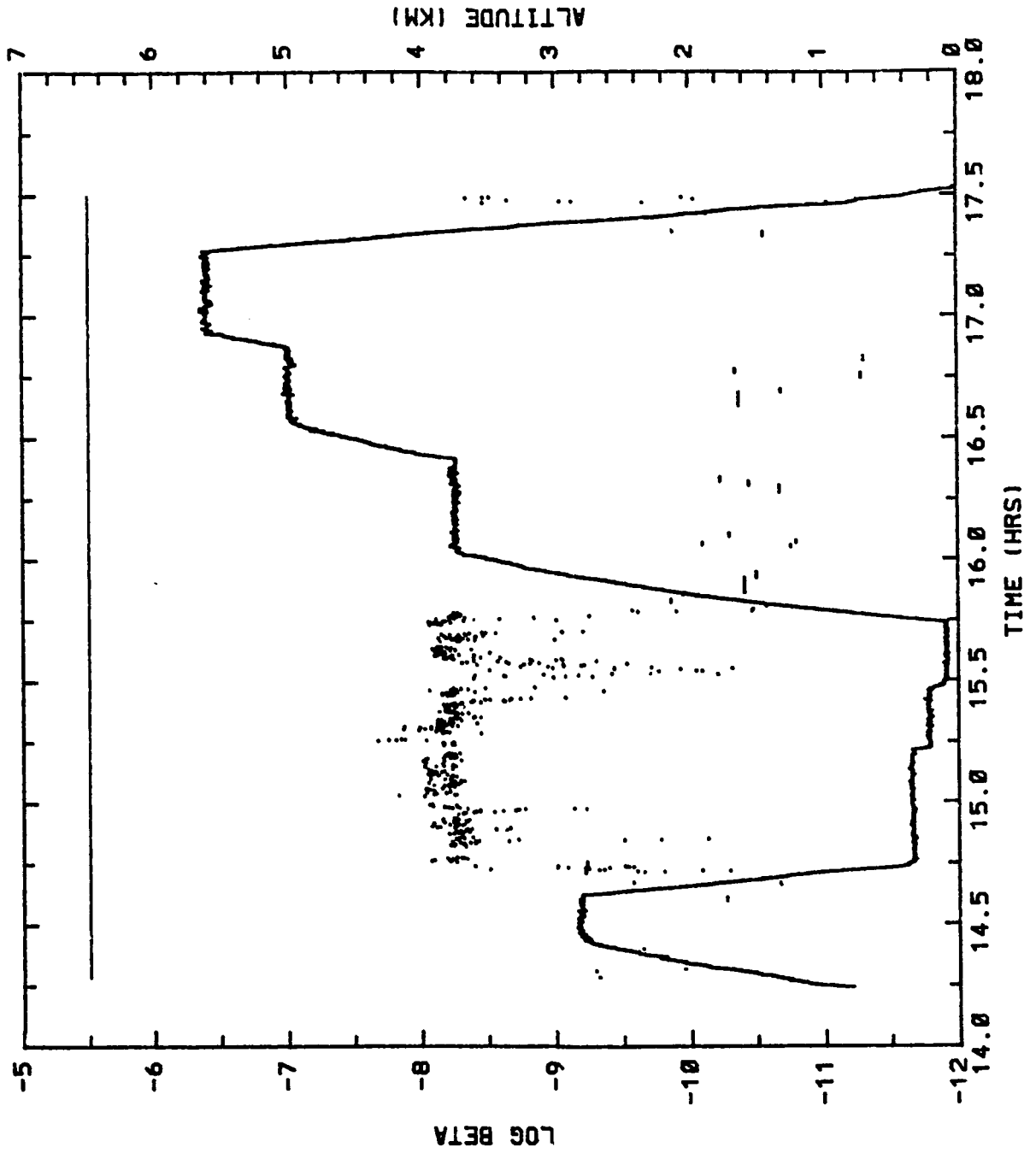


Figure 19. Volume mode backscatter and altitude vs time with clouds excluded.

9 JUNE 1986

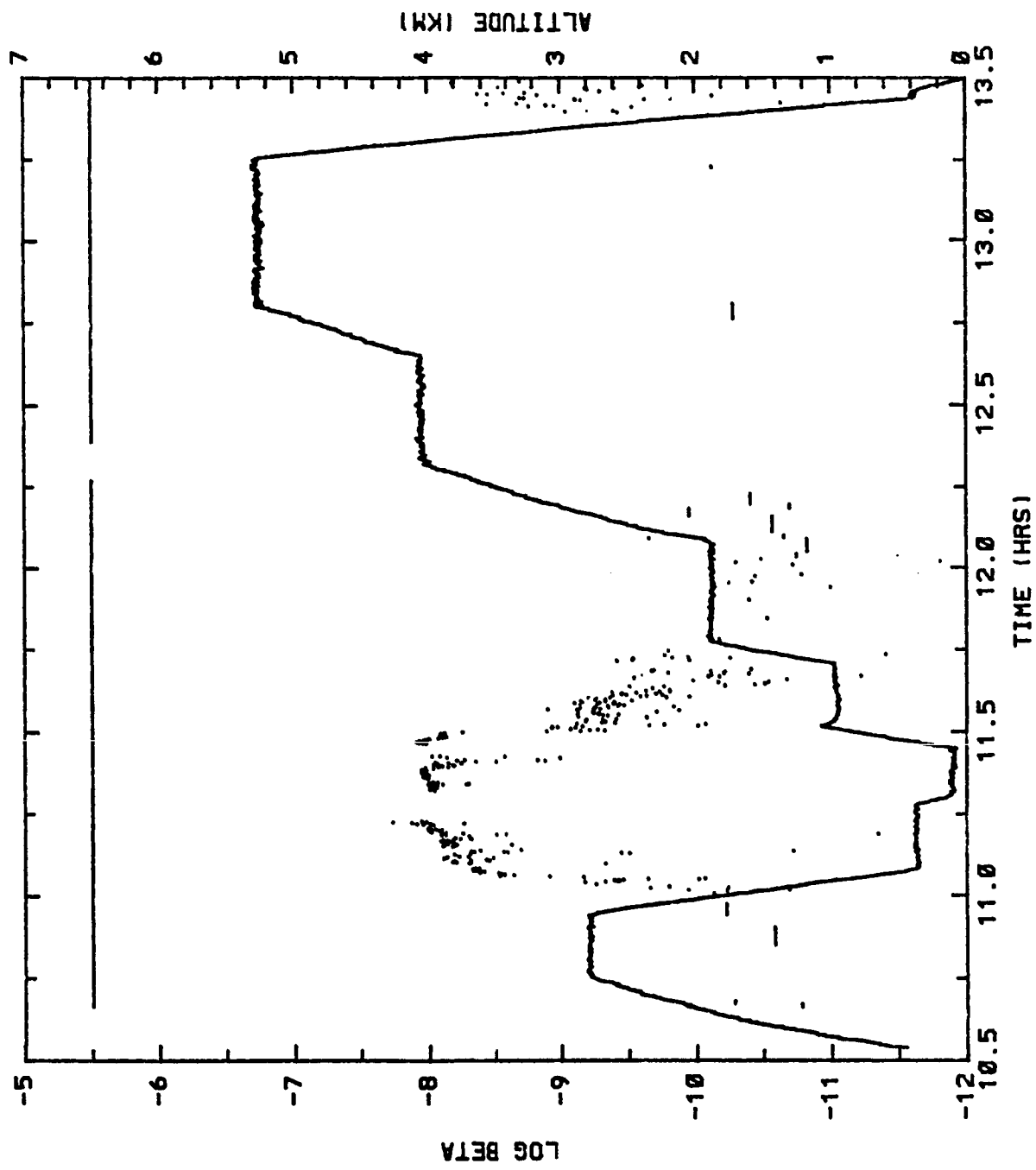


Figure 20. Volume mode backscatter and altitude vs time with clouds excluded.

10 JUNE 1986

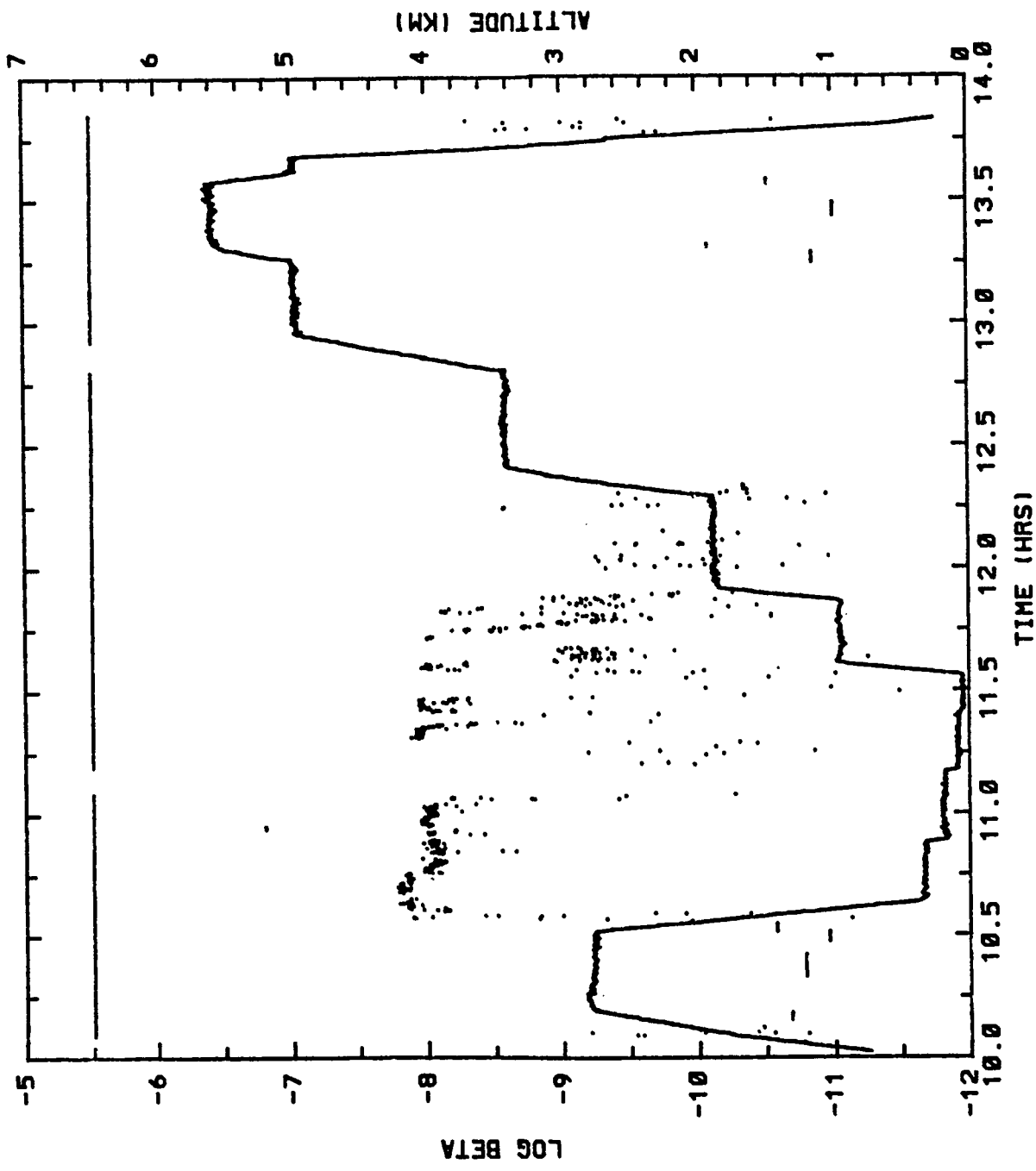


Figure 21. Volume mode backscatter and altitude vs time with clouds excluded.

11 JUNE 1986

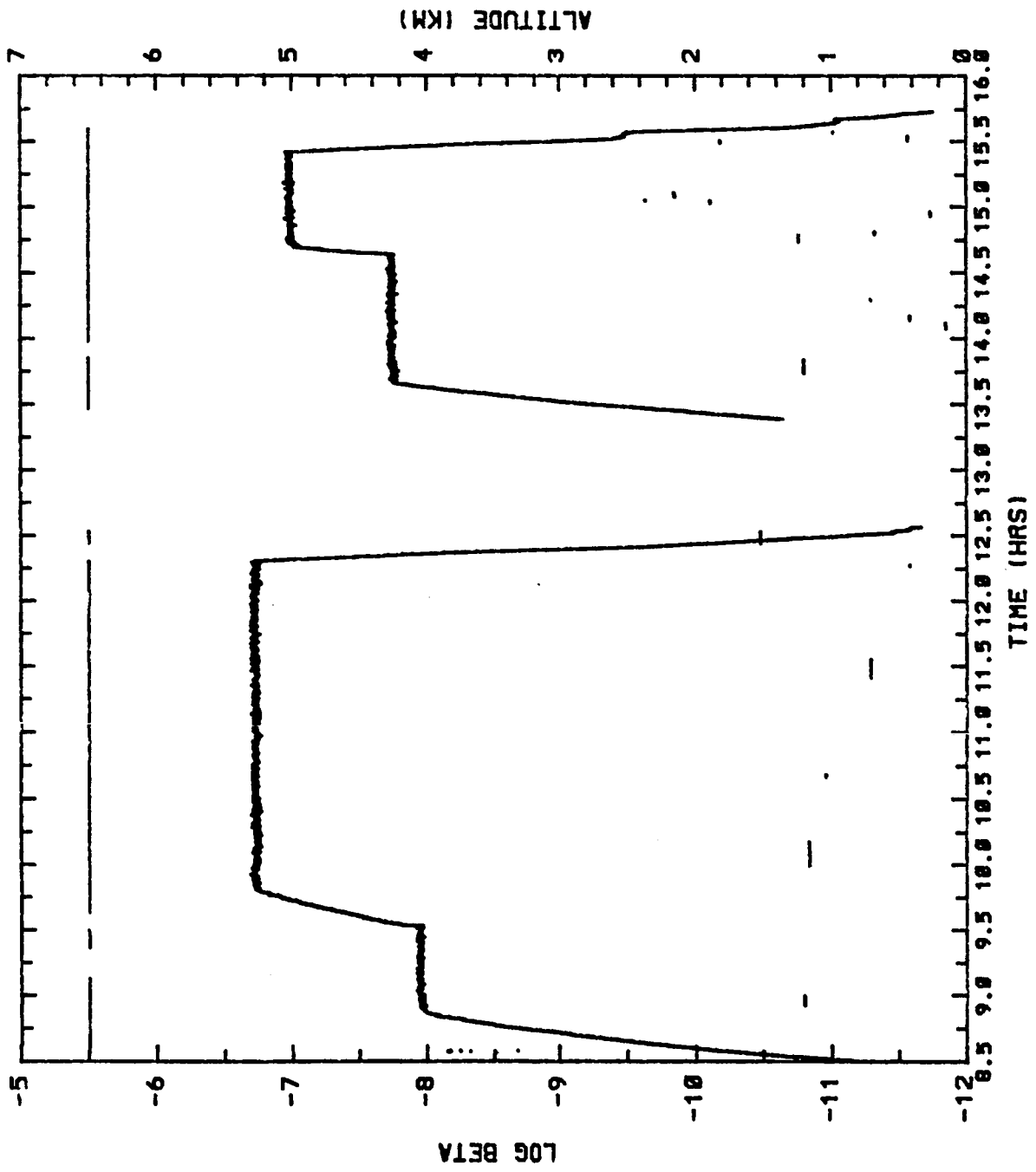


Figure 22. Volume mode backscatter and altitude vs time with clouds excluded.

Geometric mean β

May 25 - June 11

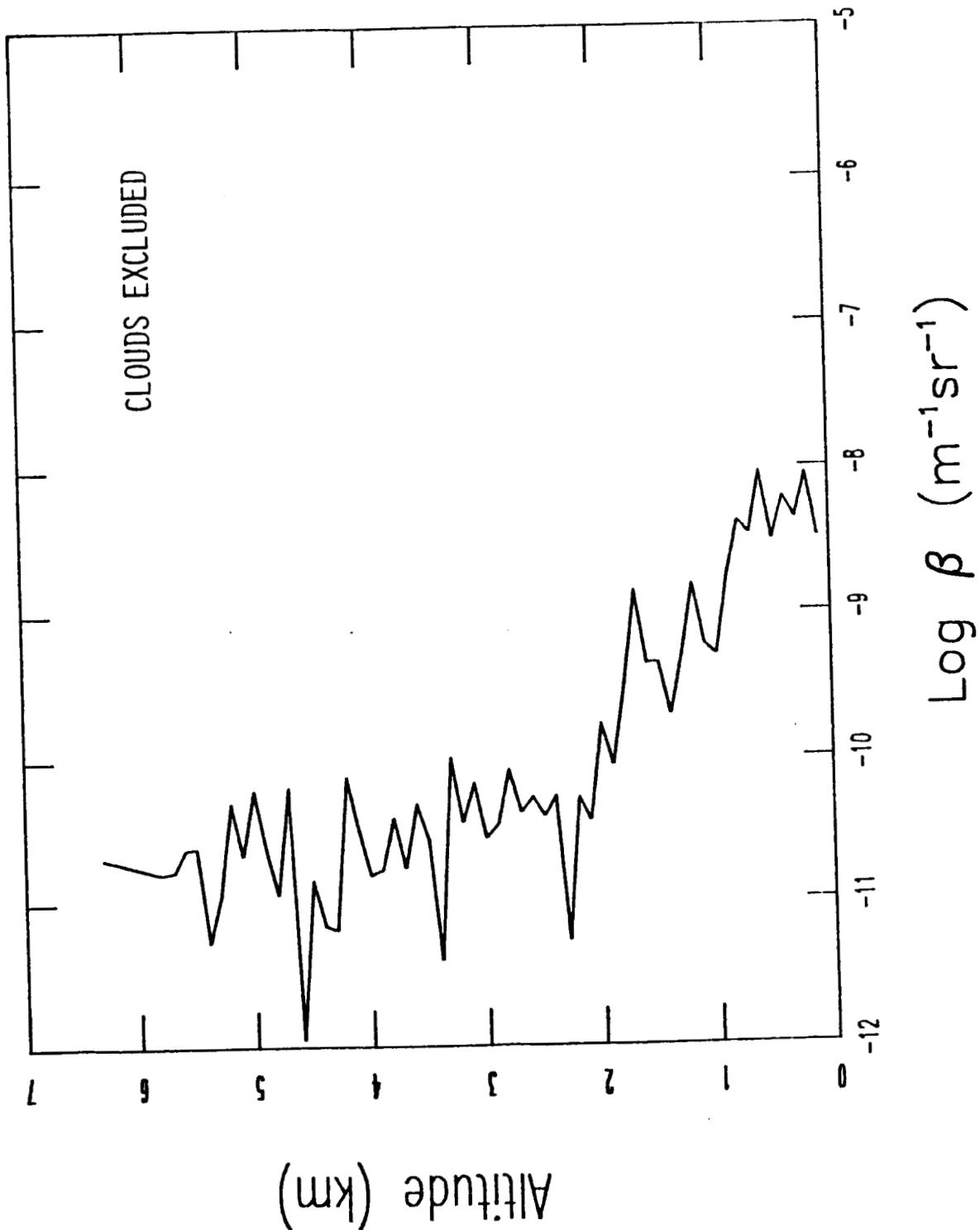


Figure 23. Mean backscatter coefficient vs altitude with clouds excluded.

NASA CW CO₂ LIDAR MEASURED BACKSCATTER

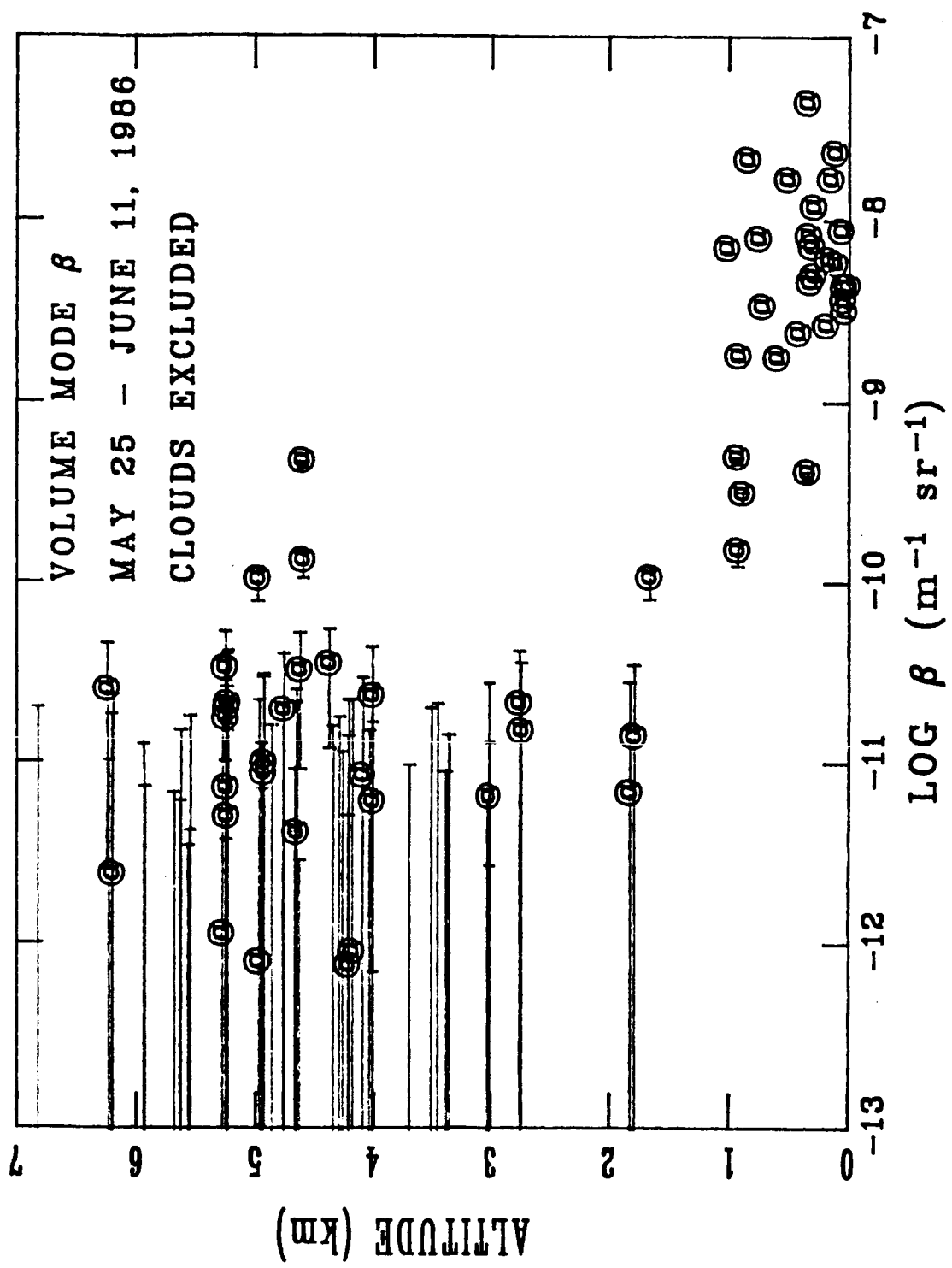
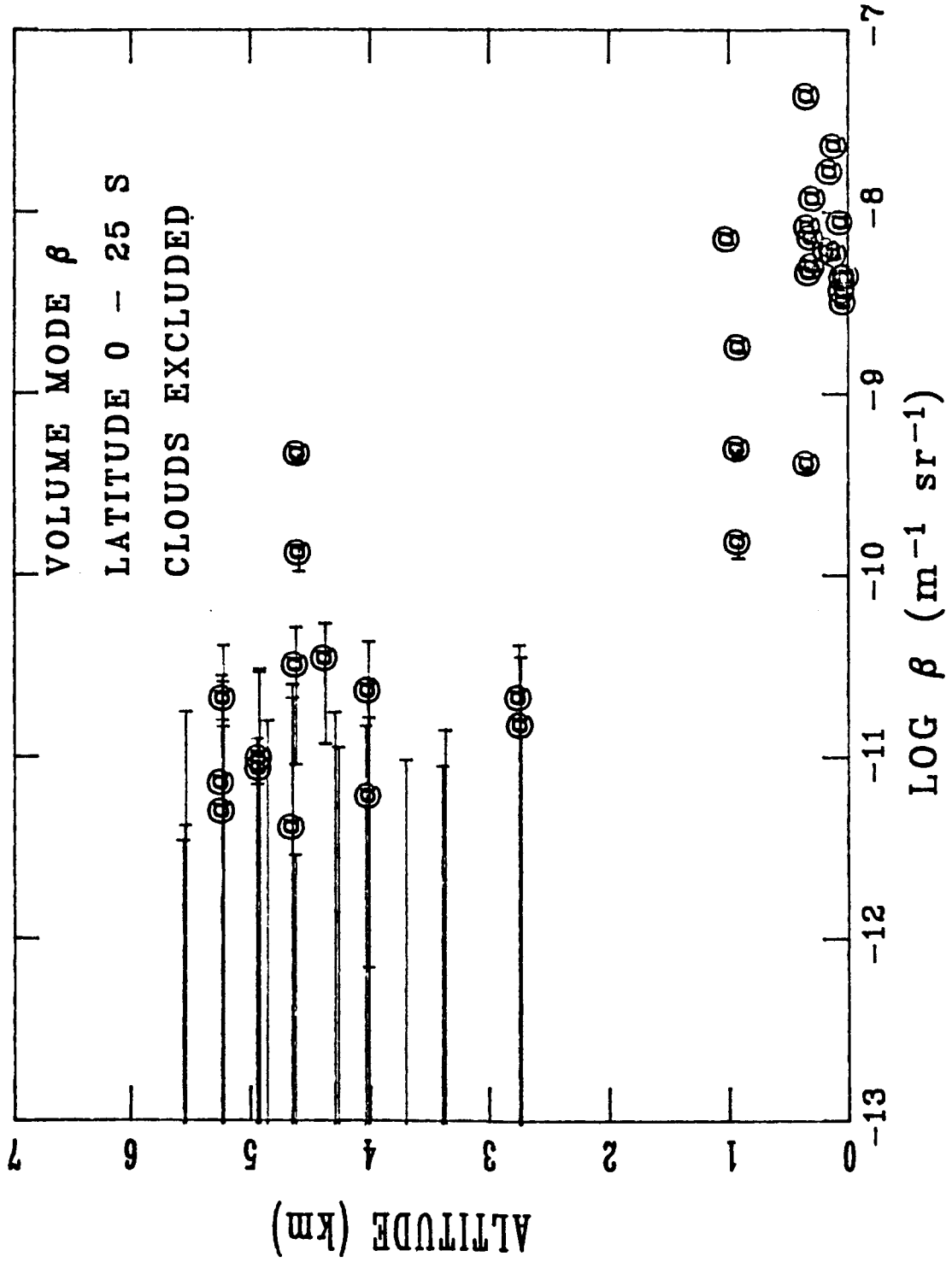


Figure 24. Backscatter coefficient vs altitude with $\pm 1\sigma$ error bars.

NASA CW CO₂ LIDAR MEASURED BACKSCATTER



NASA CW CO₂ LIDAR MEASURED BACKSCATTER

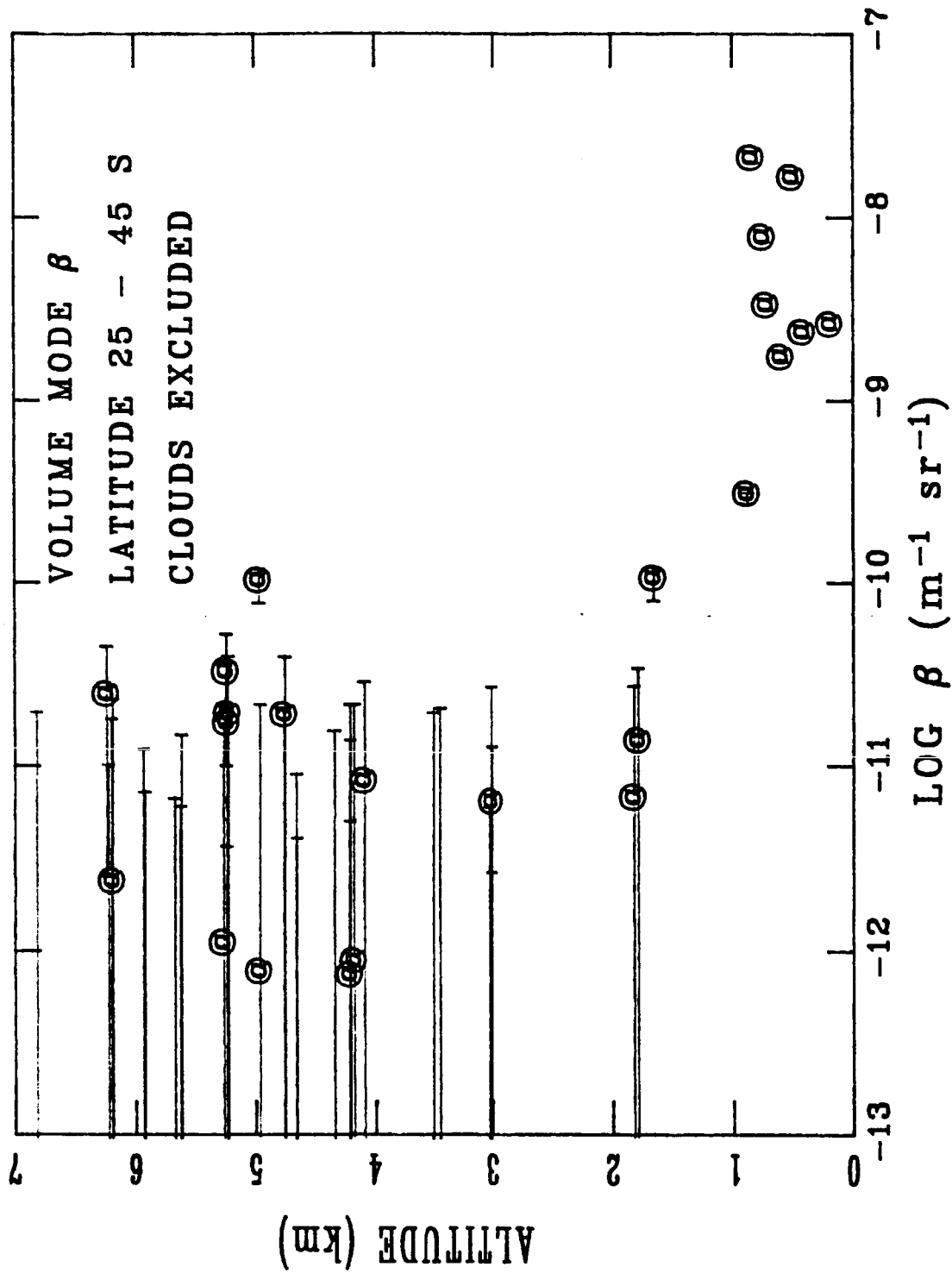


Figure 26. Same as Fig. 24 with only 25 - 45 S latitude.

NASA CW CO₂ LIDAR MEASURED BACKSCATTER

MAY 25 - JUNE 11, 1986
AUSTRALIA

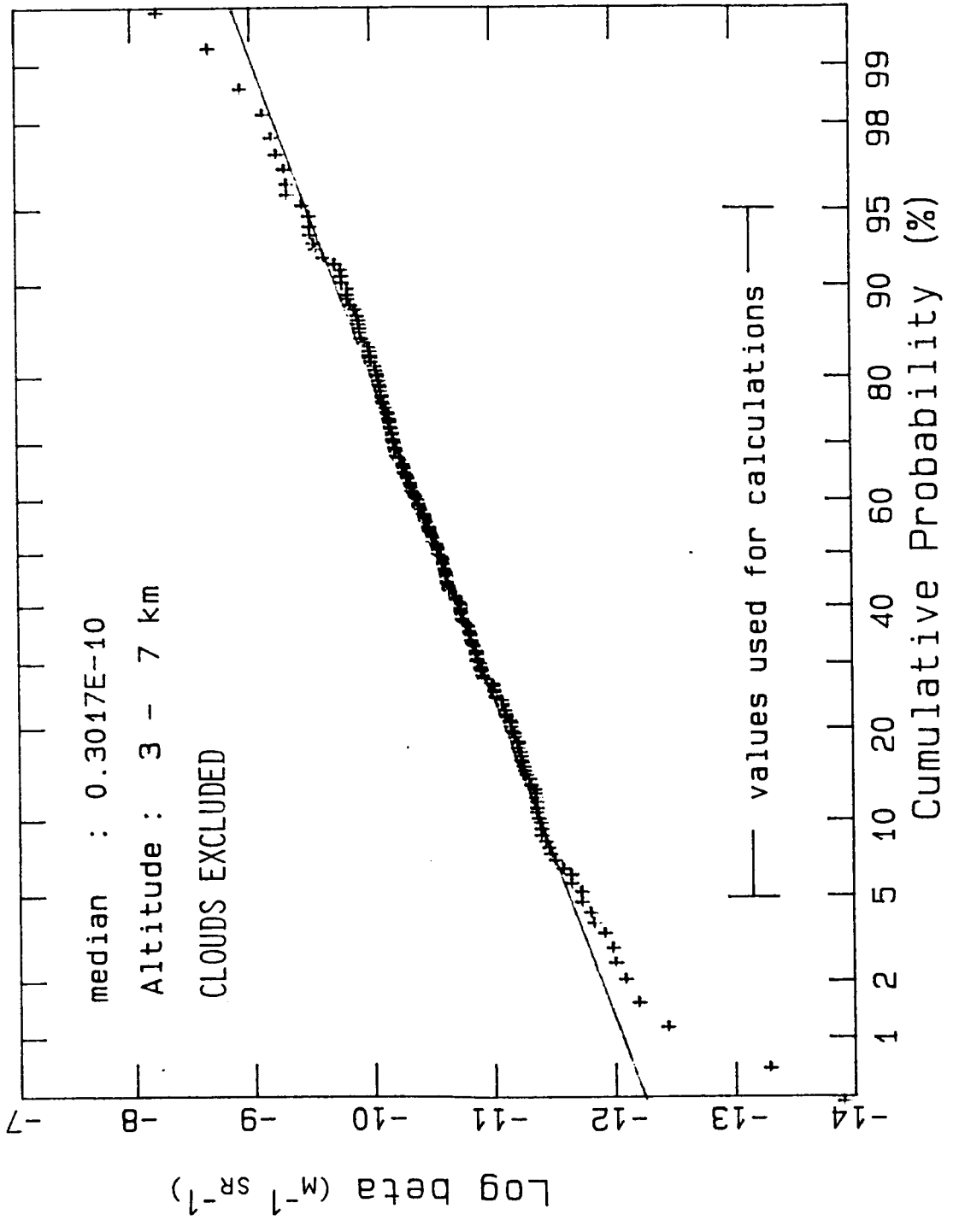


Figure 27. Cumulative probability plot of volume mode backscatter for 3 - 7 km altitude.

NASA CW CO₂ LIDAR MEASURED BACKSCATTER

MAY 25 - JUNE 11, 1986
 AUSTRALIA, NEW GUINEA

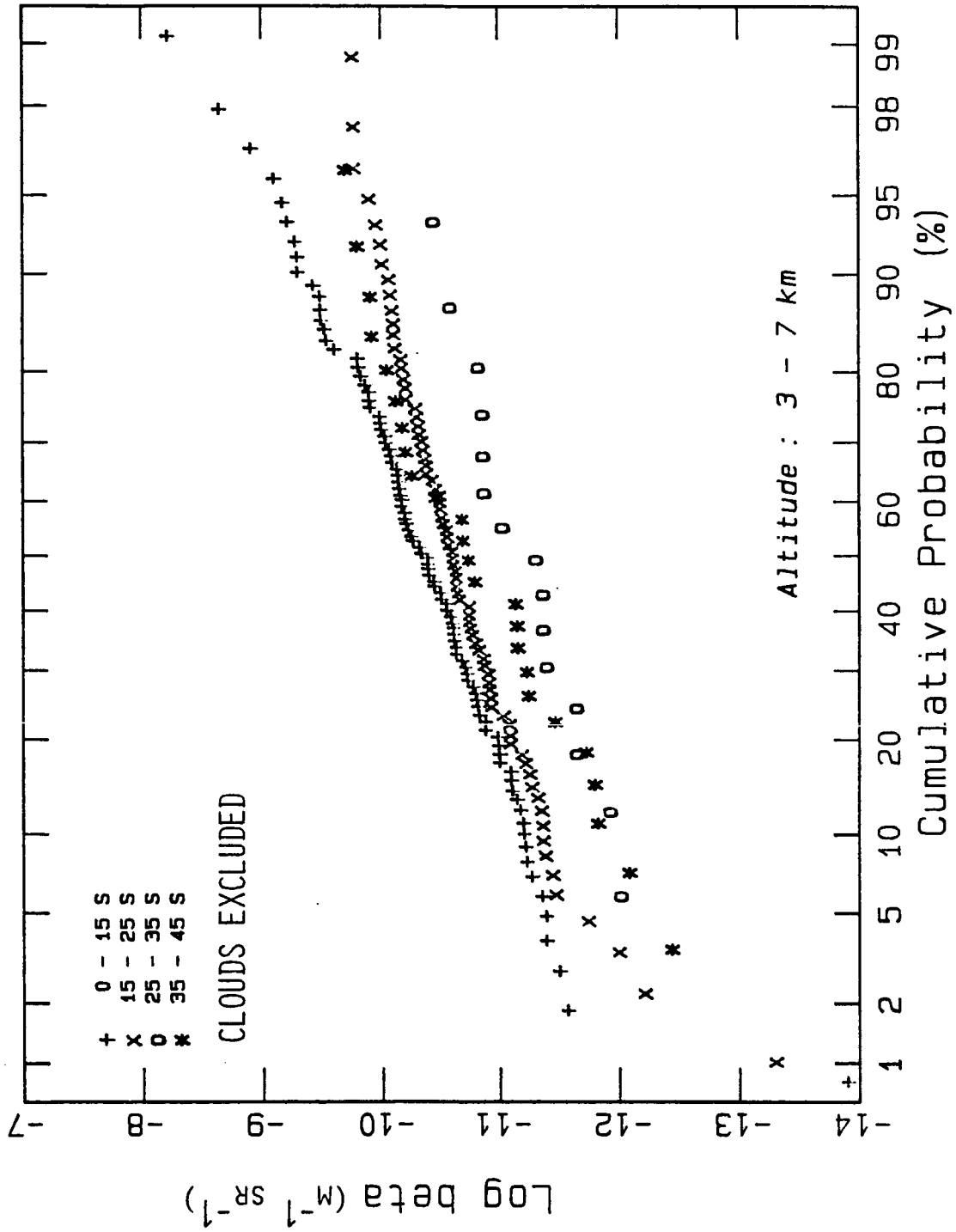


Figure 28. Same as Fig. 27 except divided into four latitude bands.

7. References

1. W.D. Jones, J.W. Bilbro, S.D. Johnson, H.B. Jeffreys, L.Z. Kennedy, R.W. Lee, and C.A. DiMarzio, "Design and calibration of a coherent lidar for measurement of atmospheric backscatter," Proc. SPIE 300, 66 (1981).
2. W.D. Jones, L.Z. Kennedy, and R.W. Lee, "Determination of Atmospheric Backscatter at 10.6 Microns," Proc. SPIE 415, 77 (1983).
3. C.M. Sonnenschein and F.A. Horrigan, "Signal-to-Noise Relationships for Coaxial Systems that Heterodyne Backscatter from the Atmosphere," Appl. Opt. 10, 1600 (1971).
4. L.D. Dickson, "Characteristics of a Propagating Gaussian Beam," Appl. Opt. 9, 1854 (1970).
5. M.J. Kavaya, "Polarization effects on hard target calibration of lidar systems," Appl. Opt. 26, 796 (1987).
6. T.R. Lawrence, D.J. Wilson, C.E. Craven, I.P. Jones, R.M. Huffaker, and J.A.L. Thomson, "A Laser Velocimeter for Remote Wind Sensing," Rev. Sci. Instrum. 43, 512 (1972).
7. M.J. Post, R.A. Richter, R.J. Keeler, R.M. Hardesty, T.R. Lawrence, and F.F. Hall, "Calibration of coherent lidar targets," Appl. Opt. 19, 2828 (1980).
8. M.J. Kavaya, unpublished (1988).
9. Final Report on Contract No. NAS8-34337, Beta Experiment, Applied Research, Inc., Huntsville, AL (June 1982).
10. Final Report on "Added Scope" to Contract No. NAS8-34337, Beta Experiment, Applied Research, Inc., Huntsville, AL (April 1983).
11. Final Report on Contract No. NAS8-35329, Beta Systems Error Analysis, Applied Research, Inc., Huntsville, AL (January 1984).
12. Operating manual for "Beta Signal Processor", Lassen Research, Manton, CA 96059 (March 1981).
13. W.D. Jones, L.Z. Kennedy, J.W. Bilbro, and H.B. Jeffreys, "Coherent focal volume mapping of a CW CO₂ Doppler lidar," Appl. Opt. 23, 730 (1984).

APPENDIX C

THE JOINT CSIRO/NASA WINDSAT EXPERIMENT:
ATMOSPHERIC BACKSCATTER MEASUREMENTS AT 0.694 μm

S. Banks and C.M.R. Platt

CSIRO Division of Atmospheric Research
Aspendale, Victoria

and

D. Booth

Footscray Institute of Technology
Melbourne, Victoria

and

R. Dubinsky[#]

[#]Temporary Research Assistant at CSIRO, DAR
Now at NASA Langley Research Centre, Hampton, VA.

1. Introduction

During the period May 25-31, 1986, CSIRO DAR operated a groundbased ruby lidar at Sale, SE Victoria, as part of the CSIRO/NASA WINDSAT experiment. The measurements were aimed at determining the level of backscatter in the free troposphere above the atmospheric boundary layer. Accompanying measurements from the CSIRO F-27 aircraft of backscatter coefficients obtained in situ with a CW CO₂ lidar at 10.6 μm and with backscatter coefficients calculated from aerosol size distributions measured in situ are described in accompanying appendices.

This article presents the data obtained with the DAR pulsed ruby lidar system together with the data reduction and analysis.

Comparisons between the ruby and CO₂ lidar backscatter coefficients and the calculated values from the aerosol size distributions are given in the main part of the report.

2. The CSIRO Ruby Lidar System

The CSIRO Division of Atmospheric Research pulsed ruby lidar is housed in a transportable caravan. The lidar consists of a Q-switched ruby laser mounted on the side of a 14 inch (35.6 cm) Schmidt-Cassegrain telescope. The system is not coaxial and maximum overlap between the laser beam and telescope field of view is reached at a range of approximately 500 m. The detector is an RCA 7265 photomultiplier with an S20 photocathode. Various combinations of neutral density filter, aperture and polarizer may be rotated into the receiver optics for use in specific applications. When the return signal is small, as it is, for instance, when the laser pulse is backscattered from high altitudes, the photomultiplier output is amplified and electrically low-pass filtered in order to reduce any noise. It is then digitised by a Biomation 8100 transient digitiser and displayed on an oscilloscope screen. The signal returned from each lidar shot is saved on magnetic tape along with the relevant system parameters for use in the data analysis. The entire data acquisition process is controlled by a Hewlett-Packard HP2100 mini-computer and is initiated by a fire pulse from the laser energy monitor. Some relevant system parameters are presented in Table 1.

Description of Data Collected

During the period of the experiment daily measurements were made of the aerosol backscatter coefficient. Data were recorded twice a day for five days, usually in the early afternoon and evening, and when conditions were cloudless. A measurement was made in the morning only on the last day of the study. A summary of all the data taken is presented in Table 2.

In order to collect data up to an altitude of 19 km a sequence of several separate series of lidar shots was recorded, each with different sampling intervals and trigger delays. Thus, for instance, a 10 ns sampling interval with zero delay was used to collect data at altitudes from 0 to 3 km. Similarly, the data in the range 2.1 to 8.25 km was measured with a sampling interval of 20 ns and a trigger delay of 13.6 μs. For the low altitude data no amplification of the photomultiplier output was necessary. For those shots which included ranges above 8.5 km, however, an amplifier gain of 93 was used. Unfortunately, the amplifier developed excessive noise during the experiment and it was necessary in some cases to use the low-pass filter with a cut-off frequency of 1 MHz in order to reduce this. Even after having done this, however, it was not

possible to analyse a large amount of the high altitude data due to the difficulty in establishing a reliable sky signal value for these shots.

The laser energy was typically between 0.5 J and 1 J throughout the experiment. For the altitudes below 8.5 km up to 100 shots were recorded during each run. For altitudes higher than this up to 200 shots were recorded. Usually, one shot was recorded every 5 seconds.

Examples of some lidar returns which were obtained during the experiment are shown in figures 1(a)-1(c). On the final two days of the experiment cloud cover often prevented any aerosol data above 1 km and little useful information was obtained on those days.

Data Analysis

During daytime hours an appreciable sky radiance D.C. signal was evident in the data and was measured as follows for each sequence of shots. The average of the last 25 data values (corresponding to the highest altitude) in each shot was obtained and plotted against the measured energy of the laser pulse. A straight line fit extrapolated to zero laser energy gave an estimate of the sky signal at that time. In some cases, however, the scatter in the data points was too great for a good straight line fit to be obtained and a second method was then used which relied on those occasions when the Biomation triggered early due to noise on the fire pulse. In these cases the recorded signal was due to the D.C. sky signal alone.

The value obtained by either of the above methods was subtracted from the data for the remaining shots and the results were then converted into an output signal voltage using the known settings on the transient digitiser. The voltages thus obtained were corrected for electrical attenuation, for the range-squared decrease in the signal and for shot-to-shot variations in laser pulse energy. Voltage values were then smoothed over 20 m intervals. Finally, the results from all the shots in the measurement sequence were averaged and standard deviations calculated.

Total attenuated backscatter coefficients were obtained in the following manner. The quantity measured by the lidar is:

$$V_T(r)^* = \frac{V_T(r)r^2}{E}$$

$$= K \left[\beta_M(r) + \beta_A(r) \right] \exp^{-2} \int_0^r \left[\sigma_M(r') + \sigma_A(r') \right] dr' \quad (1)$$

In this equation $\beta(r)$, $\sigma(r)$ and $V(r)$ are the backscatter and extinction coefficients and the voltage induced in the photomultiplier due to scattering at the range r . The subscripts M, A and T refer to molecular, aerosol and total scattering respectively. $V_T(r)^*$ is the range-corrected voltage normalised to unit E. Pulse energy K is a system constant which includes such factors as the photomultiplier sensitivity, the impedance of the photomultiplier load, and the optical losses introduced by the receiver optics. In this equation it has been assumed that any contribution to the extinction due to molecular absorption is negligible.

The second measured quantity is obtained from the aircraft observations of the temperature and pressure profiles. These are used to calculate an attenuated molecular backscattering coefficient:

$$\beta_M^{\text{att}}(r) = \beta_M(r) \exp\left(-2 \int_0^r \sigma_M(r') dr'\right), \quad (2)$$

where

$$\beta_M(r) = 0.1119 \sigma_M(r),$$

and $\sigma_M(r)$ is calculated using the usual Rayleigh scattering equation. We introduce a calibration constant C so that at a particular range R_0 , where the air is very clean, we may assume that the backscattering is totally molecular and hence $\beta_A(R_0) = 0$. We then have the relation:

$$\begin{aligned} \beta_M^{\text{att}}(R_0) &= \frac{1}{C} V_T(R_0)^* \\ &= \frac{K}{C} \beta_M(R_0) \exp\left(-2 \int_0^{R_0} \sigma_M(r') + \sigma_A(r') dr\right) \\ &= \beta_M(R_0) \exp\left(-2 \int_0^{R_0} \sigma_M(r') dr'\right) \end{aligned} \quad (3)$$

which allows the calibration constant C to be evaluated as:

$$C = K \exp\left(-2 \int_0^{R_0} \sigma_A(r') dr'\right). \quad (4)$$

This calibration constant, which to a good approximation should depend on system parameters only if the aerosol loading of the atmosphere is low, may then be used at all the other altitudes to calculate an attenuated total backscatter coefficient $\beta_T^{\text{att}}(r)$:

$$\beta_T^{\text{att}}(r) = \frac{V_T(r)^*}{C}$$

$$= \beta_T(r) \exp-2 \int_0^r \sigma_M(r') dr' \exp-2 \int_{R_0}^r \sigma_A(r') dr' . \quad (5)$$

This is the quantity which is plotted in figure 2. We may also define an attenuated scattering ratio $S^{\text{att}}(r)$ to be:

$$S^{\text{att}}(r) = \frac{\beta_T^{\text{att}}(r)}{\beta_M^{\text{att}}(r)} = \frac{\beta_T(r)}{\beta_M(r)} \exp-2 \int_{R_0}^r \sigma_A(r') dr' . \quad (6)$$

and this also plotted in Figures 3.

The practice of fitting the total backscatter $\beta_T(r)$ to a molecular (Rayleigh) backscatter atmosphere at an altitude where the atmosphere is known to be 'clean' of aerosols is standard lidar practice. It is only an approximate method, however, because there is always some aerosol content at every altitude. We can rewrite the scattering ratio $S^{\text{att}}(r)$

$$S^{\text{att}}(r) = \left(1 + \frac{\beta_A(r)}{\beta_M(r)} \right) \exp-2 \int_{R_0}^r \sigma_A(r') dr'$$

it is found that $\beta_A(r)/\beta_M(r)$ usually decreases somewhere in the troposphere to less than 0.1, so that C can be obtained to at least the same accuracy.

In the present series of measurements, determination of a suitable normalization altitude was assisted by the availability of aerosol number concentrations and size distributions made in situ at a number of altitudes from the CSIRO F-27 aircraft (see Appendix A). These measurements showed a decrease in number concentration of usually several orders of magnitude between 500m and about 4000 to 5000m altitude (or sometimes lower). As the maximum scattering ratio was never more than about 5, this implied that assuming linearity between total concentration and backscatter coefficient, the ratio $\beta_A(r)/\beta_M(r)$ usually fell to less than 0.01 at about 4000m.

As the available signal to noise ratios in the lidar return degraded rapidly due to the (range)² effect, (see Figures 1a to 1c), the total backscatter $\beta_T(r)$ could safely be normalised at some suitable altitude above 4000m without losing much meaningful information. [In fact, on one day, the normalization altitude was much lower. The implications in that case will be discussed later].

The normalization procedure is shown in Figure 2 where data are fitted to the calculated molecular scattering atmosphere. Figure 3 illustrates the resultant scattering ratio $S^{\text{att}}(r)$. It can be seen that the accuracy of the determination of $\beta_A(r)/\beta_M(r)$ must diminish rapidly with altitude. The increase in random noise at the high altitudes due to the (range)² effects is also obvious [e.g. Figures 1a to 1c].

The derived profiles of aerosol backscatter coefficient $\beta_A(r)$ are shown in Figures 4a to 4e. A correction has been made for extinction using a value of backscatter to extinction (β/σ) ratio of $\beta/\sigma = 0.057 \text{ sr}^{-1}$ obtained from Mie calculations on the measured size distributions. As a first approximation, it was assumed that the backscatter coefficients found from the analysis of the lidar data were unattenuated and, using the assumed value of backscatter-to-extinction ratio, were used to calculate extinction coefficients at each height. From these and the measured molecular values the attenuation up to each height was calculated and used to correct the original lidar data. The process was then repeated by calculating new values of extinction and continued until succeeding iterations produced no change. The total two-way transmission to 8 km is about 0.65.

In Figure 4d, the broken line indicates the result of inserting arbitrarily a gross error in the normalization where the data is now normalized to the lowest excursion in the random noise, rather to the mean noise. The uncertainty in $\beta_A(r)$ due to this error in normalization is seen to become large above about 4 km, as expected.

A feature on 26th May 1986 for both runs during that day [Figures 4b and 4c] is the local sharp minimum in backscatter at an altitude of about 1.2 km near the top of the boundary layer inversion. The signal to noise ratio in the lidar return is good at these altitudes and the minimum appeared to be a distinct feature. It was also the point of normalization so that the error at the specific normalization height is again infinite but decreases again at the higher altitudes.

There is some evidence for an increase in aerosol content at higher altitudes on 25th May 1986 and 29th June 1986, but the uncertainty there is high.

There are several sources of error which have to be considered. The results of an arbitrary "fitting error" are shown in Figure 4d, and numerical estimates are given in Table 3, where the error is once again due to a normalization on the lowest 'swing' of the noise. Random errors due to the noise itself are also shown. Another error, which can be significant, is due to an incorrect specification of the background 'sky noise'. This would have only been a significant problem in the two daytime runs on 26th May and 27th May. However, a similar 'offset error' can occur on the higher gain values of the signal amplifier. This can cause the backscatter coefficients on various amplifier ranges to be offset from each other in overlapping altitude ranges. The result of offset errors is generally an anomalous increase or decrease with altitude depending on the (range)² factor. Although the ratios of the gains on the various amplifier ranges have been normalized in overlapping height ranges, some error will remain.

The uncertainty in the value of β/σ is in the region of 30%. However, the total two-way transmittance from 0 to 6 km is about 0.64, so that a 30% error causes a maximum error of about 10% in the transmittance, which is small compared to the other errors.

Acknowledgements

Assistance in computing was provided by Mr. G. Patterson. Mr. G. Grauze looked after the caravan and hardware and took the measurements.

TABLE 1
Ruby Lidar System

TRANSMITTER

Laser wavelength	694.3 nm
Laser energy	0.2 - 1.5 Joule
Laser pulse length	60 ns
Beam divergence	1 mrad
Maximum prf	1 Hz

RECEIVER

Telescope diameter	14 inch (35.6 cm)
Receiver field of view	10 mrad max (full angle)
Detector	RCA 7265 PMT

DATA RECORDER

Biomation 8100 transient digitiser	100 megasamples/sec 100 MHz bandwidth with 2k 8-bit words
Computer	HP 2100 minicomputer

TABLE 2
Summary of Daily Lidar Data

Day	Time	Comments
Sun 25/5/86	1321 to 1425	0-3 km, 1.5-4.6 km, 2.1-8.3 km, 3.8-19.2 km ¹ Many mistriggers of transient recorder
Sun 25/5/86	1643 to 1847	0-3 km, 1.5-4.6 km, 2.1-8.3 km, 3.8-19.2 km ¹ Many mistriggers of transient recorder
Mon 26/5/86	1217 to 1508	0-3 km, 1.5-4.6 km, 2.1-8.3 km, 3.8-19.2 km ¹ 5.1-11.3 km ¹ , 9.9-31.0 km ¹ Trigger problems solved
Mon 26/5/86	1914 to 1947	0-3 km, 1.5-4.6 km, 2.1-8.3 km, 5.1-11.3 km ¹ Night time run so sky signal close to zero
Tues 27/5/86	1118 to 1201	0-3 km, 1.5-4.6 km, 2.1-8.3 km, 5.1-11.3 km ¹ 99.0-31.0 km ¹ No direct sky signal measurement
Tues 27/5/86	2100 to 2110	0-3 km Night time run so sky signal close to zero Layer at 2.5 km altitude
Thurs 29/5/86	1503 to 1632	0-3 km Clouds above 700 metres in all of the data
Thurs 29/5/86	1845 to 1934	0-3 km, 1.5-4.6 km, 2.1-8.3 km Aeroplane reported very clean air above the inversion
Fri 30/5/86	1129 to 1622	0-3 km, 1.5-4.6 km, 2.1-8.3 km Low clouds present
Fri 30/5/86	1639 to 1733	0-3 km Low clouds present
Sat 31/5/86	0925 to 1028	0-3 km Low clouds present

Notes: ¹ : The data taken for this range interval have not been analysed due to amplifier faults

TABLE 3

Errors in $\beta_A(r)$ due to incorrect normalization and due to random noise (background sky photon noise and signal photon noise)

Altitude of normalization (km)	Normalization error in $\beta_A(r)^*$ ($m^{-1} sr^{-1}$)	Random error in $\beta_A(r)$ ($m^{-1} sr^{-1}$)
2	3.9×10^{-9}	8×10^{-10}
4	7.1×10^{-9}	1.4×10^{-9}
6	1.5×10^{-8}	3×10^{-9}

* : This is due to an error of normalizing on the least random noise value instead of the average noise value.

Fig.1a: Raw lidar data taken on the 29th May 1986. This plot shows the return from the 0-3 km range.

Fig.1b: Raw lidar data taken on the 29th May 1986. This plot shows the return from the 1.5-4.6 km range.

Fig.1c: Raw lidar data taken on the 29th May 1986. This plot shows the return from the 2.1-8.3 km range.

Fig.2: Relative attenuated total backscatter coefficients fitted to the molecular backscatter profile at a range of 5.5 km. Data for 27/5/86.

Fig.3: Derived scattering ratio $S^{att}(r)$ on 27/5/86.

Figs.4a-4e: Profiles of aerosol backscatter coefficients $\beta_A(r)$ for 25/6 to 29/6/86. The dotted line illustrates the molecular Rayleigh backscatter coefficient and the dashed line, (in Figure 4c), the profile of $\beta_A(r)$ obtained with normalization on the lowest extreme value^A of the random noise. [Normalized at a different range on 27/6 compared to the full line].

TITLE: LIDAR BIOMATION DATA
 X-AXIS: BIOMATION MEMORY LOCATIONS
 Y-AXIS: BIOMATION MEMORY CONTENTS
 DATE: 290586 TIME: 1845 FILE: 0245
 SHOT: 000003 EXPT: 0030 SEQ: 0013
 SCALING: MULT. X-ORD BY 10**(3) - Y-ORD BY 10**(2)

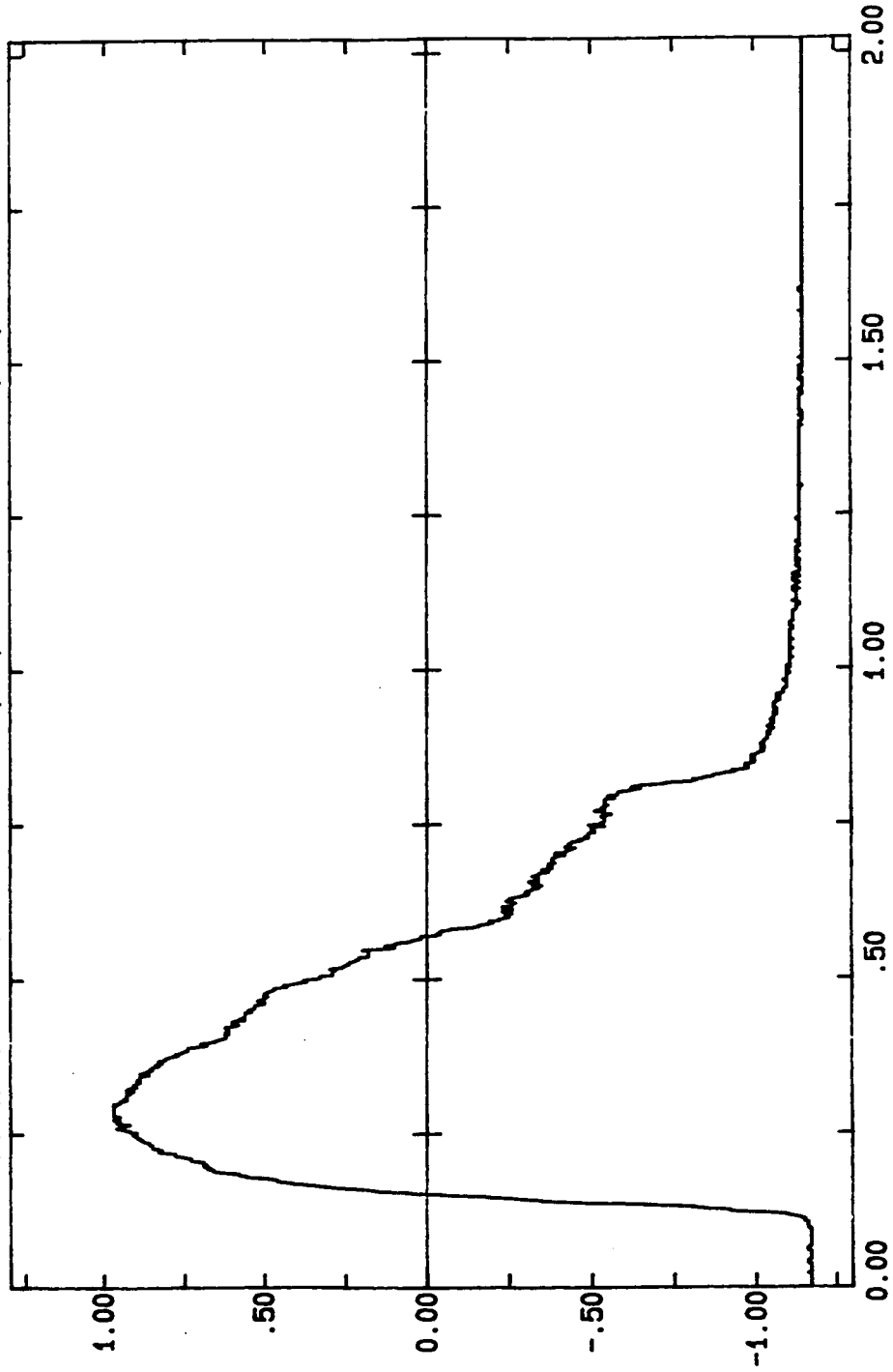


Figure 1a
 Raw lidar data taken on the 29th May 1986. This plot shows the return from the 0-3 km range.

TITLE: LIDAR BIOMATION DATA
X-AXIS: BIOMATION MEMORY LOCATIONS
Y-AXIS: BIOMATION MEMORY CONTENTS
DATE: 290586 TIME: 1853 FILE: 0245
SHOT: 000029 EXPT: 0030 SEQ: 0013
SCALING: MULT. X-ORD BY 10** (3) - Y-ORD BY 10** (2)

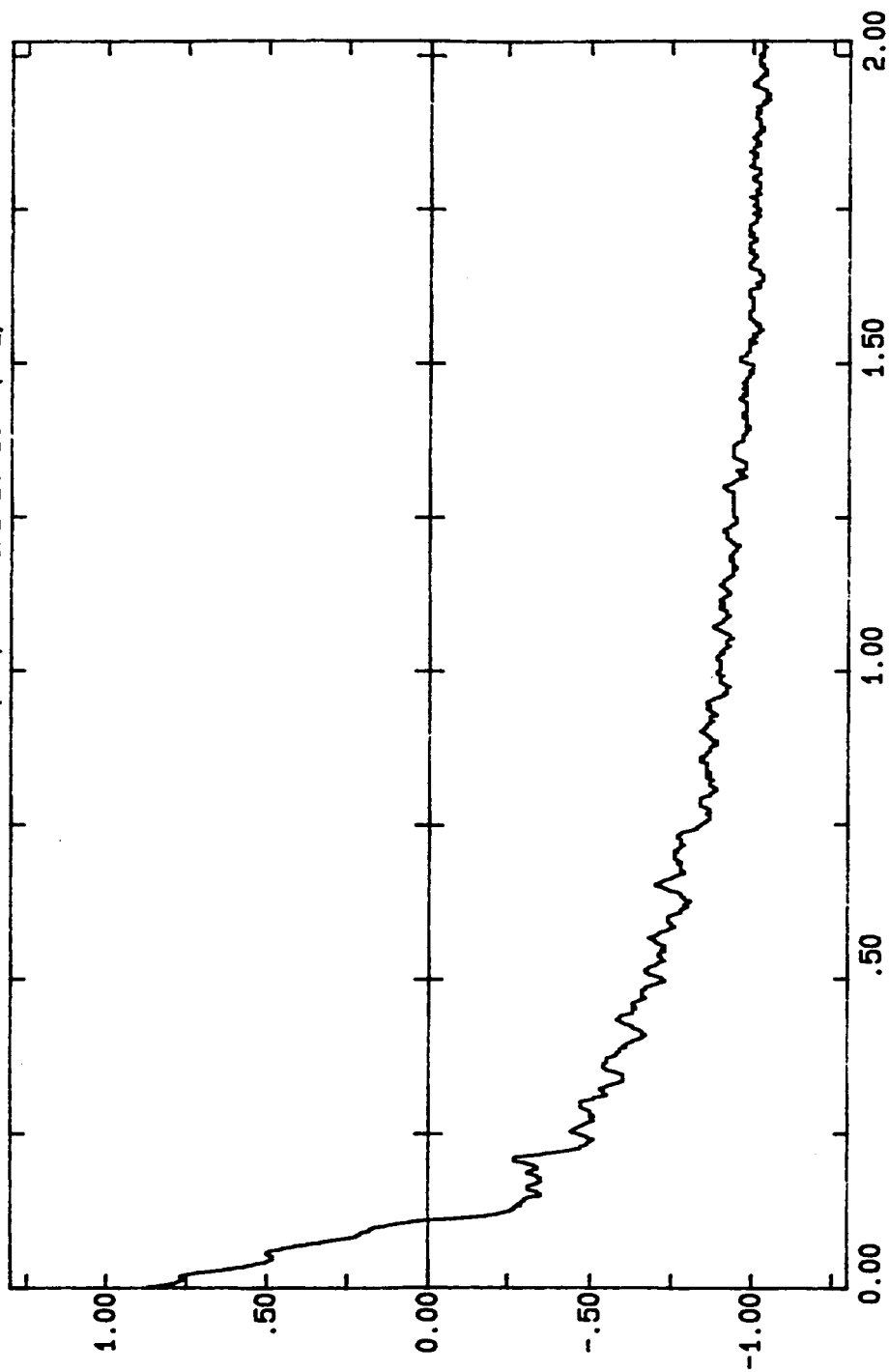


Figure 1b
Raw lidar data taken on the 29th May 1986. This plot shows the return from the 1.5-4.6 km range.

TITLE: LIDAR BIOMATION DATA
X-AXIS: BIOMATION MEMORY LOCATIONS
Y-AXIS: BIOMATION MEMORY CONTENTS
DATE: 290586 TIME: 1858 FILE: 0245
SHOT: 000058 EXPT: 0030 SEQ: 0013
SCALING: MULT. X-ORD BY 10** (3) - Y-ORD BY 10** (2)

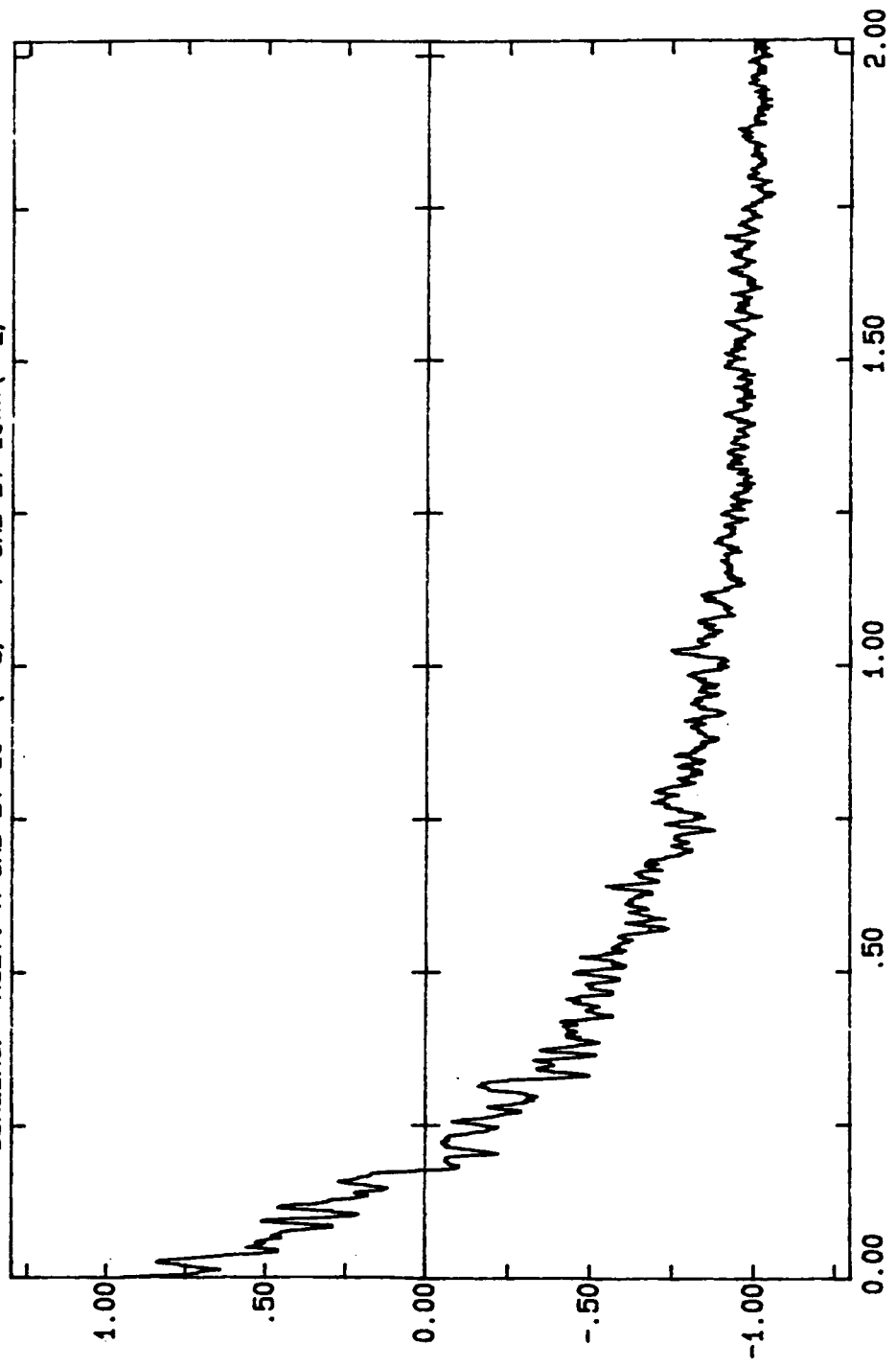


Figure 1c

Raw lidar data taken on the 29th May 1986. This plot shows the return from the 2.1-8.3 km range.

CSIRO Ruby Lidar, Sale, Victoria

27/5/86 1118hrs

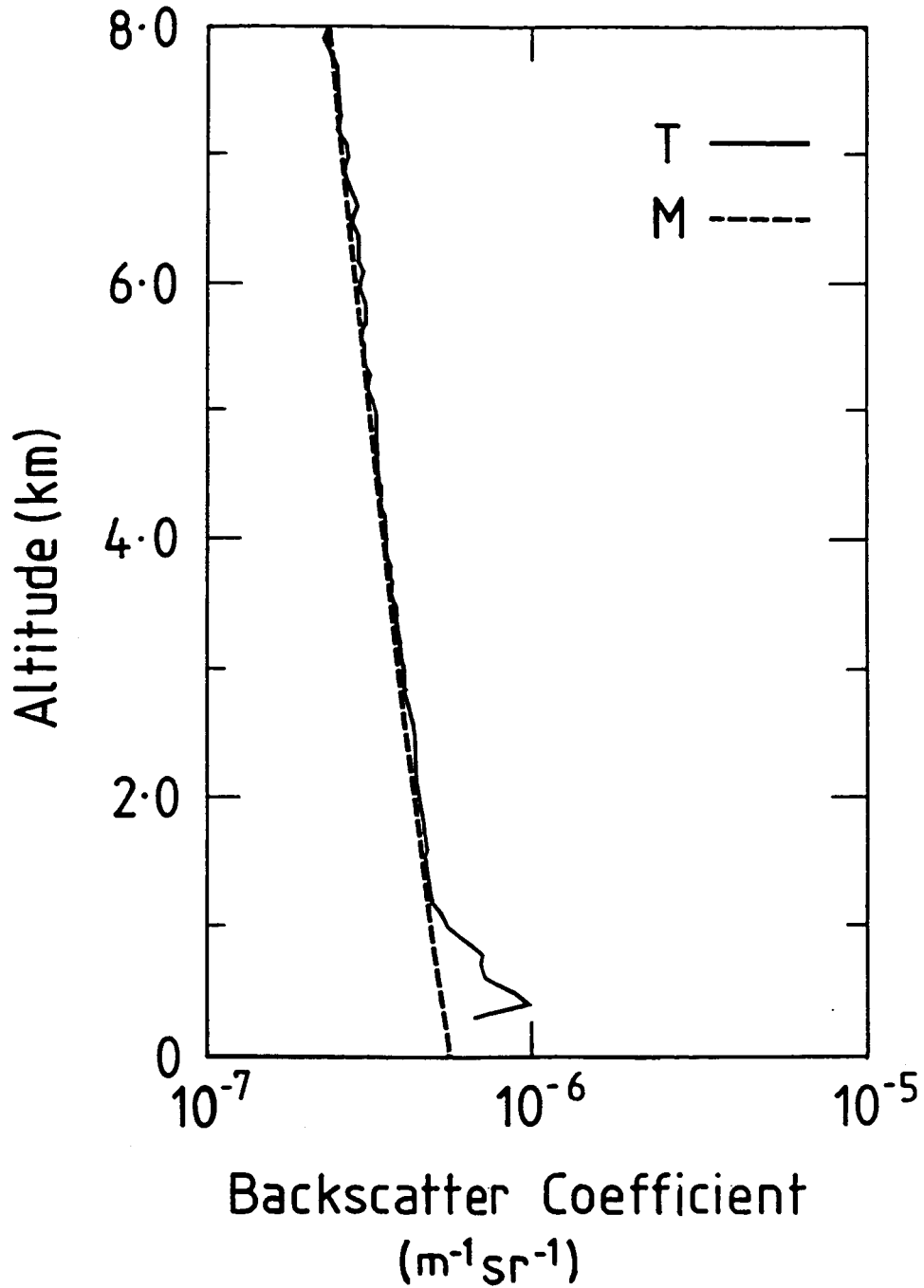


Figure 2

Relative attenuated total backscatter coefficients fitted to the molecular backscatter profile at a range of 5.5 km. Date for 27/5/86

CSIRO Ruby Lidar, Sale, Victoria

27/5/86 1118 hrs

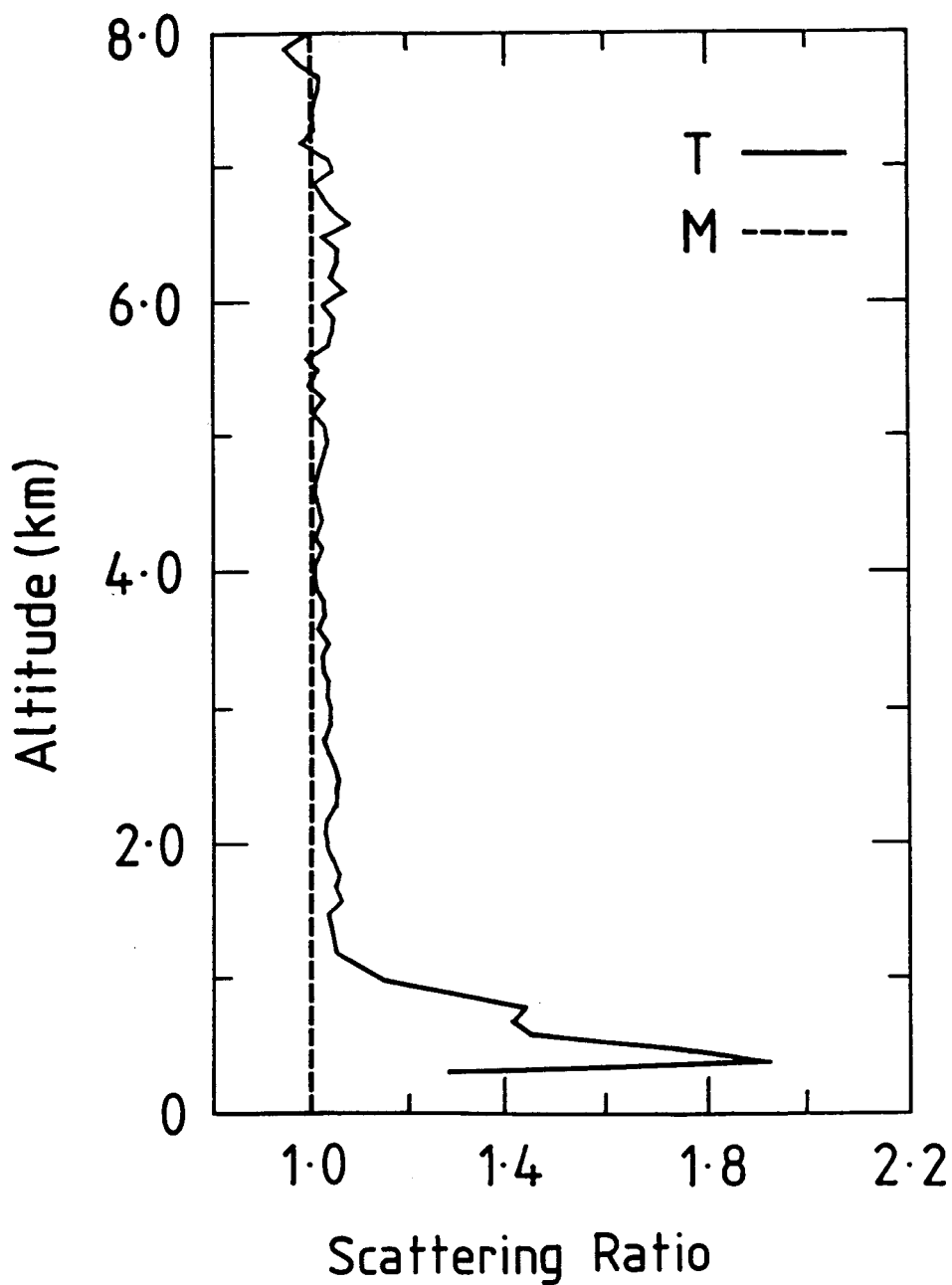


Figure 3

Derived scattering ratio $S^{\text{att}}_{(r)}$ on 27/5/86

CSIRO Ruby Lidar, Sale, Victoria

25/5/86 1643 hrs

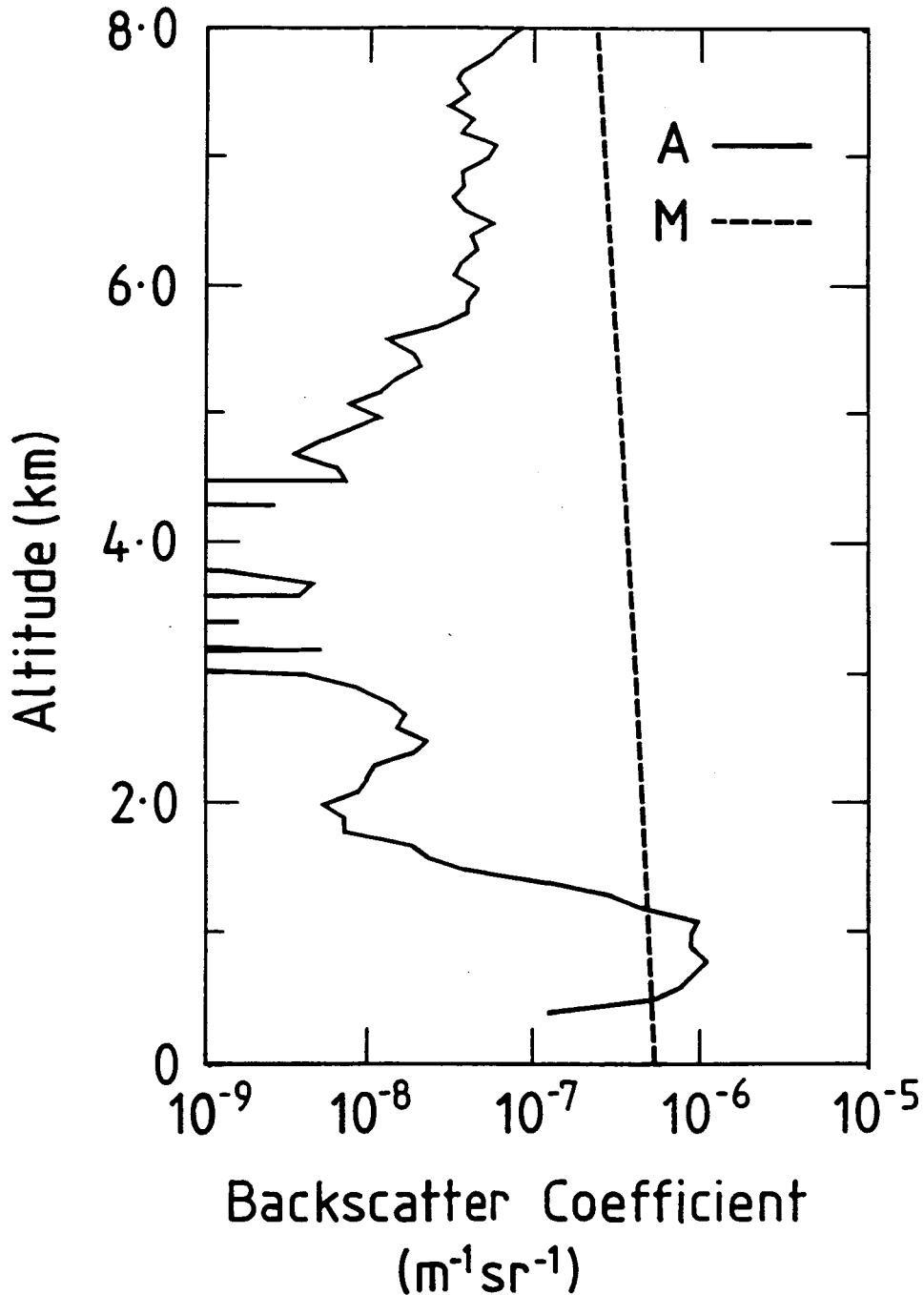


Figure 4a

Profiles of aerosol backscatter coefficients $B_A(r)$ for 25/6 to 29/6/86. The dotted line illustrates the molecular Rayleigh backscatter coefficient and the dashed line, (in Figure 4c), the profile of $B_A(r)$ obtained with normalization on the lowest extreme value of the random noise. (Normalized at a different range on 27/6 compared to the full line).

CSIRO Ruby Lidar, Sale, Victoria

26/5/86 1217hrs

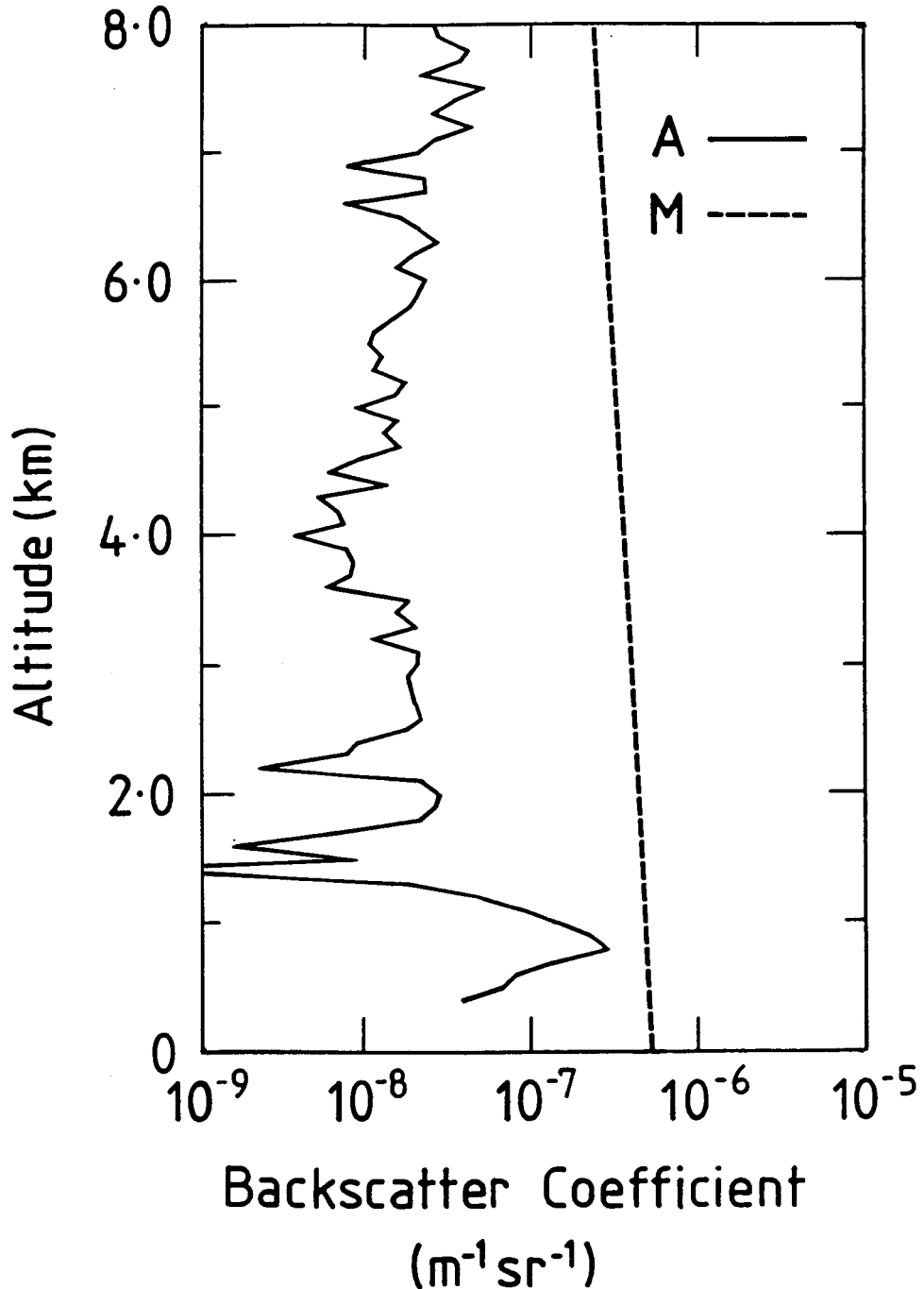


Figure 4b

Profiles of aerosol backscatter coefficients $B_A(r)$ for 25/6 to 29/6/86. The dotted line illustrates the molecular Rayleigh backscatter coefficient and the dashed line, (in Figure 4c), the profile of $B_A(r)$ obtained with normalization on the lowest extreme value of the random noise. (Normalized at a different range on 27/6 compared to the full line).

CSIRO Ruby Lidar, Sale, Victoria

26/5/86 1914 hrs

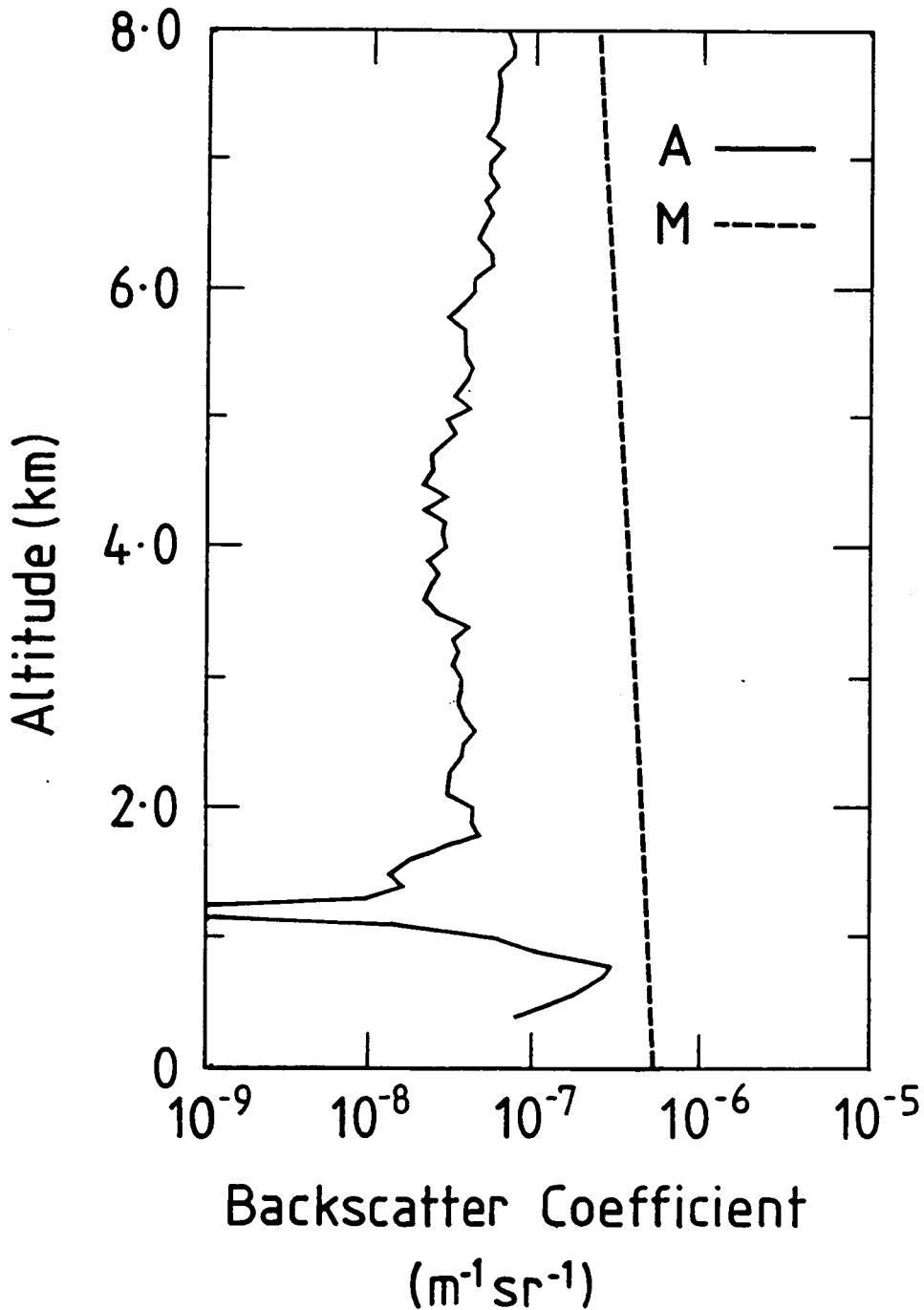


Figure 4c

Profiles of aerosol backscatter coefficients $B_A(r)$ for 25/6 to 29/6/86. The dotted line illustrates the molecular Rayleigh backscatter coefficient and the dashed line, (in Figure 4c), the profile of $B_A(r)$ obtained with normalization on the lowest extreme value of the random noise. (Normalized at a different range on 27/6 compared to the full line).

CSIRO Ruby Lidar, Sale, Victoria

27/5/86 1118 hrs

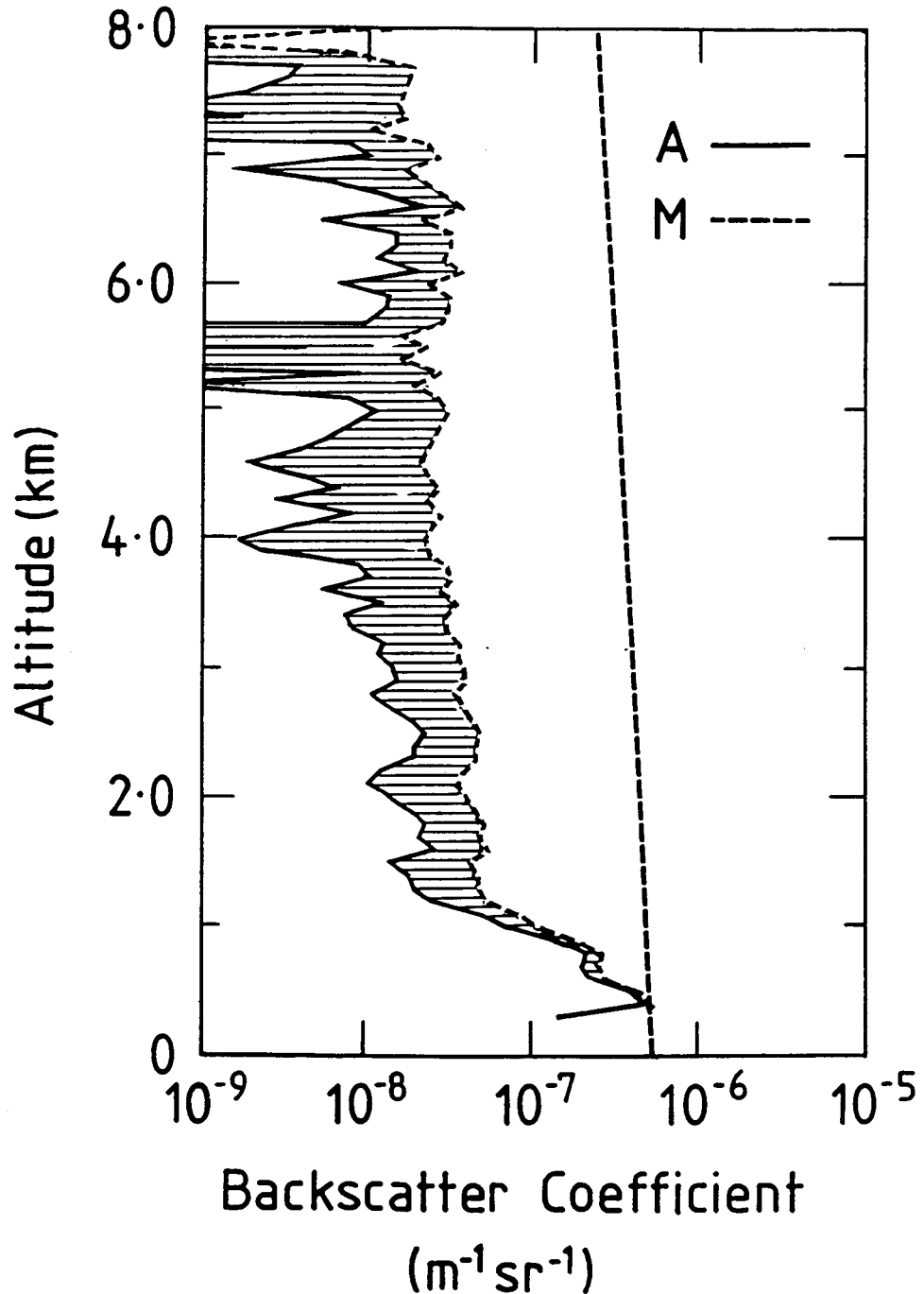


Figure 4d

Profiles of aerosol backscatter coefficients $B_A(r)$ for 25/6 to 29/6/86. The dotted line illustrates the molecular Rayleigh backscatter coefficient and the dashed line, (in Figure 4c), the profile of $B_A(r)$ obtained with normalization on the lowest extreme value of the random noise. (Normalized at a different range on 27/6 compared to the full line).

CSIRO Ruby Lidar, Sale, Victoria

29/5/86 1845 hrs

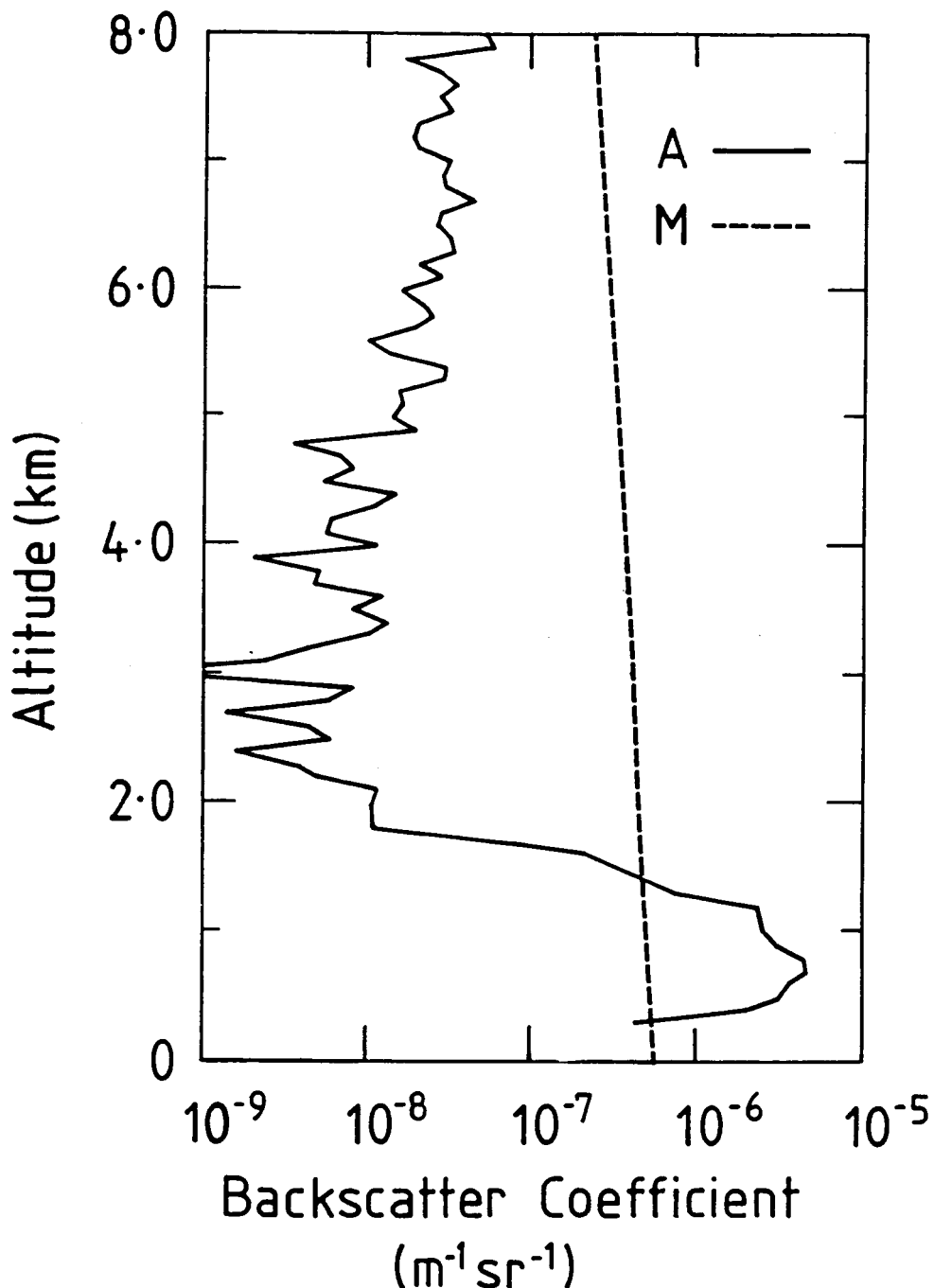


Figure 4e

Profiles of aerosol backscatter coefficients $B_A(r)$ for 25/6 to 29/6/86. The dotted line illustrates the molecular Rayleigh backscatter coefficient and the dashed line, (in Figure 4c), the profile of $B_A(r)$ obtained with normalization on the lowest extreme value of the random noise. (Normalized at a different range on 27/6 compared to the full line).

APPENDIX D

LIDAR OBSERVATIONS OF TROPOSPHERIC AEROSOLS AT
COWLEY BEACH, NORTH QUEENSLAND : MAY-JUNE 1986

S.A. Young^{1,2}, M.J. Lynch¹ and D. Cutten³

¹School of Physics and Geosciences,
Curtin University of Technology, Western Australia

²now at CSIRO Division of Atmospheric Research,
Aspendale, Victoria

³DSTO Surveillance Research Laboratory,
Optoelectronics Division, Salisbury, South Australia

1. INTRODUCTION

The lidar operated by the School of Physics and Geosciences at Curtin University of Technology (formerly Western Australian Institute of Technology) has been employed during the period 1984 to 1986 in the study of tropospheric marine aerosols at coastal sites in Western Australia (Woodman Point and Garden Island) and north Queensland (Cowley Beach 100km SE of Cairns). Four field trips were conducted at the Western Australian sites representing temperate climates and three at the tropical site in Queensland. This report presents results obtained during the first Queensland study when comparative airborne data were obtained by the CSIRO Division of Atmospheric Research using the instrumented F-27 aircraft.

2. THE CURTIN LIDAR

The lidar uses a Quanta Ray DCR IIA frequency-doubled Nd:YAG laser as the transmitter and a 254mm diameter Newtonian telescope as the receiver. The 532nm backscattered radiation is detected using an EMI 9816B photomultiplier tube with an S-20 photocathode. The output signal from the detector is amplified using either linear or logarithmic amplifiers and digitised before storage on floppy discs. Digitiser operation and data storage are controlled via an LSI 11/23 computer. Table D1 summarises the lidar's features.

During operation the lidar was scanned in elevation from 0° to 90° in a direction over the ocean. Frequently the lidar was operated at fixed elevation angles and 50 shot averages were recorded to improve the signal-to-noise ratio. Occasionally data were recorded with a polariser inserted in the receiver and aligned alternately parallel and perpendicular to the plane of polarisation of the transmitted laser pulse.

The lidar data were complemented by on-site measurements of meteorological and aerosol parameters. Temperature, relative humidity and wind speed and direction were recorded at ground level and profiles of temperature and relative humidity were obtained from radiosondes launched from the site during each three-hour observational period. A MRI nephelometer, a CSASP particle counter and a radon counter provided surface data on aerosol extinction, number, size and origin.

3. METEOROLOGICAL CONDITIONS

The period of observation (from 29th May to 11th June 1986) was characterised by SE (on shore) winds and an air temperature which varied between 22° and 24°C during the measurement sessions. During the earlier part of this period (29th May to 7th June) winds were consistently between 7 and 11 m.sec⁻¹, relative humidities between 80% and 96% and there were frequent rainshowers from low cumulonimbus clouds. Conditions moderated during the last three days; winds dropped to between 3 and 5 m.sec⁻¹, relative humidities dropped to between 50% and 80%, clouds only formed after midday and there was no rain during the measurement sessions.

4. METHODS OF DATA ANALYSIS

The lidar data have been analysed to produce several different outputs. Data averaged over many shots and acquired from horizontal firings in regions of horizontal atmospheric homogeneity have been analysed to produce values of the aerosol backscatter-to-extinction ratio (β_A/σ_A) in the near-surface layer. Data acquired at higher elevation angles have been analysed to produce profiles of backscatter and extinction. In the absence of measured values of (β_A/σ_A) throughout the troposphere, the value measured at the surface was used in the analysis of these latter data.

4.1 The Determination of the Aerosol Backscatter-to-Extinction Ratio

The lidar equation for the backscattered power received from a range r can be written as

$$P(r) = K(\beta_A(r) + \beta_m(r)) \exp\left[-2 \int_0^r (\sigma_A(r') + \sigma_m(r')) dr'\right] / r^2 \quad , \quad (D1)$$

where $\beta(r)$ and $\sigma(r)$ are, respectively, the volume backscatter function and volume extinction coefficient and K is a system constant. The subscripts A and m refer to the aerosol and molecular contributions to these quantities. Note here that the extinction terms are assumed to be due to scattering only; molecular and aerosol absorptions at the wavelength used are negligible (Elterman (1964), McClatchey et al. (1972)).

For a lidar firing horizontally through a homogeneous atmosphere D1 can be rewritten.

$$P(r) r^2 = K\bar{\beta}_T \exp[-2 \bar{\sigma} \cdot r] \quad , \quad (D2)$$

where

$$\bar{\beta}_T = \bar{\beta}_A + \bar{\beta}_m \quad (D3)$$

is the total backscatter function and

$$\bar{\sigma}_T = \bar{\sigma}_A + \bar{\sigma}_m \quad (D4)$$

is the total extinction coefficient. The bars indicate averaged values, as small variations about a mean are acceptable. Taking natural logarithms of D2 gives

$$\ln [P(r) r^2] = \ln [K\bar{\beta}_T] - 2\bar{\sigma} \cdot r \quad . \quad (D5)$$

D5 is a linear function of r and a linear regression of $\ln [P(r) r^2]$ against r yields values of $\bar{\sigma}$ and $K\bar{\beta}_T$.

Using D3 and following a method similar to that of Waggoner et al. (1972)

$$\begin{aligned} K\bar{\beta}_T &= K\bar{\beta}_A + K\bar{\beta}_m \quad , \\ &= K \left(\frac{P_A(\pi)}{4\pi} \right) \cdot \bar{\sigma}_A + K\bar{\beta}_m \quad . \end{aligned} \quad (D6)$$

Here the aerosol extinction and backscatter are related by the equation

$$\beta_A = \left(\frac{P_A(\pi)}{4\pi} \right) \sigma_A \quad (D7)$$

where $P_A(\pi)$ is the aerosol phase function for the case of backscatter (e.g. Deirmendjian, 1964), and the quantity in brackets is equivalent to the aerosol backscatter-to-extinction ratio. Note that this value is averaged over the ensemble of particles in the scattering medium.

If D6, which is equivalent to equation 6 of Waggoner et al., is normalised by dividing by β_m , then measurements made over an extended time period or range of altitudes will all provide a linear graph of $K\bar{\beta}_T/\beta_m$ against $\bar{\sigma}_A/\beta_m$, provided that the average backscatter-to-extinction ratio remains constant. D6 then becomes

$$(K\bar{\beta}_T)/\beta_m = K \left(\frac{P_A(\pi)}{4\pi} \right) \bar{\sigma}_A/\beta_m + K \quad , \quad (D8)$$

and linear regression will produce values of both the lidar system constant K and the aerosol backscatter-to-extinction ratio.

4.2 The Determination of Profiles of Vertical Backscatter Function

The clean-air calibration method has been used in the analysis of the data. In this method, the backscatter signal at some calibration range r_{cal} is assumed to be due entirely to scattering from air molecules. Because of the lidar geometry, it is not feasible to determine the transmittance from zero range to r_{cal} , and it is convenient to combine the system constant and the transmittance in one term $[K T^2 (0, r_{cal})]$.

For ranges $r < r_{cal}$, $D1$ can be rewritten

$$P(r) r^2 = \frac{\left[K T^2 (0, r_{cal}) \right] \left[\beta_m(r) + \beta_A(r) \right]}{\exp \left[-2 \int_r^{r_{cal}} \sigma_m(r') + \sigma_A(r') dr' \right]} \quad (D9)$$

This can be expressed in numerical form:

$$P_j r_j^2 = \frac{K T_{o,jcal}^2 (\beta_{mj} + \beta_{Aj})}{\exp \left[-4\pi\delta r \sum_{i=jcal+1}^j (\beta_{mi} + \beta_{mi-1}) / P_m + (\beta_{Ai} + \beta_{Ai-1}) / P_A \right]} \quad (D10)$$

Here δr is the digitiser range increment and $P_m = 1.5$ is the molecular phase function for backscatter. A solution for β_{Aj} is found by calculating first the constant term at r_{jcal} :

$$K T_{o,jcal}^2 = P_{jcal} \cdot r_{jcal}^2 / \beta_{mjcal} \quad (D11)$$

then using this to calculate solutions at ranges $r_j = r_{jcal} - j\Delta r$:

$$\beta_{Aj} = \frac{P_j r_j^2 \exp \left[-4\pi\delta r \sum_{i=jcal+1}^j (\beta_{mi} + \beta_{mi=1}) / P_m + (\beta_{Ai} + \beta_{Ai-1}) / P_A \right]}{K T_{o,jcal}^2} - \beta_{mj} \quad (D12)$$

Note that the solution β_{Aj} is required in the summation on the right hand side of the equation. To overcome this problem this term in the summation initially is set to zero and a first approximation for β_{Aj} is obtained using D12. A better estimate is obtained by using this first solution in the summation. Iteration proceeds until the solution converges to the desired accuracy (Gambling and Bartusek, 1972).

4.3 An Estimate of Uncertainties in the Derived Aerosol Backscatter Profiles

The error (or uncertainty) in β_{Aj} in D12 is found by first calculating the relative error in the total backscatter:

$$\frac{\Delta\beta_{Tj}}{\beta_{Tj}} = \frac{\Delta P_j}{P_j} + \frac{2\Delta r_j}{r_j} + \frac{\Delta T_{j,jcal}^2}{T_{j,jcal}^2} + \frac{\Delta K T_{o,jcal}^2}{K T_{o,jcal}^2} \quad (D12)$$

where ΔP_j arises from $\frac{1}{2}$ LSB in the digitiser ADC, Δr is the uncertainty in the range = $\frac{1}{2}$ the range increment δr ,

$$\frac{\Delta K T_{o,jcal}^2}{K T_{o,jcal}^2} = \frac{\Delta P_{jcal}}{P_{jcal}} + \frac{\Delta\beta_{mjcal}}{\beta_{mjcal}} + \frac{2\Delta V_{jcal}}{V_{jcal}} \quad (D13)$$

and

$$\frac{\Delta T_{j,jcal}^2}{T_{j,jcal}^2} = \delta r \sum_{i=jcal+1}^j (\sigma_{mi} + \sigma_{mi-1}) \rho + \Delta \sigma_{Ai-1} \quad (D14)$$

The relative error in the molecular extinction term, ρ , is taken as one percent (Lenhard, 1973). Next $\Delta\beta_{Aj}$ is calculated as

$$\Delta\beta_{Aj} = \left(\frac{\Delta\beta_{Tj}}{\beta_{Tj}} \right) \cdot \beta_{Tj} + \rho\beta_{mj} \quad (D15)$$

The error in the aerosol extinction to be used in D14 at the next range increment is

$$\Delta\sigma_{Aj} = \left(\frac{\Delta P_A}{P_A} + \frac{\Delta\beta_{Aj}}{\beta_{Aj}} \right) \cdot \sigma_{Aj} \quad (D16)$$

5. RESULTS OF OBSERVATIONS AT COWLEY BEACH - MAY-JUNE 1986

5.1 Aerosol Backscatter-to-Extinction Measurements in the Surface Layer

Information on the aerosol backscatter-to-extinction ratio in the region about 2m above the water and approximately 400m to 4000m from the lidar was obtained from horizontal firings of the laser over the ocean. The lidar was situated at approximately 50m from the water's edge. Observations were made several times each measurement session.

Data have been divided into two groups for analysis. These correspond to the earlier rainy period of high humidity and the later clearer and drier period described in Section 3. As could be expected, data collected during the latter period show less scatter, and have been used for the determination of the lidar system constant K, although the value obtained from the first period is not significantly different.

Data acquired in the second period during times of horizontal homogeneity are presented in Figure 1. The 12 data points shown represent data collected at 18 different times during the 4 day period. Each is the average of 50 individual laser firings covering about 25 seconds giving a total of 900 laser firings. Note that there is remarkably little variation in the aerosol optical properties during this period. The results for $P_A(\pi)/4\pi$ and K are:

$$P_A(\pi)/4\pi = (0.0189 \pm 0.0022) = (0.238 \pm 0.027) / 4\pi \text{ sr}^{-1} ,$$

$$K = (3.56 \pm 0.19) \times 10^{10} \text{ m}^3 \text{ A.J}^{-1} .$$

The lidar system constant is the product of the optical transmission efficiency of the receiver, the effective receiving area of the mirror, the velocity of light and the conversion efficiency of the PMT which had been measured previously. The optical efficiency is the product of three reflections from aluminium, transmission through four glass surfaces and through a narrow band filter:

$$\begin{aligned} \text{i.e. } K &= \eta_o S c/2 Q \\ &= (0.247) (0.0478 \text{ m}^2) (1.499 \times 10^8 \text{ m.sec}^{-1}) (2.0 \times 10^4 \text{ A.W}^{-1}) \\ &= 3.54 \times 10^{10} \text{ m}^3 \text{ A.J}^{-1} . \end{aligned}$$

Excellent agreement exists between the directly and indirectly derived values of the constant.

Data acquired during the earlier period are presented in Figure 2 which, although it shows more scatter than in Figure 1, still indicates rather consistent aerosol properties during the five days of observation. The twelve data points consist of 24 averages of 50 shots or a total of 1200 laser firings. Linear regression of the data gives values of

$$P_A/4\pi = (0.0128 \pm 0.0035) = (0.161 \pm 0.044) / 4\pi \text{ Sr}^{-1} ,$$

and
$$K = (3.59 \pm 0.48) \times 10^{10} \text{ m}^3 \text{ A.J}^{-1} .$$

Note that the system constant derived from this data set is not significantly different from the other values. This proves that the calibration of all of the components in the lidar system remained stable during the 14 days of the study, despite the harsh environmental conditions of strong winds, heavy rain and sea spray. The components considered here are several optical surfaces, optical filters, amplifiers, ADCs and the laser output energy monitor.

The values for the aerosol phase function derived from the two data sets, .019 and .013, differ although the difference is only just significant at the one standard deviation level. An estimate of this value may also be obtained by using Mie scattering calculations and particle-sizing and nephelometer data. Total extinction at 1130 a.m. on the 10th June was $7.3 \times 10^{-5} \text{ m}^{-1}$ which gives an aerosol extinction of $6 \times 10^{-5} \text{ m}^{-1}$. A log-normal distribution was found to fit the particle sizing data and when radius limits of $r_1 = 0.2 \mu\text{m}$ and $r_2 = 5.0 \mu\text{m}$ were used with a refractive index appropriate to sea salt in Mie scattering calculations a value of 0.017 was found for the aerosol phase function at backscatter. This value compares well with the lidar derived values.

Finally, lidar derived values of aerosol extinction are plotted against nephelometer values in Figure 3. The scatter in the data points is the result of the instruments not sampling the same volume of air. The nephelometer was on the shore whereas the lidar was sampling air up to 4 km out to sea. The average ratio of the lidar to the nephelometer value is .73 with a standard deviation in this mean value of .05. As the lidar data were measured at 532 nm and the nephelometer at 470 nm a wavelength exponent of -2.6 is indicated.

5.2 Vertical Profiles of Aerosol Backscatter Function

Vertical profiles of aerosol backscatter function derived from lidar measurements on June 9th and June 10th are presented in Figure 4 and Figure 5 respectively. These data are studied here because airborne sampling of aerosols on these days allow a comparison to be made.

Figure 4 shows enhanced aerosol scattering in the boundary layer, where high relative humidity has increased the particle sizes. The lidar profile is an average of 50 firings at around 1030 EST and the molecular scattering profile was obtained from a radiosonde balloon launched from the lidar site at 1015 EST. A weaker scattering layer is apparent between 1400m and 2000m, also a region of high relative humidity. The aerosol backscatter function decreases steadily with height above this altitude which corresponds to that of the strong temperature inversion. Note that the lidar data have been normalised to the molecular backscatter signal at 4500m and this causes the graph to tend to zero near this height.

Figure 5 is the average of 50 lidar firings around 1138 EST. The radiosonde balloon was launched at 1052. Again, enhanced scattering from aerosols is detected below the temperature inversion at 2100m, a region of high relative humidity. Above this height aerosol scattering drops steadily. Normalisation to molecular scattering occurs for heights above 4000m. The aircraft particle sampling data also show the strong layer with weaker scattering above although, in contrast to the lidar data, they show roughly constant scattering with height above the inversion. The consistent difference between the two instruments in the measured magnitude of aerosol scattering is unexplained at this stage.

Note that lidar derived aerosol backscatter function profiles are influenced by two factors. The first is the need to normalise data at some height where aerosol scattering is assumed to be below the limit of detection of the lidar. If, in fact, significant aerosol scattering does exist this region, then the lidar backscatter profiles will underestimate the actual value at all heights in the profile. Such effects are likely to be small in this data set, a fact supported by the airborne measurements.

As discussed in section 4, a value of the aerosol scattering phase function in the backscatter direction (i.e. the backscatter-to-extinction ratio) is needed to calculate the transmittance correction from the backscatter measurements. If the assumed value is in error or changes with height then errors in the backscatter profile will result as shown in the analysis in section 4.3. This is not expected to be a major factor with data presented here.

Acknowledgements

The authors thank the following people for their assistance: Jim Davies for his participation in field trips and computer programming, Ross Gadene for field trip and electronics support and the staff of the JTTRE at Cowley Beach for their support in the field.

6. REFERENCES

- | | | |
|---|------|--|
| Elterman, L. | 1964 | Atmospheric Attenuation Model, 1964, in the UV, Visible, and IR Regions for Altitudes to 50 km. AFCRL-64-740, Environmental Research Papers No.46. |
| Gambling, D.J. and Bartusek, K. | 1972 | Atmospheric Environment, <u>6</u> , 181. |
| Lenhard, R.W. | 1973 | Bull.Amer.Meteorol.Soc., <u>54</u> , 691. |
| McClatchley, R.A.
Fenn, R.W.,
Selby, J.E.A.
Volz, F.E. and
Garing, J.S. | 1972 | Optical Properties of the Atmosphere. (3rd edition). AFCRL-72-0497, Environmental Research Papers No.411. |

Table D1: Curtin Lidar Technical Details

Transmitter:

Laser	QuantaRay DCR IIA Nd:YAG with frequency doubling
Wavelength	532 nm
Energy per pulse	~ 0.2 J
Pulse duration	5 ns

Steerable Receiver:

Telescope	254 mm diameter Newtonian
Detection filter bandwidth	1 nm
Receiver optical efficiency (including filter)	0.247
Detector	EMI 9816E (S-20) photomultiplier tube
PMT conversion	$2.0 \times 10^4 \text{ A.W}^{-1}$

Recording Electronics:

Amplification	linear or logarithmic
Digitiser	1024 words @ 8 bits resolution
Minimum sampling interval	50 ns
Computer	LSI 11/23+ (controls digitiser and recording of data onto 8" floppy discs Also used for data analysis)

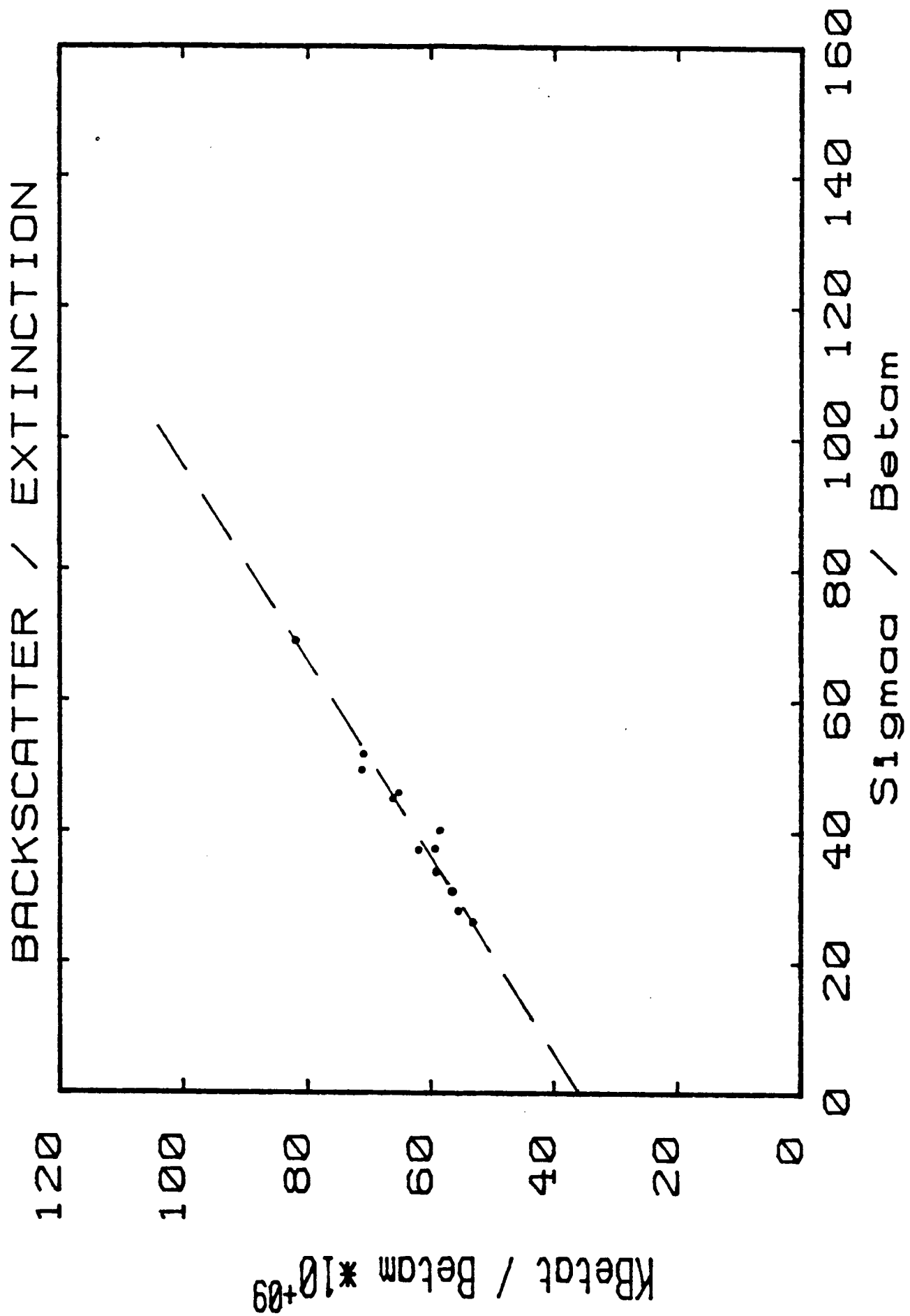


Figure 2

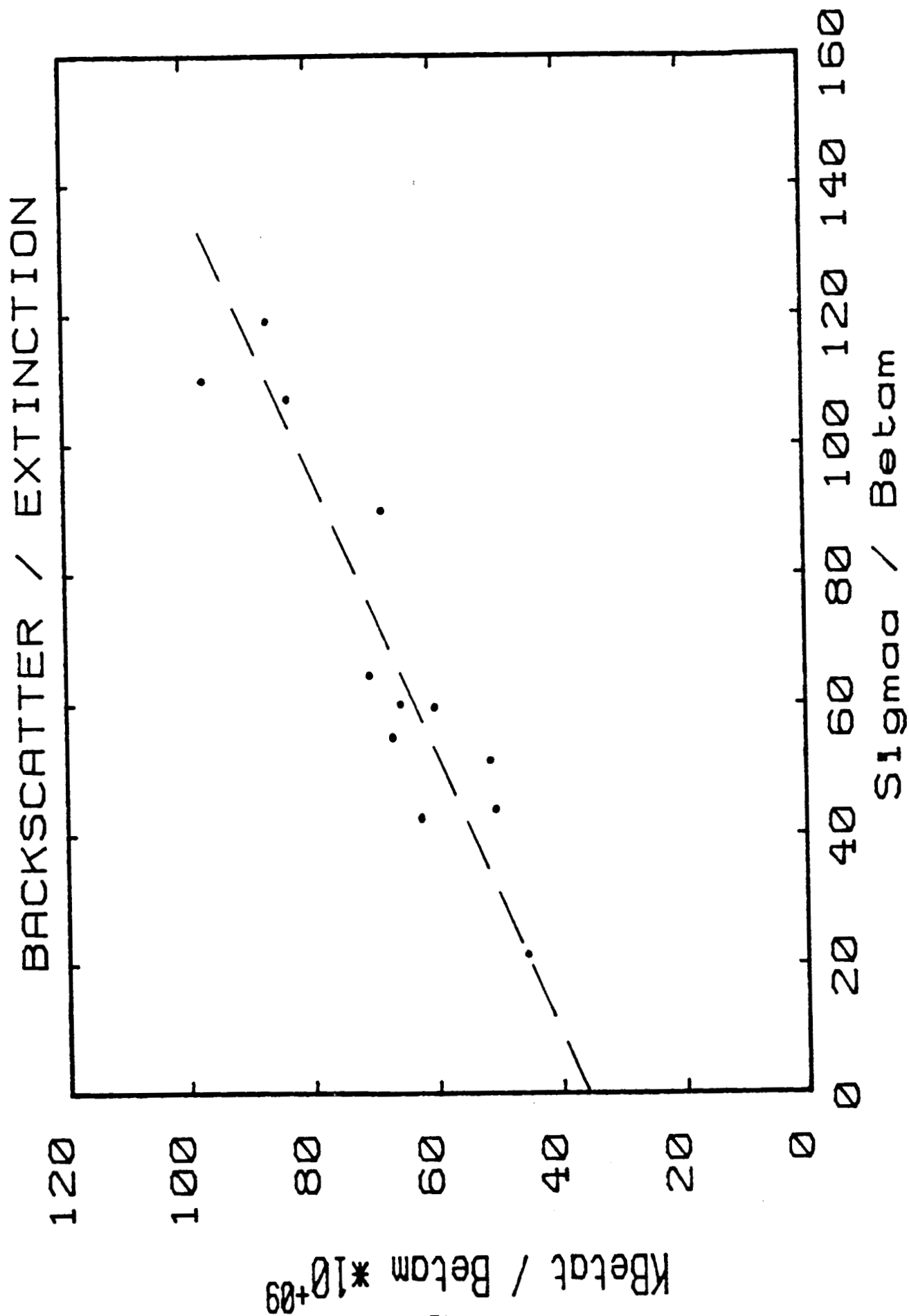


Figure 2

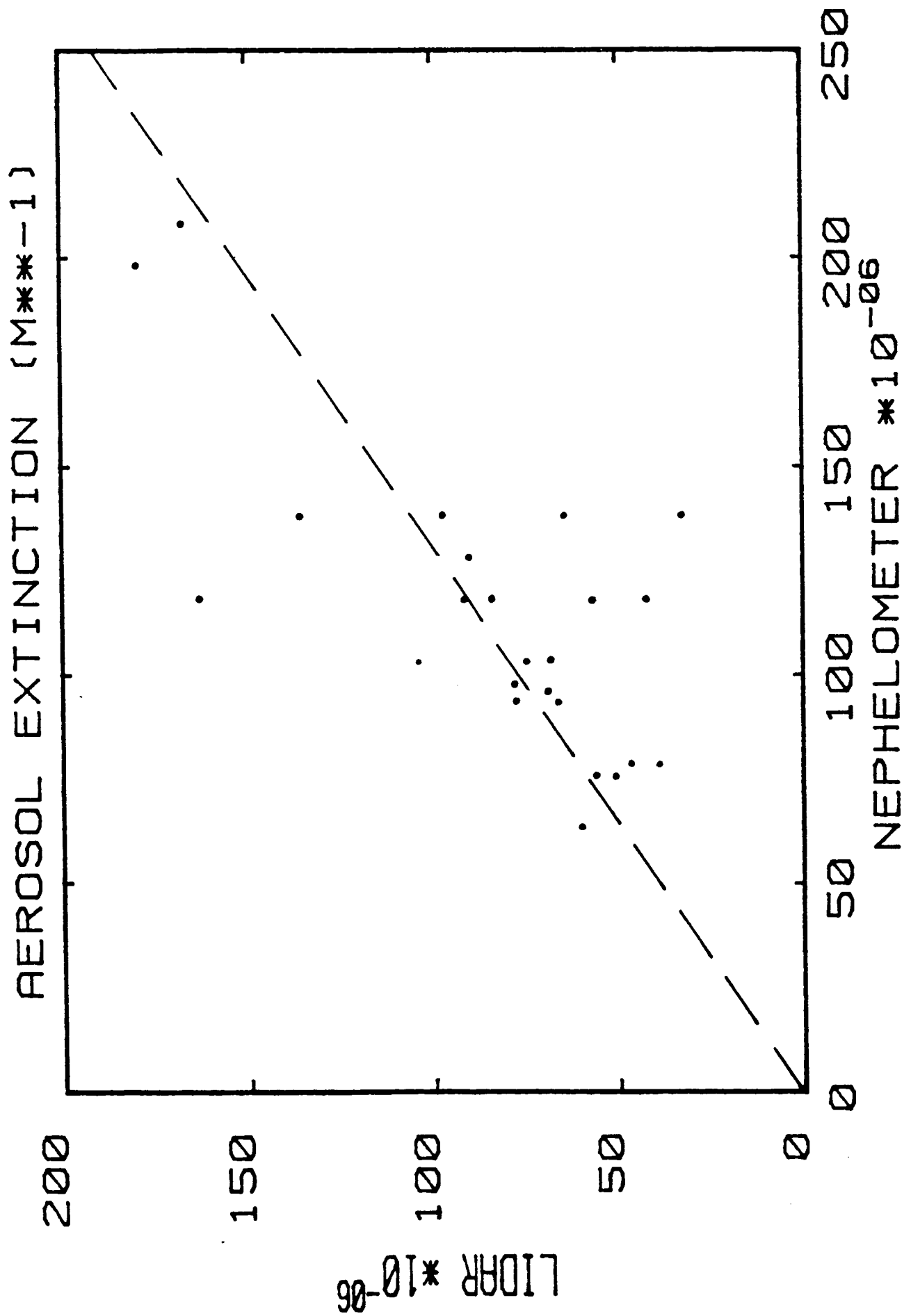


Figure 3

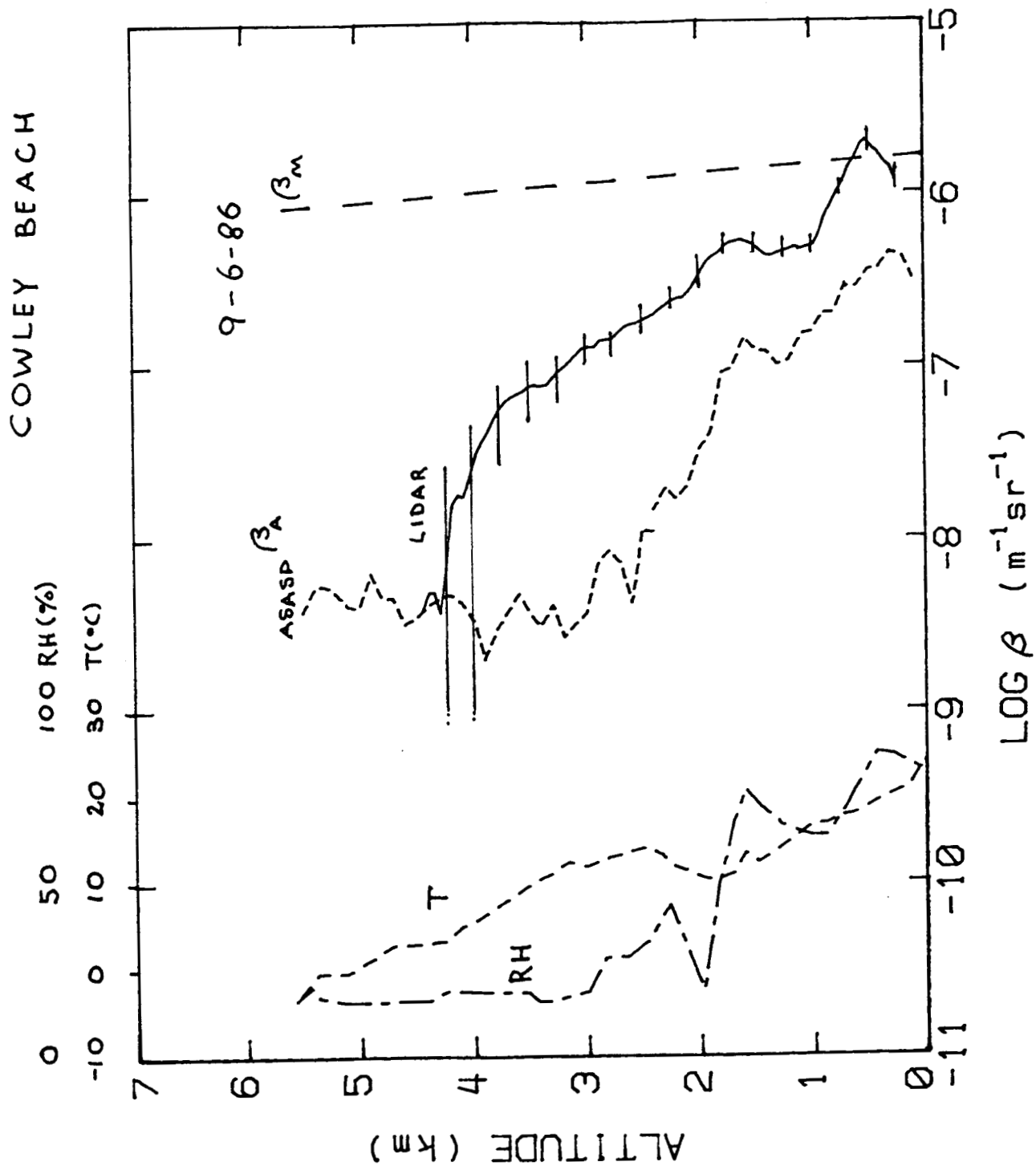


Figure 4

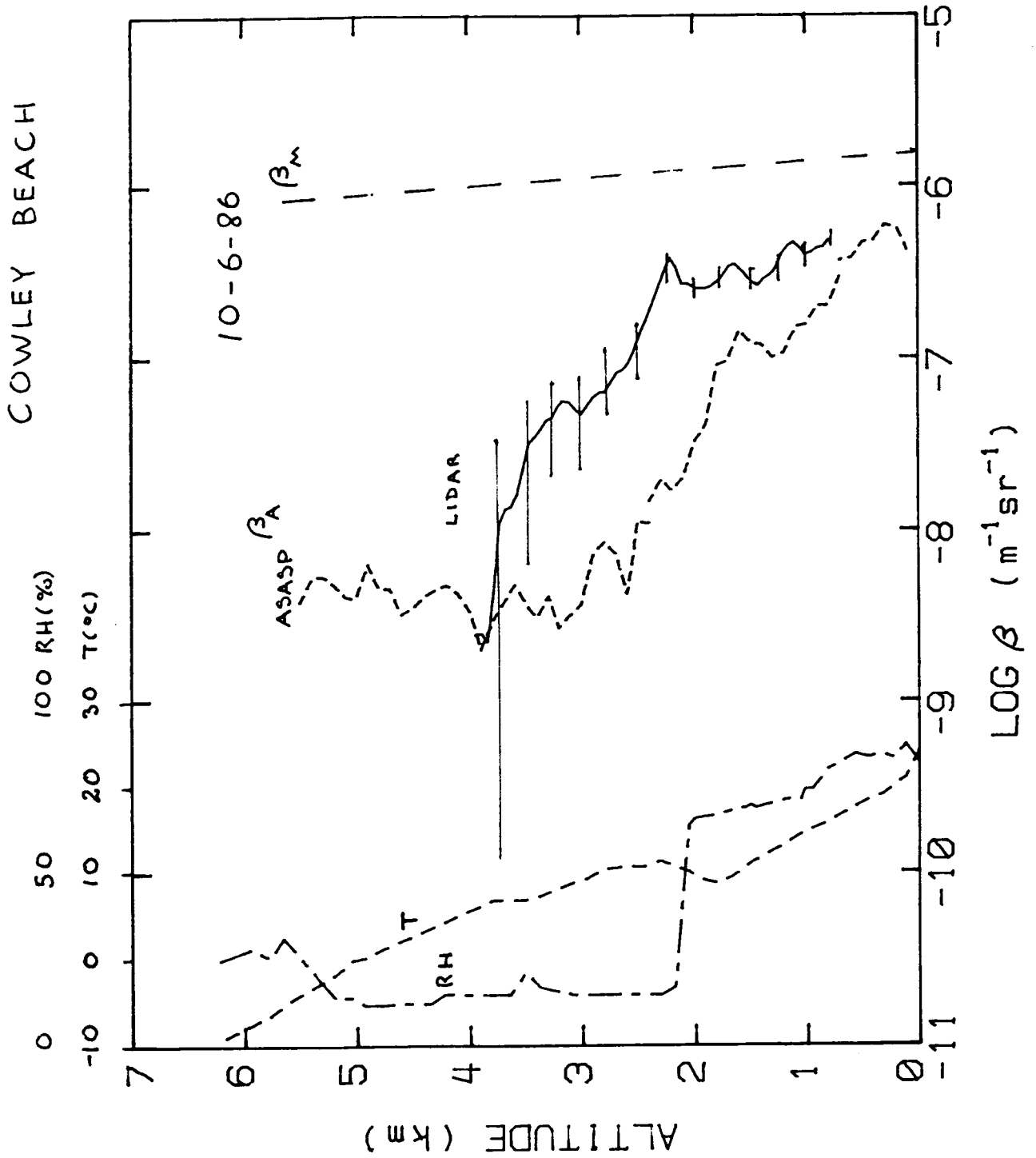


Figure 5